Light responsive cell-cell like biointerface using cadherin peptidomimetics

---

Dissertation

zur Erlangung des Grades

der Doktorin der Naturwissenschaften

der Naturwissenschaftlich-Technischen Fakultät

der Universität des Saarlandes

von

Desna Joseph

Saarbrücken, 2020

Tag des Kolloquiums: 14. Oktober 2021

Dekan: Prof. Dr. Christian Motz

Berichterstatter: Prof. Dr. Aranzazu del Campo

Prof. Dr. Alexander Titz

Vorsitz: Prof. Dr. Albrecht Ott

Akad. Mitarbeiter: Dr. Sercan Keskin

Light responsive cell-cell like biointerface using cadherin peptidomimetics

Desna Joseph

geb. in Kerala, India

DISSERTATION

INM-Leibniz Institut für neue Materialien, Saarbrucken

To my family

Abstract

Interaction between the cells plays a vital role in tissue formation and transmembrane signalling. The family of Cadherin proteins is among the important classes of adhesion molecules engaged in cell-cell interactions. Whose members mediate homophilic Ca^{2+} dependent cell-cell adhesion, and they are dynamic and spatiotemporally tightly regulated in a wide variety of tissues. Dynamic control of cadherin mediated interactions is a key to understand and modulate various cellular events for biomedical applications. This thesis presents a new strategy to spatiotemporally control cadherin mediated cell-cell interactions at biomimetic interfaces. For this purpose photoactivatable peptidomimetics of E-cadherin and N-cadherin were developed by introducing a light responsive non-natural amino acid, His[Ru(bpy)2PPh3] at the His residue of the HAV cadherin binding motif. These peptides were immobilized on poly(acrylamide) hydrogels and cadherin-mediated cell adhesion and derived cellular responses as a function of the activity of the peptide were studied. Flat and micropatterned hydrogels were used to reconstruct polarized cellular microenvironments, as they occur in epithelial or musculoskeletal tissues. Cellular morphology on the novel cadherin mimetic hydrogels was explored. Light-regulated myogenic differentiation of C2C12 cells by temporal control of N-cadherin peptide presentation was demonstrated using the photoactivatable N-cadherin mimetic peptide.

Zusammenfassung

Die Interaktion zwischen den Zellen spielt eine entscheidende Rolle bei der Gewebebildung und der Transmembransignalisierung. Die Familie der Cadherin-Proteine gehört zu den wichtigen Klassen von Adhäsionsmolekülen, die an Zell-Zell-Interaktionen beteiligt sind. Deren Mitglieder vermitteln die homophile Ca^{2+} abhängige Zell-Zell-Adhäsion, und sie sind in einer Vielzahl von Geweben dynamisch und räumlich-zeitlich streng reguliert. Die dynamische Kontrolle der durch Cadherin vermittelten Interaktionen ist ein Schlüssel zum Verständnis und zur Modulation verschiedener zellulärer Ereignisse für biomedizinische Anwendungen. In dieser Dissertation wird eine neue Strategie zur raum-zeitlichen Kontrolle von Cadherin-vermittelten Zell-Zell-Interaktionen an biomimetischen Grenzflächen vorgestellt. Zu diesem Zweck wurden photoaktivierbare Peptidomimetika von E-Cadherin und N-Cadherin entwickelt, indem eine lichtempfindliche nicht-natürliche Aminosäure, His[Ru(bpy)2PPh3] am His-Rest des HAV-Cadherin-Bindungsmotivs eingeführt wurde. Diese Peptide wurden auf Poly(acrylamid)-Hydrogelen und durch Cadherin vermittelte Zelladhäsion immobilisiert, und es wurden abgeleitete zelluläre Antworten als Funktion der Aktivität des Peptids untersucht. Zur Rekonstruktion polarisierter zellulärer Mikroumgebungen, wie sie in epithelialen oder muskuloskelettalen Geweben vorkommen, wurden flache und mikroparenchymierte Hydrogele verwendet. Die zelluläre Morphologie der neuartigen Cadherin-mimetischen Hydrogele wurde untersucht. Die lichtgesteuerte myogene Differenzierung von C2C12-Zellen durch zeitliche Kontrolle der N-Cadherin-Peptid-Präsentation wurde mit dem photoaktivierbaren N-Cadherin-Mimetikum-Peptid nachgewiesen.

Acknowledgments

I wish to express my sincere appreciation to my PhD supervisor, **Prof. Dr. Aránzazu del Campo** for giving me the opportunity to pursue my PhD research in Dynamic Biomaterials group and for her support and guidance during my PhD. I also thank **INM-Institute of New Material, Saarbrücken** for providing me all the facilities to carry out my research. I thank European union Horizon 2020, Mechano Control project for funding my research.

I would like to express my sincere gratitude to my second supervisor, **Prof. Dr. Uli Kazmaier,** University of Saarland, for his suggestions and support. I am thankful to **Prof. Andrés J. García,** Georgia Institute of Technology Atlanta, GA, USA for his valuable advice and feedback for the N-cadherin project. I thank **Dr. Johan de Rooij** and **Dr. Martijn Gloerich**, Center of Molecular Medicine, UMC Utrecht for a great collaboration on the E-cadherin project.

Furthermore, I would like to thank **Dr. Roshna Vakkeel,** for introducing me to the field of peptidomimetics and for being a wonderful mentor and an even better friend. I truly appreciate the guidance you provided and your constant support in my research pursuits.

I also thank **Dr. Aleeza Farrukh,** for training me in the preparation and characterization of polyacrylamide hydrogels and for your collaboration on the N-cadherin project.

I am very thankful to **Dr. Jennifer Yvonne Kasper** and **Dr. Mitchell Han,** for their guidance and support during the cell biology experiments and for all the discussions and advice. I also thank for your collaboration on E-cadherin project.

I would like to thank **Dr. Shifang Zhao,** for showing me the PDMS stamp preparation and **Dr. Jingnan Zhang,** for helping me with SU-8 photomask preparation. I thank **Dr. Bin li,** for helping me with data analysis and graphics design and **Dr. Jun feng**, for the SEM imaging of PDMS stamps.

I thank **Dr. Karin Kiefer, Dr. Emmanuel Terriac** and **Dr. Mitchell Han**, for introducing me the microscopy techniques. I also thank **Dr. Malgorzata Wlodarczyk-Biegun** and **Dr. Oya Ustahüseyin,** for introducing me the Rheology techniques. I thank **Stefan brück** for all his technical support.

I am especially thankful to **Dr. Maria Villiou, Qiyang Jiang, Rebecca Ludwig** and **Dr. Essak Khan** for all the scientific and non-scientific discussions and for being there for each other to support and motivate during the last 4 years.

I thank **Dr. Julieta Paez, Dr. Samuel Pearson** and **Dr. Shrikrishnan Sankaran** for their continued motivation and encouragement.

Special thanks to my office mates **Dr. Jana staudt** and **Dr. Dan Yu** for all the great support and help.

My deepest gratitude to **my parents**, who instilled in me the virtues of perseverance and commitment and relentlessly encouraged me to strive for excellence. I truly appreciate your willingness to listen even when I am stressed out and for always providing advice. Thank you for always believing in me. **Tincy**, you are a wonderful sister and a best friend. Thanks for always being there to motivate me.

I am sincerely grateful to my in-laws and family for all of your support along the way.

Finally, I would like to thank **Dr. Savin Shynu Varghese,** for supporting me throughout this journey. No matter how difficult or discouraging life has ever been, I have always been able to count on you to cheer me up. I appreciate your continued support and unwavering love to finish this thesis.

Thank You,

Desna

Abbreviations

δ	Chemical shift
ε	Molar extinction coefficient
λmax	Wavelength of maximum absorbance
v	Frequency
AAm	Acrylamide
AA	Acrylic acid
Ac	Acetyl
ACN	Acetonitrile
Ala	Alanine (A)
Asp	Aspartic acid (D)
AU	Absorbance units
Bfr Irr	Before irradiation
BSA	Bovine serum albumin
Boc	Tert-butoxycarbonyl
tBu	Tertiary butyl
c	Concentration
$CDCl_3$	Deuterated chloroform
cyclo[RGDfK]	Cyclic (arginine-glycine-aspartic acid-D-phenylalanine-lysine)
cyclo[RGDfC]	Cyclic (arginine-glycine-aspartic acid-D-phenylalanine-cystine)
Cys	Cysteine (C)
d	Doublet (NMR)
D	Dimensional
DAPI	4',6-Diamidino-2-phenylindole
DCM	Dichloromethane
DIPEA	Diisopropylethylamine

DMEM	Dulbecco's Modified Eagle´s Medium
DMF	N,N-Dimethylformamide
DMNPB	3-(4,5-Dimethoxy-2-nitrophenyl)-2-butyl ester
DMSO	Dimethylsulfoxide
E	Young´s modulus
ECD	Extracellular domain
E-cad	E-cadherin
EDC	1-Ethyl-3-(3-dimethylaminopropyl)carbodiimide
EMT	Epithelial–mesenchymal transition
eq.	Molecular equivalent
ESI-MS	Electrospray ionization mass spectroscopy
FITC	Fluorescein isothiocyanate
Fmoc	9-fluorenylmethoxycarbonyl protecting group
G´	Storage modulus
Gly	Glycine(G)
h	Hour
HANBP	2-(4′-Amino-4- nitro-[1,1′-biphenyl]-3-yl)propan-1-ol
HBTU	O-Benzotriazole-N,N,N',N'-tetramethyl-uronium-hexafluorophosphate
HeLa	Henrietta Lacks
HEPES	4-(2-Hydroxyethyl)-1-piperazineethanesulfonic acid)
His	Histidine (H)
HOBt	1-Hydroxybenzotriazol
Ile	Isoleucine (I)
Lys	Lysine
M	Molarity (mol/l)
m	Multiplet (NMR)
MDCK	Madin-Darby Canine Kidney cells

MEFs	Mouse Embryonic Fibroblasts
Milli-Q	Deionized, filtered ultrapure water
min	Minute
MS	Methyl Sulfone
MW	Molecular weight
mol%	Molar percentage
NHS	N-Hydroxysuccinimide
NMR	Nuclear magnetic resonance
ovn	Over night
PDMS	Polydimethylsiloxane
PBS	Phosphate-buffered saline
PEG	Poly(ethylene glycol)
PFA	Paraformaldehyde
PMNB	p-Methoxynitrobiphenyl
Pre irr	pre-irradiation
RP-HPLC	Reverse phase high performance liquid chromatography
S	Singlet (NMR)
SD	Standard deviation
Sec	Second
sulfo-SANPAH	(Sulfosuccinimidyl-6-(4'-azido-2'-nitrophenylamino)hexanoate)
Ser	Serine (S)
r.t.	Room temperature
TIS	Triisopropyl silane
TFA	Trifluoroacetic acid
TEMED	Tetramethylethylenediamine
TFE	2,2,2-trifluoroethanol
Thr	Threonine (T)

Trp	Tryptophan (W)
UV	Ultraviolet
UV/VIS	Ultraviolet–visible spectroscopy
Val	Valine (V)
VEGF	Vascular endothelial growth factor
VIS	Visible spectral range
^{1}H-NMR	Proton NMR spectroscopy
^{13}C-NMR	Carbon NMR spectroscopy

All other abbreviations, such as physical and chemical units have their normal definition unless otherwise specified.

Table of Contents

Motivation

Cell-cell interactions play a pivotal role in maintaining tissue integrity and organization. The spatiotemporal regulation of these interactions is crucial during embryogenesis and wound healing, and dysregulation is involved in cancer progression. The development of tools to interfere and eventually control cell-cell interactions dynamically and with spatiotemporal resolution is important to progress in our understanding of biological processes.

During the last two decades, useful approaches to regulate interactions between cells and the extracellular matrix based on biomimetic materials have been proposed. Light responsive peptidomimetics of matrix adhesive proteins presented on biomaterial surfaces have been developed as synthetic biointerface with dynamic biofunctionality. Cell responses to changes in the composition or mechanical properties of the extracellular matrix have been studied using these artificial microenvironments. This thesis takes advantage of this progress and presents a similar platform to regulate cell-cell adhesive interactions.

Cadherins are major membrane adhesive proteins that mediate the connection between adjacent cells and form adherent junctions. Biomaterial surfaces decorated with cadherin proteins can promote cellular processes activated by cell-cell interactions such as cell adhesion, proliferation, and differentiation. Cadherin-cadherin interactions have been extensively studied and the molecular design of the interacting interface is known. This has facilitated the development of cadherin peptidomimetics as small molecules that can bind to cadherins and be used to reconstruct cell-cell like interfaces. In this thesis, advanced cadherin peptidomimetics with light-regulated bioactivity will be presented and applied to design cell-cell like interfaces with dynamic properties.

Cell-matrix and cell-cell interactions in the epithelial cellular environment are spatially segregated with apical-basal polarity. Micropatterned hydrogels have been proposed as synthetic microenvironments to mimic a polarized receptor distribution. In this thesis, dynamic polarized microenvironments that allow independent activation of cell-cell and cell-ECM interactions are presented using photoactivatable cadherin mimetic peptides. The functionality of this biomimetic platform is demonstrated by triggering the adhesion of epithelial cells and myogenic differentiation of fibroblasts upon light exposure.

This thesis details the synthesis and characterization of photoactivatable cadherin mimetic peptides containing a non-natural amino acid with a photoremovable protecting

group. Photoactivatable peptidomimetics of N-cadherin and E-cadherin are presented. The light-regulated bioactivity of the compounds was tested in cell adhesion experiments on flat poly(acrylamide) hydrogels modified with the peptidomimetics. Special effort was devoted to optimizing the ligand concentration and mechanical properties of the hydrogel for cell attachment. The adhesion of epithelial cells was tested on E-cadherin modified hydrogels. Micropatterned hydrogels with spatial separation of cadherin and matrix adhesive peptides were developed. The ability to control N-cadherin mediated cellular processes on-demand using photoactivatable N-cadherin peptidomimetic was demonstrated in N-cadherin mediated myogenic differentiation assay.

The thesis is organized as follows:

Chapter 1 describes the state-of-the-art of literature about cell adhesion, cell-cell interaction, cadherin receptor family, synthetic models of cell-cell biointerface, Dynamic biointerface, and polarized microenvironments.

Chapter 2 explains the selection and synthesis of photoactivatable E & N- cadherin peptidomimetics and shows the physiochemical and photochemical characterization of developed photoactivatable peptides

Chapter 3 presents the development, physiochemical characterization, biofunctionalization, and photolysis of 2D and 2.5D polyacrylamide hydrogels copolymerised with acrylic acid and methylsulfone acrylate.

Chapter 4 entails the interactions between E-cadherin mimetic peptides and epithelial cells on 2D polyacrylamide hydrogels.

Chapter 5 describes cellular assays to demonstrate the light-triggered bioactivity of N-cadherin peptidomimetic, and applies it to regulate N-cadherin mediated myogenic differentiation.

Chapter 6 summarizes the most important conclusions of the work.

Chapter 1

Background and Literature review

1.1 Cell adhesion

The interactions of cells with their natural microenvironment guide cellular behavior[1]. In particular, the adhesion of cells to the extracellular matrix (ECM) and to the neighboring cells are crucial for many cellular processes. Cells attach to the matrix and to cells via adhesion receptors (cell adhesion molecules) that form complexes with complementary partners at the ECM or at the membrane of neighboring cells. Through them, cells sense and communicate information from and to their environment. Cell adhesion is dynamically controlled in space and time during cell differentiation[2,3], migration, or proliferation processes. For instance, during cell motility cells need to release attachment points to the matrix and establish new ones as they move forward. Understanding how cell adhesion works at the molecular level would provide new information on cellular biology and opportunities to regulate cellular processes[4].

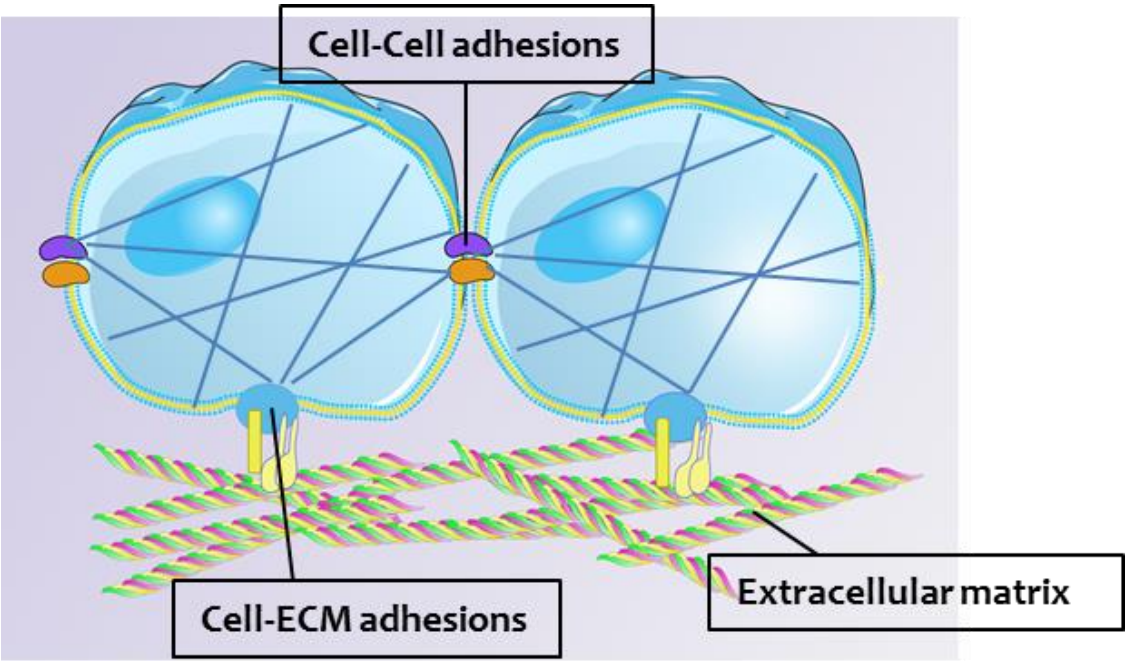

Fig. 1.1 *Schematic representation of Cellular microenvironment and interaction between cell-cell and cell- extracellular matrix.*

Cell adhesion molecules (CAMs) are proteins present on the cell membrane, which mediate the cell adhesion by either interacting with neighboring cells or to the extracellular matrix[5]. The intracellular part of most CAMs is associated with components of the cytoskeleton[6]. The five major classes of CAMs are: Integrins, cadherins, Immunoglobulin (Ig) superfamily, lectins, and mucins **(Fig. 1.2)**. The Integrins are involved in cell-matrix interaction, while the others are involved in cell-cell interaction[7]. Cell-cell attachment including cadherins and selectins relies upon Ca^{2+} ions, while adhesions including integrin and Ig-superfamily CAMs don't.

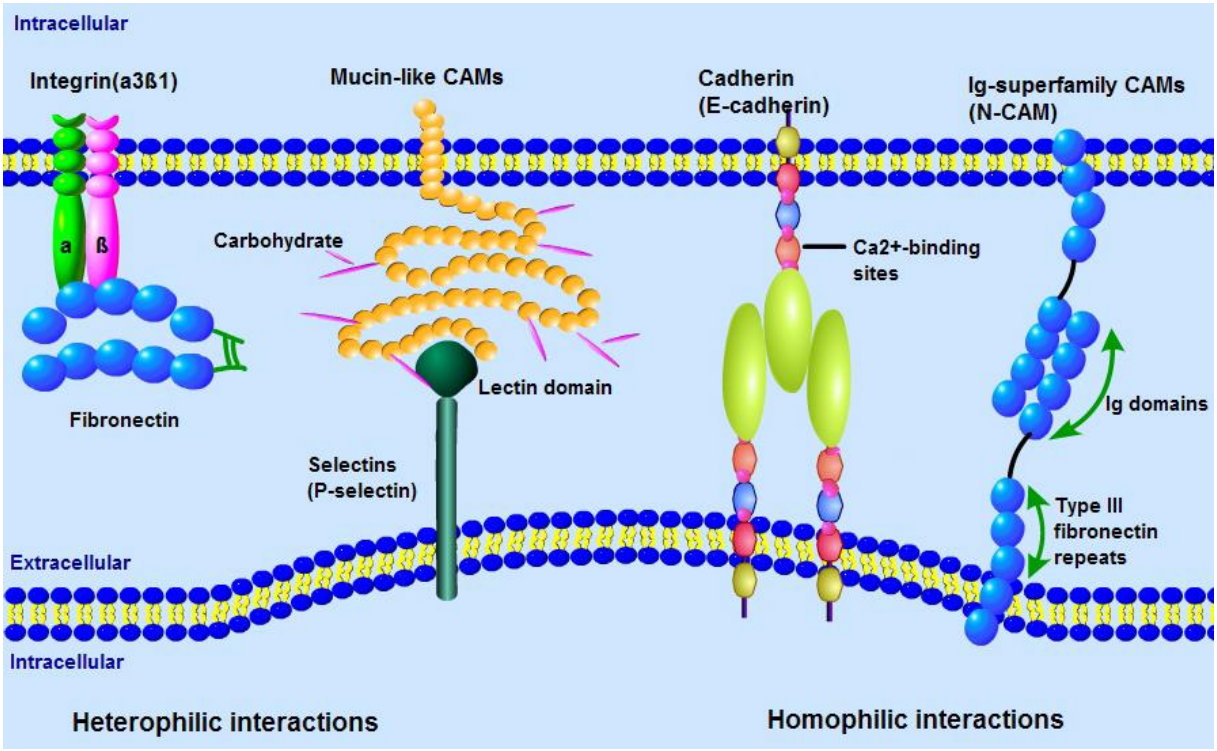

Fig. 1.2 *Families of cell-adhesion molecules (CAMs); Cadherin and the immunoglobulin (Ig) superfamily of CAMs mediate homophilic cell-cell adhesion. Integrin and selectins form heterophilic adhesion, Copyright sabbiotech company.*

1.2 Cell-ECM Interactions

The extracellular matrix is a complex meshwork of structural and functional proteins and carbohydrates. Which plays a significant role in tissue and organ morphogenesis and structure and function maintenance of cells and tissues. ECM's composition and morphology contribute to the particular characteristics and specific function of individual tissues and

organs. During growth, development, and wound repair, the ECM is also significant: it functions as a reservoir for soluble signaling molecules and mediates migration, proliferation and differentiation of cells[8].

The family of trans membrane glycoproteins called integrins mediates interactions of cells with the ECM. Integrins are heterodimers consisting of an α and a β subunit[9]. Integrins in vertebrates can be constructed from 18 different α and 8 different β subunits[10]. The various combinations of α and 8 β subunits generates 24 distinct integrins. Each integrin has specific binding partners, it is involved in distinct signaling pathways, and presents distinct distribution in individual tissues[10,11]. Integrins recognize adhesive sites at ECM proteins such as collagen, laminin and fibronectin or vitronectin[12]. Cell-matrix adhesion sites form a physical connection between the extracellular scaffold and the intracellular cytoskeleton, having a relevant structural and communication role in tissue formation and homeostasis. Furthermore, signaling between the cells and ECM is bidirectional and maintained through adhesion complexes[13].

1.3 Cell-cell interactions

The capacity of cells to communicate with each other is key feature of multicellular organisms[7]. Cells share information with neighboring cells to coordinate their behavior and a controlled functioning of the whole organism. Many cells in tissues are in physical contact with other cells. Cell-cell communication tools involve intracellular receptors, cell surface receptors and physical contact to the partner cell in the form of cell-cell junctions. These cell junctions can be classified attending to their function in different classes: tight junctions, adherens junctions, desmosomal junctions and gap junctions[7].

Tight junctions seal neighboring cells together by connecting the plasma membrane of adjacent cells in a sheet. This prevents the leakage of molecules between the cells and through the sheet[1]. Tight junctions have ribbon-like bands connecting adjacent epithelial cells. Each strand in these systems is composed of transmembrane proteins (claudins and occludin) that prevent leakage of fluid across the cell layer[7].

Adherens junctions join the actin cytoskeleton of neighboring cells. Adherens junctions are normally situated close to the apical surface just underneath the tight junctions. The adherens junctions play out different functions including inception and adjustment of cell-cell adhesion, guideline of the actin cytoskeleton, intracellular signaling and transcriptional

signaling. The center of the adherens junctions involves transmembrane glycoproteins of the cadherin superfamily, e.g. E-cadherin, and the catenin family including p120-catenin, β-catenin, and α-catenin[1,7,14].

Desmosomal junctions connect the cytoskeleton of adjacent cells by joining the intermediate filaments. Desmosomal junctions are formed by desmogleins and desmocollins, members from the cadherin superfamily, proteins called desmosomal cadherins[1,7].

Gap junctions link the cytoplasm of nearby cells. They allow small water-soluble ions and molecules to diffuse uninhibitedly between neighboring cells. However, anticipating the section of proteins and nucleic acids through plasma membrane. Gap junctions are composed of transmembrane glycoproteins called connexons. The gap junction is dynamic in nature; it can open or close in light of an assortment of components, including Ca^{2+} and H^{+} particles[1,7].

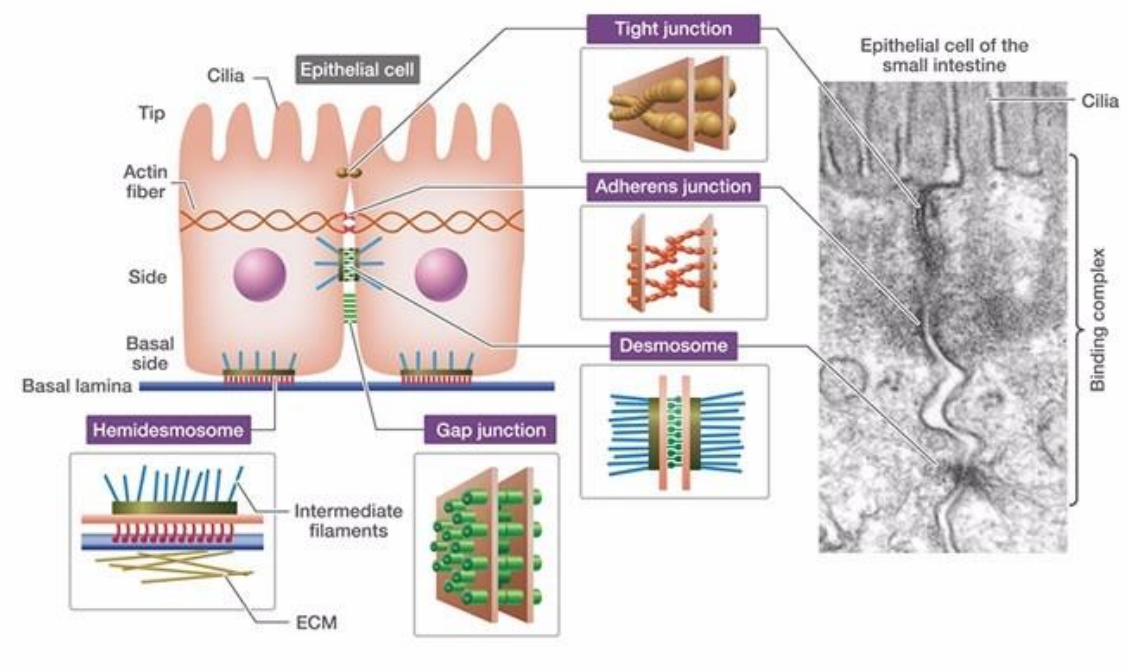

Fig. 1.3 *Schematic diagram showing cell junctions in epithelial tissue. They are held together by specialized membrane proteins that form specialized junctions between adjacent cells, copy right creative proteomics.*

1.4 The cadherin receptor family

Cadherins are transmembrane receptor proteins with a major role in cell-cell adhesion[7]. The cadherin superfamily comprises more than 40 members and can be organized in two major subfamilies: classical and non-classical cadherins (Table 1.1). Cadherins are highly conserved

over species and are comprised of three domains; i.e., an extracellular domain, transmembrane domain, and intercellular domain[7].

Table 1.1 *Cadherins and their distribution in different tissues*[15].

Cadherin	**Tissue distribution**
E-Cadherin	epithelia, skin, liver, pancreas, kidney, sensory neurons
N-cadherin	nervous system, lens, cardiac and skeletal muscle
P-cadherin	skin, breast (myoepithelial cells), prostate (basal cells)
VE-cadherin (Cadherin-5)	vascular endothelium
R-cadherin (Cadherin-4)	eye (retina), brain, skeletal muscle
K-cadherin (cadherin-6)	brain, cerebellum, kidney, lung, pancreas
Cadherin-8	brain
Cadherin-9	brain
Cadherin-10	brain
OB-cadherin (cadherin-11)	osteoblasts, skeletal muscle, fibroblasts
M-cadherin (cadherin-15)	developing skeletal muscle, satellite cells, cerebellum
PB-cadherin	pituitary, brain
Li-cadherin	liver, intestine
HPT-cadherin	gastrointestinal tract

1.4.1 Classical cadherins

Classical cadherins (E-, N-, P- cadherins) are type 1 integral membrane glycoprotein of 720-750 amino acids that facilitate the cell-cell adhesion by their capacity to self-associate (between identical molecule types)[7]. The homotypic association of cadherins is significant for the arrangement of cells during embryogenesis, tissue organization and for the function of tissue[16,17]. Nearly, all cadherin molecules comprise a N-terminal extracellular domain, a trans membrane region and a C-terminal cytoplasmic tail. The architecture of the extracellular domain of classical cadherins is the same. It has five extracellular domains (ECD1-ECD5; 1-5

numbering from the outer most domain) and the repeated sequences are vital for Ca^{2+} binding and cell-cell adhesion[18]. Binding of Ca^{2+} molecules between the extracellular domains turns it into stiff hooks that link cells together. Sequences corresponding to cell-cell adhesion and self-association are located at the ECD1. Different classes of cadherins have almost 50-60 percent of identical sequence[7].

The intracellular domain is highly preserved within the cadherin family and associates with several proteins in the cytoplasm, collectively called catenins[7]. The term "classical cadherin" refers to the ability form catenin complexes. The cadherin-catenin association is pivotal for the interaction between cadherins on the neighboring cells, Furthermore, to balance out the cadherin-cadherin interaction[12] **Fig. 1.3**. The catenins have three major binding partners; α-catenin, β-catenin or γ-catenin and plakoglobin/p120. β-catenin or γ-catenin binds to the cytoplasmic tail of cadherin and α-catenin attaches to β-catenin or γ-catenin[19]. α-catenin has the ability to interact with actin cytoskeleton, subsequently it connects the cadherin/ β-catenin complex to the actin cytoskeleton, which is essential for cadherin activity[20].

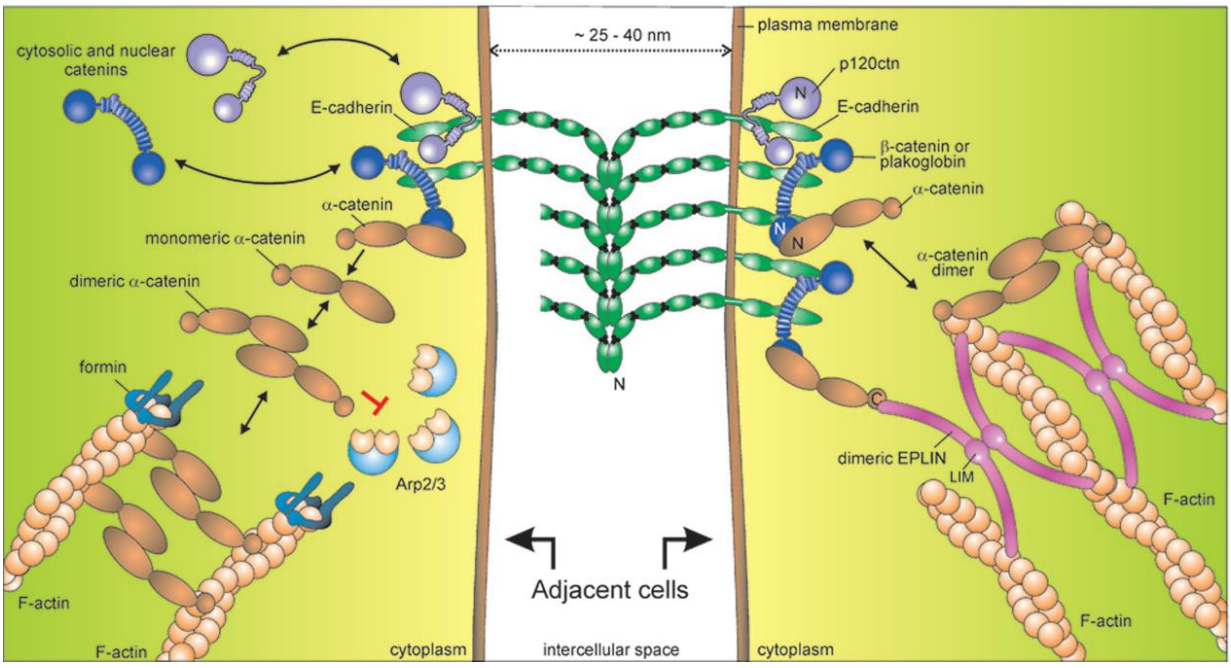

Fig. 1.4 *Schematic representation of homophilic cadherin interaction between adjacent cells, Reproduced with permission from SpingerLink*[20].

1.4.1.1 E-cadherin

E-cadherin (epithelial cadherin) is also referred to as cadherin-1, encoded by the CDH1 gene holds most epithelial layers together. Different layers of polarized epithelial cells, for example those that line the small intestine or kidney, and skin is rich in E-cadherin[7]. E-cadherin is important for tissue morphogenesis and maintaining mature tissues[21]. It is involved in many *in vivo* and *in vitro* development and differentiation processes of ESCs, MSCs, iPSCs and whole embryos[22]. E-cadherin mediated cell-cell interaction directly influence hepatocytes to maintain their differentiated phenotypes by developing a 3D spheroid arrangement or a multi-layer cell aggregates[23,24]. During the early phases of embryogenesis, E-cadherin facilitates cell-cell adhesion is mostly rearranged to regulate cell migration, cell sorting, and tissue function, indicating close cooperation with E-cadherin in the maintenance, proliferation and differentiation of stem cells[21,25,26]. Cell-cell contact mediated by E-cadherin regulates early keratinocyte cell differentiation[27]. Keratinocytes that lack E-cadherin display in vitro downregulated differentiation markers[28]. The down regulation of E-cadherin in cancer cells lead to the loss of cadherin mediated cell adhesion and a transition from benign epithelial to mesenchymal state[29]. Misregulation of the dynamics of E-cadherin may contribute to the promotion of metastasis[22].

1.4.1.2 N-cadherin

N-cadherin or neural cadherin is also referred to as cadherin-2, encoded by the CADH2 gene in humans[24]. N-cadherin (neuronal cadherin) is another type of classical cadherin and predominantly expressed on central nervous system, endothelial, and invasive cancer cells. The amino acid sequences on the extracellular domain and cytoplasmic tail of E- and N-cadherins shares about 64% and 70% similarity respectively and 84% in the β-catenin binding domain[30].

Cells undergo an epithelial-mesenchymal transformation (EMT) during embryogenesis that initiates N-cadherin up regulation and E-cadherin down regulation in the mesoderm[31]. In the early stage of embryonic development, N-cadherin expression was identified in mesoderm and notochord, which is subsequently also apparent in neural tissue[32], certain epithelial tissues, heart myocardium[33] and limb cartilage[34,35]. N-cadherin levels were found to increase during differentiation of osteoblasts and decrease during adipogenic differentiation, indicating their participation in appropriate differentiation mechanisms[36].

Neural crest cells associated with neural tube express N-cadherin; nonetheless, the expression of N-cadherin is downregulated after EMT process and which results in the migration of cells and they transform into different types of tissues and cell populations, such as peripheral nervous system, cartilage, bone and melanocytes[24]. These shows that N-cadherin mediated interactions are crucial for tissue development, morphogenesis and maturation[37].

1.4.2 *Cis* and *Trans* interactions in cadherins

Classical cadherins forms cell-cell adhesion through the extracellular domain by the formation of linear zipper-like ribbon structure[20]. The structure is formed by a combination of adhesion dimers and strand dimers[38]. Adhesion dimers connect the neighboring cell surfaces (t*rans* dimer), while strand dimers organize the cadherin molecules from the same cell surface in a parallel direction (c*is* dimer)[38]. The adhesive interface in this structure includes a highly conserved Trp at position 2 as well as an evolutionarily conserved His 79- Ala 80- Val 81, (HAV) tripeptide in the N-terminus of ECD1 (**Fig 1.6)**. The side chains of the HAV motif account for the 14% adhesion interface[38]. The conserved Trp and His-Ala-Val plays a key role in *cis* and *trans* dimerization[39–42].

A large HAV tripeptide containing dimer interface is involved in c*is* adhesion and *trans* interaction involves the mutual exchange of Trp 2 and their inclusion into hydrophobic pockets on EC1 of the juxtaposing protein[38]. The Trp 2 from ECD1 of a cadherin monomer interacts with the acceptor pocket from the ECD1 of a neighboring cell. During the *cis* or strand dimer formation Ala 80 provide a hydrophobic pocket for the side chain of Trp 2 on the second cadherin monomer[38]. The His and Val make adhesion contacts with the ECD2 of the same cell and these record for under 5% of the adhesion interface[38,43].

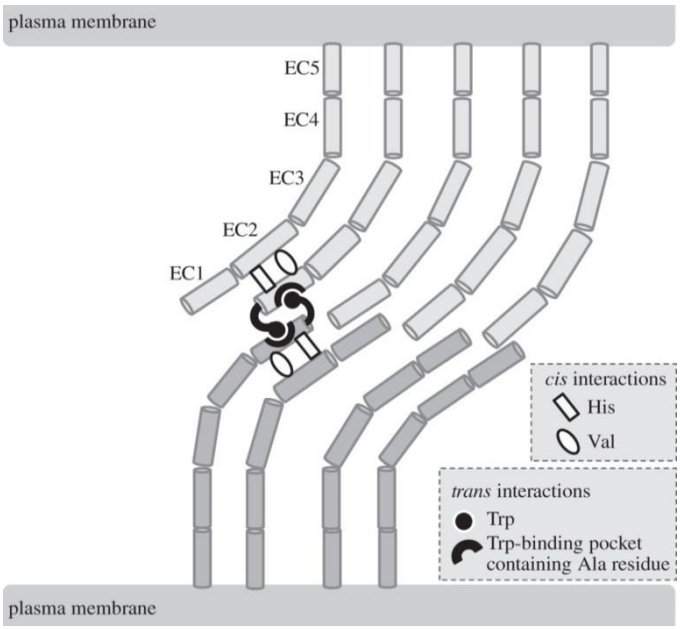

Fig. 1.5 *Schematic representation of cis and trans interaction between the extra cellular domain of two cadherin proteins from neighboring cells , Reproduced with permission from Royal Society*[44]*.*

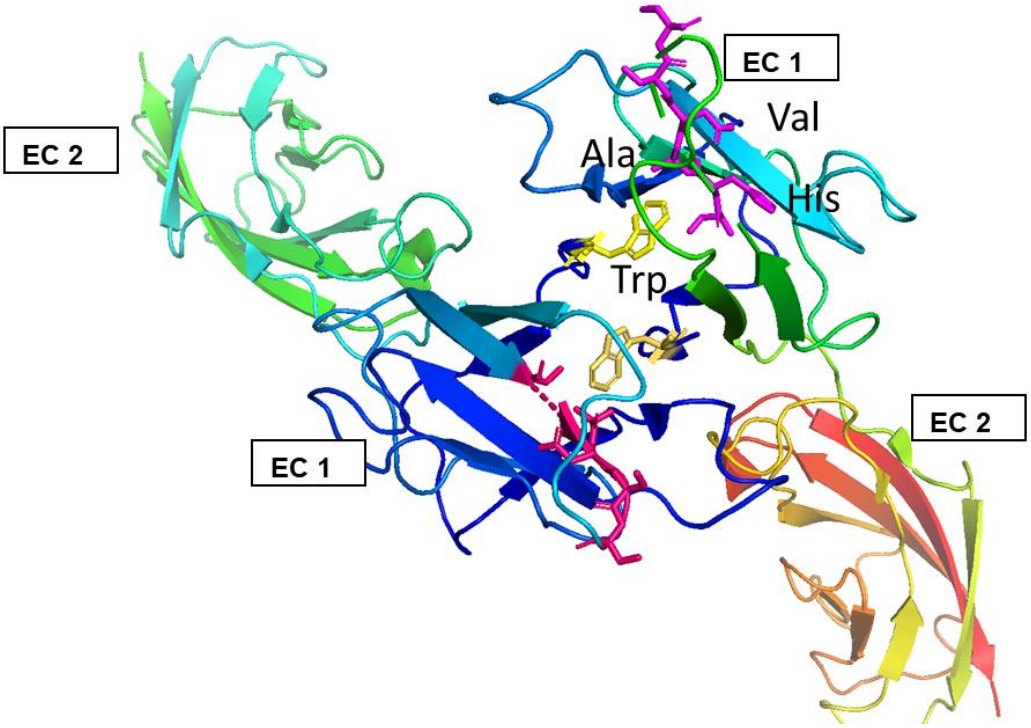

Fig. 1.6 *Crystal structure of the E-cadherin strand swapped trans dimer (ribbon view). Conserved HAV sequence (magenta sticks) and Trp 2 in the hydrophobic pocket of Ala 80 are labeled (yellow sticks), PDB CODE 3Q2L*[40]*.*

1.5 Synthetic models of the cell-cell biointerface

The study of cadherin interactions and associated cell responses at the cell-cell interface is experimentally complicated. Different minimal models of the cell membrane have been developed and used to reconstruct artificial cell-cell interfaces as models to study cell-cell communication. In this case cell-cell adhesive receptors are immobilized on synthetic surfaces to which cells are cultured. The properties of the artificial biointerface (the concentration of the adhesive protein, or the coexistence of others) can be easily defined. These platforms have been widely used to generate cell-cell (and also cell-matrix) adhesive complexes and look at cell responses. This section describes the most relevant platforms used to study cell-cell interactions.

Supported phospholipid bilayers (SLBs) functionalized with cell membrane receptors are useful models to investigate cell-cell interactions. SLBs can easily form on hydrophilic solid supports. These systems allow lateral mobility of the CAMs incorporated in the bilayer, in a manner that imitates the membrane of a cell[45–47]. Since E-cadherin has low mobility in natural cellular membrane[48], in recent study, SLBs functionalized with E-cadherin protein using His-tag technology have been used to understand cell-cell adhesion in epithelial layers related to SLB fluidity[46] (**Fig. 1.7A)**. When MKN-28 epithelial cells cultured on mobile E-cadherin SPBs (**Fig. 1.7B),** enrichment of E-cadherin was less, suggesting that no junctions were produced. However, when the E-cadherin was functionalized on low mobility SLBs, effective cell-cell junctions were formed (**Fig. 1.7C).** Cells on immobile SLBs failed to form cell-cell junctions. The authors proposed that E-cadherin's intracellular domain has a critical function in the formation of junctions on low mobility SPBs, the interaction between E-cadherin protein functionalized on the SLB and E-cadherin on the cell surface form the cadherin-cadherin intermediate bond, which leads to the activation of actin fiber nucleation process resulting in stable cell-cell junctions[46] **(Fig. 1.7B-C).**

SLBs functionalized with the N-cadherin have also been used to guide progenitor cells from skeletal tissue during mesenchymal condensation, chondrogenesis and bone formation[49]. It was found that with higher cell densities during seeding, cells were lead to a pre-mesenchymal condensation state[49]. Lately, it has been reported that SLBs functionalized with extracellular domain of N-cadherin protein promote neural adhesion, neurite extension, and maturation[50]. E-18 cortical neurons cultured on N-cadherin SLBs promote cell adhesion with homogeneous cell distribution and network formation, while the cultured cortical

neurons show an extensively developed finely meshed neural network architecture after 7 days of culture[50] **(Fig. 1.7 D-E)**.

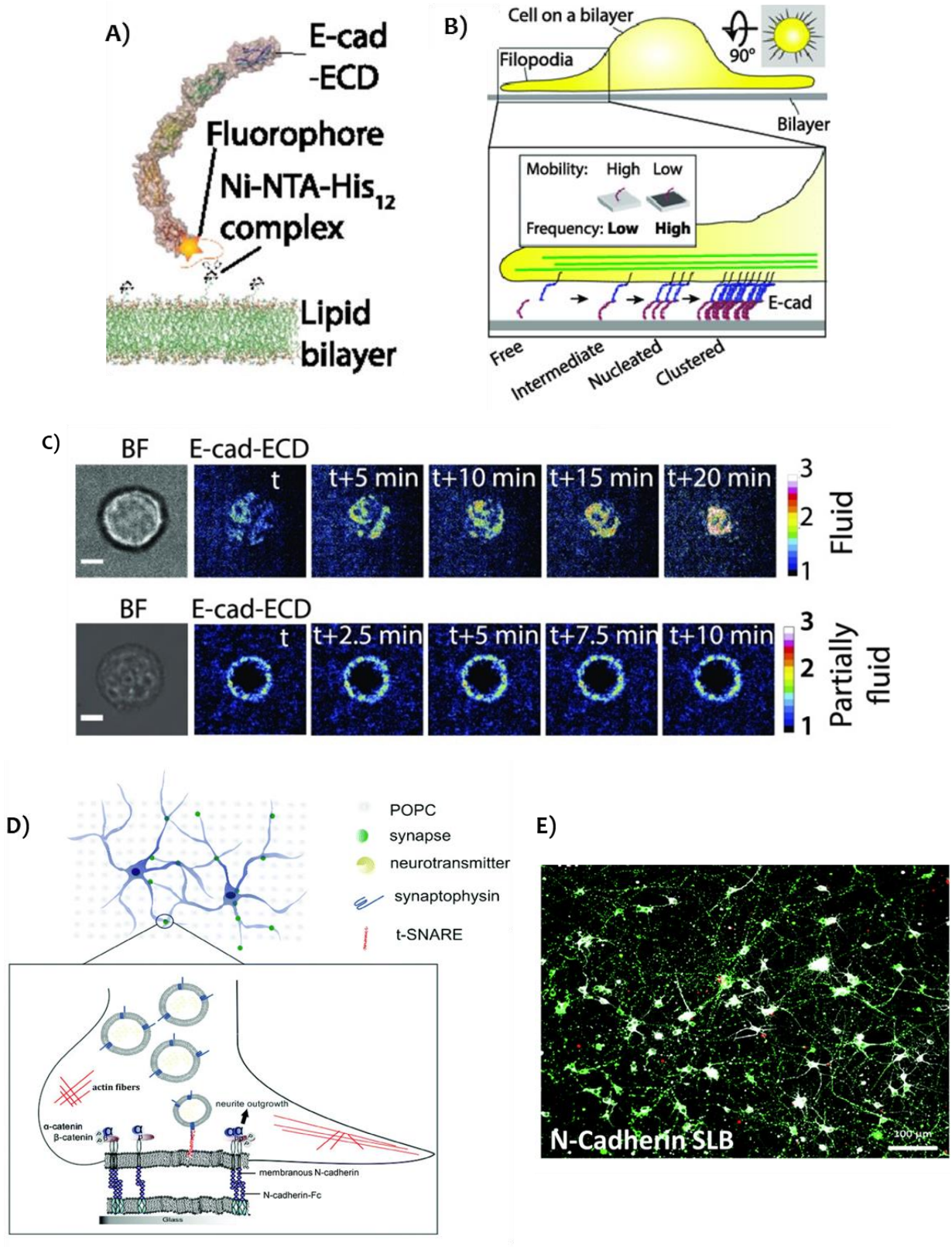

Fig. 1.7 *(A) SLBs functionalized with extracellular domain of E-cadherin carrying a fluorophore, using Ni^{2+}-NTA-His12 chelation. (B) E-cadherin mediated cadherin-cadherin interaction on SLBs. (C)*

Fluorescent time-lapse images of MKN-28 epithelial cells on mobile (fluid) and low mobility (partially fluid) E-cadherin functionalized SPBs. Left: bright field mode. Color bars show fold enhancement in surface density of E-cadherin (scale bars: 5µm), Reproduced with permission,[46] *Copyright (2015), National Academy of Sciences. (D) Schematic representation of the interaction between N-cadherin from cell surface and N-cadherin on SLBS. (E) Cell adhesion and neurite formation of neuronal cells cultured on N-cadherin functionalized SLBs, Reproduced with permission from Royal Society* [50].

2D solid surfaces modified with E-cadherin have also been used to model the cell-cell biointerface[51]. For example, polystyrene surfaces (PS) modified with E-cadherin induced spreading of embryonic stem cells and enhanced proliferation and paracrine function of MSCs[52] **(Fig. 1.8A)**. Glass coverslips coated with N-cadherin has used to investigate the response of cells to cadherin activation relying on distinct signaling pathways[53]. Myogenic cells adhered on this N-cadherin substrate with extensive spreading and they exhibited a fried egg morphology characterized by large lamellipodium. It was found that homophilic liganding of N-cadherin can specifically induce the co-organization of cadherin-catenin complexes and actin cytoskeleton in cadherin adhesions[53] **(Fig. 1.8B)**.

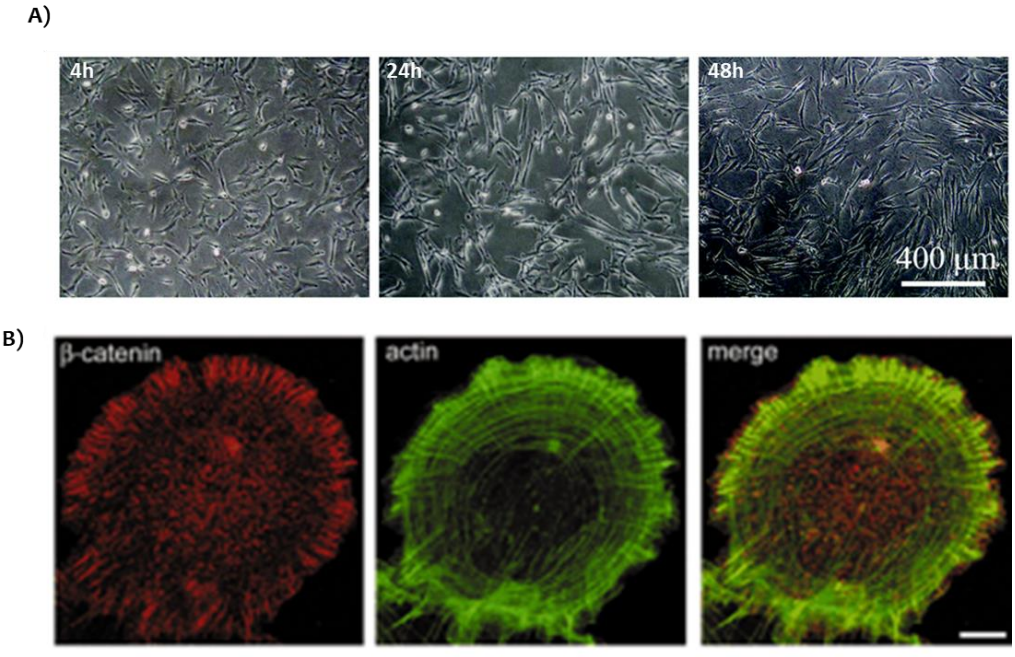

Fig. 1.8 *(A) Phase-contrast images of hUCB-MSCs cultured on PS surfaces modified with E-cadherin for 4, 24 and 48 h, Reproduced with permission from Royal Society*[52] *(B) Cell spreading on N-cadherin modified substrate induces the formation of cadherin adhesions after 2 h, red (β-catenin)*

and green (F-actin), scale bar 10 µm Reproduced with permission from THE COMPANY OF BIOLOGISTS LTD.[53]*.*

Self-assembled monolayers (SAMs) of peptide alkanethiols (ATs) have also used as excellent platforms to explore cell-cell interactions[54–56]. In one study, the Gold (Au) nanopatterns of various sizes (100-800 nm) has functionalized with E-cadherin protein to show the threshold size required for cell adhesion and formation of adherence junction. The Au surfaces have been modified with hydrophobic ATs and then the E-cadherin protein was deposited by sequential addition of neutravidin, biotinylated protein A and E-cadherin respectively. Epithelial cells cultured on homogeneous surfaces adhered and spread with large lamellipodia showing strong interaction with the surface. Cell adhesion on 100 nm patterns was weak, whereas cells cultured on larger pattern sizes show good adhesion, spreading, and defined cortical actin **(Fig. 1.9A)**. This work shows the importance of ligand patch size in cadherin mediated cell-cell contacts[55]. In another study, SNAP-tag immobilization technique has used to functionalize Au surfaces with E-cadherin protein. The Au surfaces was modified with ATs carrying a benzylguanine (BG) head group. The SNAP-tag (fused to the C terminal of E-cadherin) is an enzyme that covalently binds to the benzyl group of benzylguanine (BG) by releasing guanine **(Fig. 1.9B)**. This covalent immobilization method allows proper orientation and density control of ligand on surface. E-cadherin functionalized SAMs efficiently promotes cell spreading and generates single cadherin and cell adhesion forces[54] **(Fig. 1.9C)**.

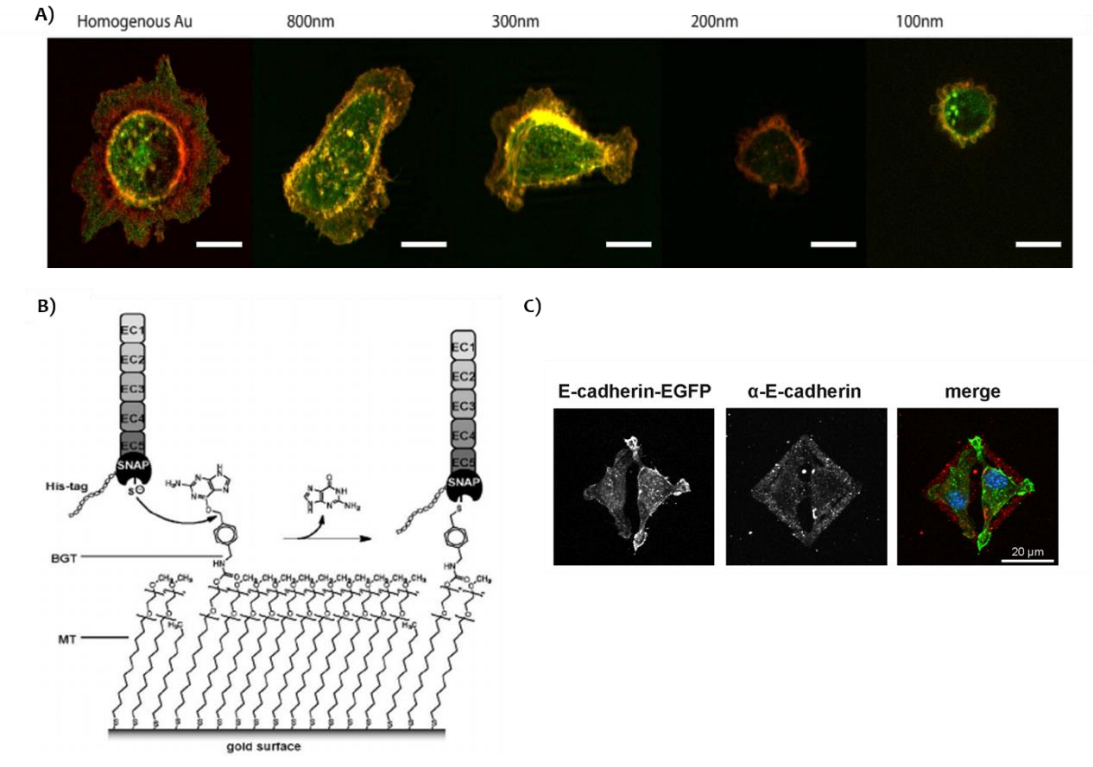

Fig. 1.9 *(A) Fluorescent microscopy images of L-cells, murine fibroblasts which lack endogenous cadherins on E-cadherin functionalized different patch sizes; actin (red) and E-cadherin GFP (green), scale bar 10 µm, Reproduced with permission*[55]*, Copyright 2012, American Chemical Society. (B) Schematic representation of covalent binding of E-cadherin using SNAP-tag. (C) fluorescence image of EcadEGFP/L-cells on E-cadherin functionalized surfaces, Reproduced with permission* [54]*, Copyright 2014, The authors.*

Hydrogels have also been used as 2D interfaces to study cell-cell interactions. The capacity of hydrogels to retain high amounts of water and their soft nature makes them interesting platforms to mimic the cellular interface. Cell adhesion through cadherin proteins responds to mechanical changes in the microenvironment and activate cell signaling pathways as (RhoA, ROCK, YAP/TAZ) and also organize cytoskeleton[57,58]. The response of cell-cell contacts to mechanical parameters of the microenvironment can be studied using biointerfaces, typically hydrogels, with different mechanical properties. p(AAm) is one of the mostly used hydrogel for reconstructing biointerfaces[59]. p(AAm) hydrogels have been functionalized with E/N-cadherin proteins or cadherin peptidomimetics to investigate cadherin mediated cell-cell interactions. N-cadherin expressing myogenic C2 cells cultured on N-cadherin protein coated p(AAm) hydrogels with young's modulus of 95 kPa showed a typical fried egg morphology characterized by a large circular lamellipodium similar to the results observed on glass substrates **(Fig. 1.10A)**. While cells on soft substrates (E = 11 kPa) exhibited less spreading and no lamellipodium extension. Cells on rigid substrates recruited N-cadherin-catenin complexes at the cell substrate interface and the actin cytoskeleton was formed a circular network of filaments surrounding the nucleus. In contrast, recruitment of N-cadherin-catenin complexes and stress fibers were not detected in soft substrates[60] (**Fig. 1.10B)**. In a recent study, E-cadherin protein were covalently linked to a p(AAm) hydrogel surface with a protein surface linker sulfo-SANPAH and explored the rigidity sensing by E-cadherin during cell adhesion. E-cadherin dependent adhesion of MDCK cells on soft p(AAm) hydrogels (E = 1 & 9 kPa) did not promote cell adhesion and spreading **(Fig. 1.10C-D)**. Cells cultured on 30 kPa substrates showed weak attachment with small lamellipodium protrusions, and had very few F-actin bundles. Whereas cells adhered to a 60 kPa p(AAm) hydrogels appeared to have larger spread area and extended lamellipodia-like protrusions[58,60] **(Fig. 1.10E)**. These studies showed that the mechanical properties of the hydrogel (i.e. its Young's modulus) lead to changes in cell morphology, actin organization and membrane dynamics.

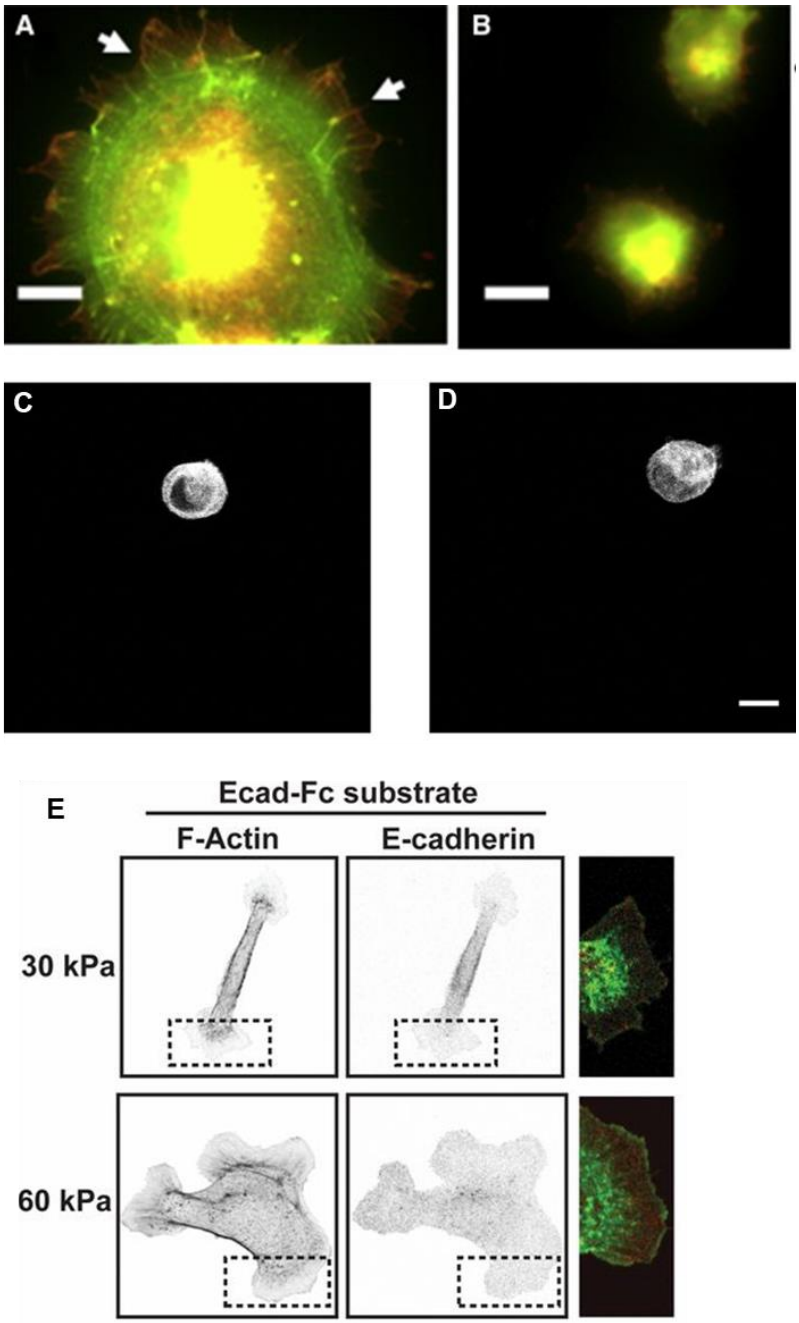

Fig. 1.10 *(A-B) Fluorescent microscopy images of C2 cells on p(AAm) hydrogels coated with N-cadherin with different rigidities E = 95 kPa and E = 10 kPa respectively, β-catenin (red), F-actin (green) scale bars: 10 μm, cadherin adhesions is marked with arrows. Reproduced with permission*[60]*, Copyright, 2010 Biophysical Society. (C-D) MDCK cells cultured on p(AAm) hydrogels coated with E-cadherin with different rigidities E = ~1 kPa and E = 9 kPa respectively, stained with phalloidin. (E) Confocal images of MDCK cells on E-cadherin functionalized substrates of different rigidities E = 95 kPa and E = 10 kPa. The dotted box in each image is combined and enlarged, F-actin(green), E-cadherin: dsRed (red), scale bar, 10* μm*. Reproduced with permission*[58]*, Copyright 2017, NATIONAL ACADEMY OF SCIENCES.*

To more closely mimic native cellular environments, cellular response in 3D biointerfaces has been developed recently. Cell-cell interactions in 3D culture have also been explored using hydrogels. In this case, cells were embedded in the hydrogel matrix modified with N-cadherin ligands and studied the importance of N-cadherin in regulating chrondrogenesis and cartilage matrix deposition using encapsulated mesenchymal stem cells (hMSCs)[61]. When MSCs were encapsulated in methacrylated hyaluronic acid (HA) hydrogels functionalized with N-cadherin mimetic peptides, promoted early chondrogenesis of MSCs and cartilage-specific matrix production[61] (**Fig. 1.11**). Later the same system has been used to show the role of N-cadherin specific interaction in osteogenesis from hMSCs[62].

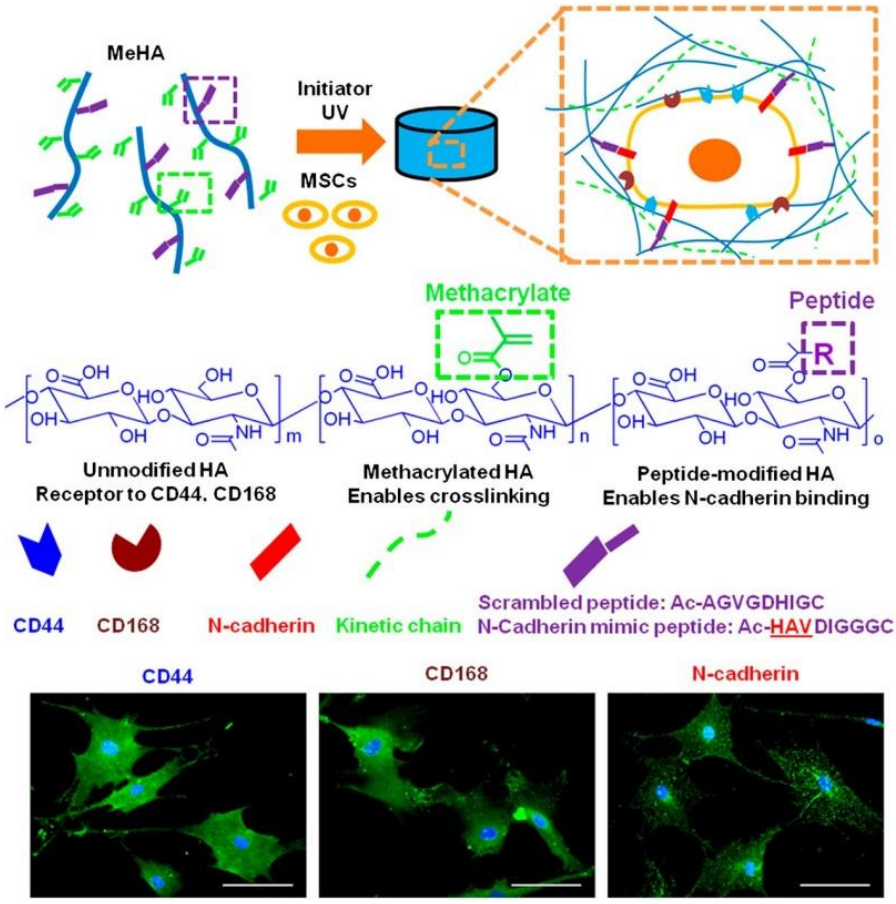

Fig. 1.11 *Fluorescence images of hMSCs encapsulated on methacrylated hyaluronic acid hydrogel modified with N-cadherin ligands; CD44, CD168, N-cadherin (green) and nuclei (blue), Reproduced with permission [61], Copyright (2013), National Academy of Sciences.*

1.6 Dynamic biointerfaces

Cell-cell interactions in tissues are highly dynamic, and their changes are spatially and temporally regulated during embryogenesis or regenerative processes[63,64]. Dysregulation of such interactions occurs in pathological cases, like tumor progression and metastasis[65,66].The ability to control cell-cell interactions dynamically and spatiotemporally is a key to understand and regulate cell-cell interactions mediated biological process. In order to study cell-cell interactions at model biointerfaces, tools to regulate the presence and concentration of adhesive ligands at the material surface with spatial and temporal control would be of great help.

Light-based strategies to regulate the interactions of cells at interfaces are particularly attractive from an experimental point of view. Light is fully orthogonal to most cellular components and can be controlled precisely in location and time. Two main strategies have been used for the photochemical regulation of cell adhesive ligands on materials surface. (i) The use of reversible light-sensitive molecules, such as spiropyran or diazobenzene. These molecules are attached to the adhesive ligand and undergo conformational changes upon irradiation with UV or visible light that change the orientation and exposure of the ligand at the surface reversibly[67]. (ii) The use of photolabile protecting groups (PPG) linked to the adhesive ligand of interest at the respective binding position to the CAM. The PPG deactivates the biological function temporally. The biological activity can be restored upon illumination with light, which cleaves the PPG from the molecule and activates the binding of complementary receptor. The photoactivation in this case is irreversible. This strategy has rendered the highest selectivity and contrast in the control of cellular processes, and will be elaborated in this section and applied further in this thesis.

The first example of a photoregulated biointerface for the control of cell adhesion was reported in 2008[68,69]. In this case the widely use peptidomimetic cyclo[RGDfK] was used as cell-adhesive peptide to target integrins. The cyclo[RGDfK] was modified with DMNPB photolabile protecting group at the side chain COOH group of the Asp. This modification inhibited binding of integrins. Substrates functionalized with cyclo[RGD(DMNPB)fK] peptide did not support cell adhesion. However, after the removal of DMNPB group from the peptide by activating the hydrogel with 350 nm light, the bioactivity was restored. cyclo[RGD(DMNPB)fK] peptide modified surface was used to control migration of human umbilical vein endothelial cells (HUVECs) using photopatterning approach and was compared with a wound healing

assay[70](**Fig. 1.12A)**. More recently, a different photoactivatable RGD variant attached with a two-photon photolabile protecting group, PMNB allowed control of adhesion, migration and angiogenic morphogenesis of endothelial cells encapsulated in a hydrogel[71]. cyclo[RGD(PMNB)fC] peptide modified PEG hydrogel was used to demonstrate the adhesion and angiogenic morphogenesis of endothelial cells in a spatially and temporally controlled manner[71](**Fig. 1.12B)**. A similar approach was applied to the cell adhesive peptide YAVTGRGDSPAS. Modification of the amide bond between the Gly and Arg residues with an o-nitrobenzyl group inactivated the biological activity of peptide. This peptide was used to phototrigger the attachment of HeLa cells[69,72].

Photo-activatable variants of laminin mimetic peptides have also been demonstrated to promote integrin-mediated adhesion of neuronal cells and were used to direct axonal growth on synthetic biomaterials[73]. In this case the laminin mimetic peptide IKVAV was modified with a HANBP on the Lys residue[74]. Longer peptidomimetics, CASIKVAVSADR were also derivatized with DMNPB and HANBP PPGs at the amine terminal group of Lys and resulted in spatiotemporal regulation of neuronal cell attachment and differentiation using light[73] (**Fig. 1.12C&D**).

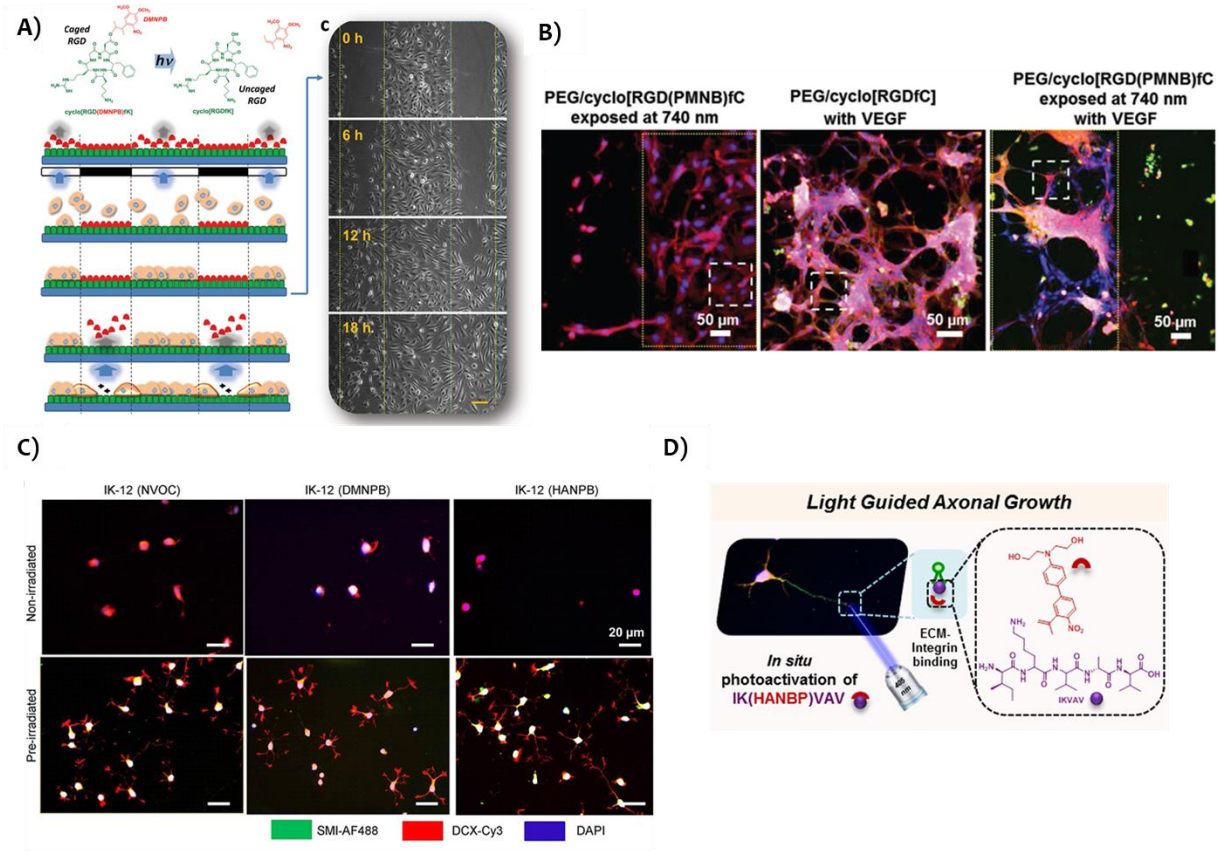

Fig. 1.12 *Light controlled cellular attachment and spatiotemporal activation of biological process on biomaterial substrates;(A) Photo-activatable cell migration assay; Migration of HUVECs on a cyclo[RGDfK] patterned SAMs, Reproduced with permission[70], Copyright 2013, John Wiley and Sons (B) PEG Gels functionalized with cyclo[RGD(PMNB)fC]/VEGF and containing HUVEC formed interconnected microvascular network within the exposed regions in 3d, Reproduced with permission[71], Copyright 2018, John Wiley and Sons (C) Morphology of neural progenitor cells cultured on non-irradiated and pre-irradiated hydrogels functionalized with light responsive IKVAV peptides, Reproduced with permission[73], Copyright 2018, John Wiley and Sons (D) Site-selective guidance of neurites extension on photoactivated hydrogel surface. Reproduced with permission[74], Copyright 2018, American Chemical Society .*

It is important to note that in these approaches for photocontrol, photoresponsive peptidomimetics and not whole proteins were used for binding to the cellular receptors. Peptidomimetics are short peptides, easier to synthesize and manipulate than the native proteins, and which retain part of the biological function of a the natural protein[75]. They are commonly used as protein substitutes in biomaterial science because of their higher stability,

synthetic feasibility, defined structure and lower synthetic effort. On the PPG side, a variety of groups are available, including o-nitro aryl groups, aryl carbonylmethyl, coumarin derivatives or metal coordination complexes[76]. These PPGs can be activated over a broad spectrum of wavelengths (220-890 nm). The most commonly used PPGs are nitrobenzyl compounds, and their dimethoxy derivatives (nitroveratryl)[76], since precursors are commercially available.

1.7 2.5D Biointerfaces to mimic natural polarized microenvironments

Cells in their natural microenvironment establish cell-cell and cell-matrix adhesion complexes. These complexes are typically formed in spatially different interfaces, but are mechanically connected intracellularly through the cellular cytoskeleton. Hydrogels presenting mixed matrix and cell adhesive molecules have been used to study cooperative effects and derived responses of cells to changes in cell-cell and cell-matrix adhesions[57,60,61]. However, such systems fail to represent the spatial and mechanical differentiation of cell-matrix and cell-cell interfaces in natural tissues. This is particularly relevant for polarized tissues like epithelium, endothelium, nerve or muscle tissue, where the spatial localization of receptors and differential mechanics at cell-matrix and cell-cell interfaces are crucial signals for cellular differentiation, tissue formation and functional performance[77–79]. This scenario cannot be represented in homogeneously coated substrates with adhesive proteins.

Initial attempts to mimic the polarized distribution of adhesive receptors in 2D epithelial cultures have made use of micropatterned substrates on glass with stripes of matrix and cell-cell adhesive ligands[47,62,80,81] (**Fig. 1.13A&B**). A more advanced experimental approach used hydrogels with micropatterned squares of matrix proteins to confine cell doublets that formed a basal cell-matrix interface with the substrate and a cell-cell interface in the lateral plane[82]. The results indicated that spatial distribution of cell-cell and cell-ECM interactions control the force balance in multicellular epithelial interactions, highlighting the need for alternative experimental cell culture approaches to study such processes[82]. Two recently reported experimental designs have progressed in mimicking a 2.5D organization of cell-cell and cell-ECM contacts. Viasnoff *et al.* used a 9-steps microfabrication process to obtain arrays of 30 x 30 x 30 µm wells with a PDMS bottom coated with ECM proteins, and acrylate walls homogeneously coated with Ecadh-Fc[83]. Hepatocyte doubles cultured within the wells formed a lumen depending on the spatial localization of ECM-adhesion and cell–cell-adhesions. Nelson

et al. presented a simple 2.5D microenvironment for a biomimetic cell-cell junction comprised of 3D silicon vertical walls (barriers) modified with E-cadherin protein attached to a surface coated with matrix protein (fibronectin)[84]. Epithelial cells formed stable cadherin-cadherin junction with the functionalized wall and formed apical-basal polarity guided by the spatial distribution of E-cadherin. These two examples represent a step forward to incorporate mechanical factors in polarized synthetic microenvironments[85](**Fig. 1.13C&D**). However, the mechanical properties of the interfaces offered to the cell have little to do with the mechanical properties of the natural interfaces. Moreover, these systems do not allow differential or variable mechanical cues in the basolateral and lateral planes.

In del Campo's Lab, a 2.5D biomaterial microenvironment that allows presentation of different and independent biochemical and mechanical signals to cells on the basal and lateral directions has been recently developed and is presented in Chapter 3. This platform allows independent modulation of the properties of cell-matrix and cell-cell-like interfaces in a polarized environment. The system is based on polyacrylamide hydrogels and can be adapted within a wide range of stiffness (1-750 kPa), adhesive ligands and geometries. This system will be used in this thesis (Chapter 5).

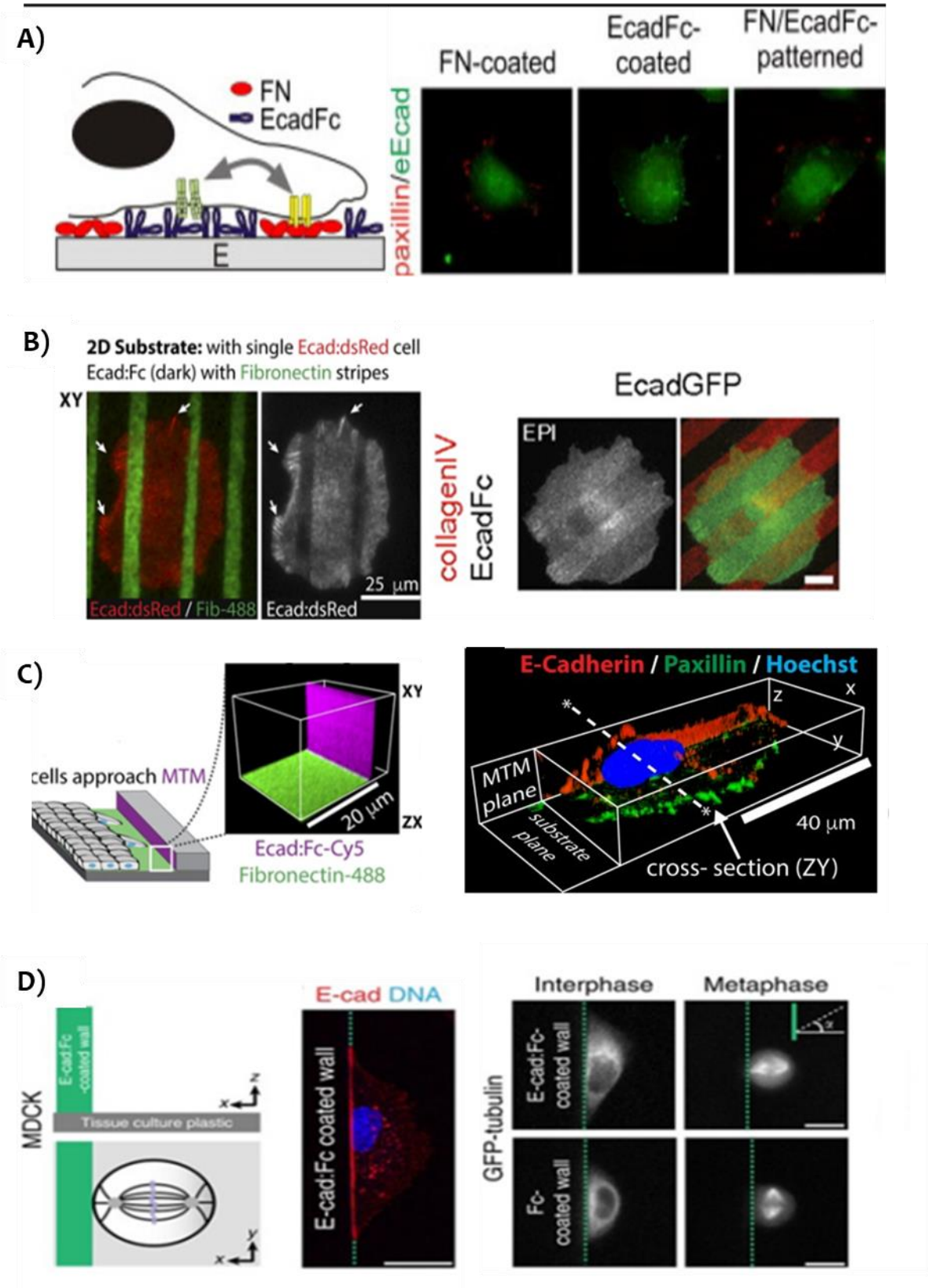

Fig. 1.13 *Biointerfaces functionalized with extra cellular domain of E-cadherin protein and fibronectin (A) Integrin-cadherin cross talk on dual-component surfaces present spatially separated regions of E-cadherin and fibronectin proteins*[86] *(B) Cell adhesion on a dual E-cadherin/ECM copatterned 2D substrates; Ecad-dsRed expressing MDCK cells on*

Fibronectin:EcadFc [84]*& EcadGFP-expressing MDCK cells on collagenIV:EcadFc surfaces*[80] *(C) Hybrid junctions between cells and the E-cadherin coated side wall, confocal image of single cell junctioning to the E-cadherin functionalized PDMS wall*[84] *(D) Schematic representation of E-cadherin coated vertical silicone sidewall and uncoated bottom surface; Localization of E-cadherin in MDCK cells between the sidewall and cell junction and expression of mitotic spindle angle relative to the sidewall*[87]*.*

Chapter 2

Synthesis of photo-activatable cadherin mimetic peptides

In this chapter, photoactivatable variants of cadherin mimetic peptides based on the HAV sequence are presented. For this purpose, the photolabile protecting group $[Ru(bpy)_2PPh_3]^{2+}$ is used to form a complex with the imidazole side chain of the histidine residue. The presence of the photolabile protecting group temporally prevents the recognition of the peptide by cadherin proteins. The activity of the peptide can be restored upon irradiation with light of appropriate wavelength and intensity. The synthesis and characterization of physicochemical properties of the photoactivatable peptides are described.

2.1 Introduction

2.1.1 Peptidomimetics of classical cadherin proteins

Protein mimetic peptides (peptidomimetics) are short peptides that imitate part of the function of a natural peptide or protein and retain the ability to interact with the biological target and produce the same (or part) of its biological effect[75]. They are often used as matrix protein substitutes in biomaterial science because of their higher stability, synthetic feasibility, defined structure, solubility and lower synthetic effort.

Cadherin peptidomimetics mimic the cadherin-cadherin binding domain[88]. The most explored cadherin peptidomimetics contain the evolutionary conserved sequence His-Ala-Val (HAV)[88]. Selectivity for the different cadherin types is provided extending this sequence with flanking amino acids, which vary between the different cadherins types[88]. The interactions of the flanking amino acids at the binding site contribute to the binding energy[89].

2.1.1.1 E-cadherin peptidomimetic sequences

E-cadherin peptidomimetics have been explored as antagonists to block E-cadherin biological functions. For example, addition of E-cadherin peptidomimetics in solution increased paracellular porosity[90,91], modulated blood brain barrier permeability[92,93] and inhibited E-cadherin mediated cell-cell adhesion of MDCK and Caco-2 cells[88]. Sequences from the ´groove´ region consisting of a conserved HAV peptide sequences (Ac-LFSHAVSSNG-NH_2 and Ac-SHAVSS-NH_2) and `bulge´ region containing an ADT sequences (Ac-QGADTPPVGV-NH_2 and Ac-ADTPPV-NH_2) of ECD1 have been reported to mimic E-cadherin activity[91] (**Fig. 2.1)**. The SHAVSS sequence with flanking Ser has also been proven to bind to E-cadherin specifically. Exchanging the hydrophilic Ser with a hydrophobic residue diminished the capacity of the peptide to modulate cadherin-cadherin interaction[90]. Another important site for E-cadherin- E-cadherin interactions is situated in the bulge region of the ECD1 of E-cadherin, which has an ADTPPV sequence[91]. This sequence appears to recognize the SHAVSS sequence situated in another E-cadherin molecule[91]. Both synthetic linear and cyclic versions of these peptide sequences have been studied in detail[90–95].

The synthetic linear decapeptides Ac-LFSHAVSSNG-NH_2 (HAV-10), Ac-QGADTPPVGV-NH_2 (ADT10) and the hexapeptides Ac-SHAVSS-NH_2 (HAV-6) and Ac-ADTPPV-NH_2 have been shown to inhibit cadherin mediated cell-cell interactions, lead to the opening of paracellular junctions[91,96]. They have been used to enhance paracellular penetration of peptides and proteins[91,96]. Compared to decapeptides, the short hexapeptides have demonstrated a stronger inhibitory effect in the intercellular junctions. The hexapeptides are smaller and might penetrate the tight junctions more easily to bind E-cadherin and disturb cadherin homophilic interactions[96]. Cyclic peptides, Ac-CHAVC-NH_2 (cHAVc3) and Ac-CADTPPV-NH_2 (ADTC5) have shown to modify the blood brain barrier to improve the delivery of diagnostic and therapeutic agents to the brain[92]. This has been shown using an *in situ* brain perfusion model[93]. Recently, it has been reported that Au surface immobilized with synthetic linear LYSHAVSSNG-$(PEG5)_2$-CCC peptide regulates the adhesion and clustering of epithelial cells[51].

Along with theses sequences, the linear peptide H-SWELYYPLRANL-NH_2 has also been identified as E-cadherin antagonist[97]. This peptide derives from the N-terminal sequence of cadherin protein and harbors a Trp residue (W) in the second position[98]. The biological function of this peptide remains to be investigated in detail.

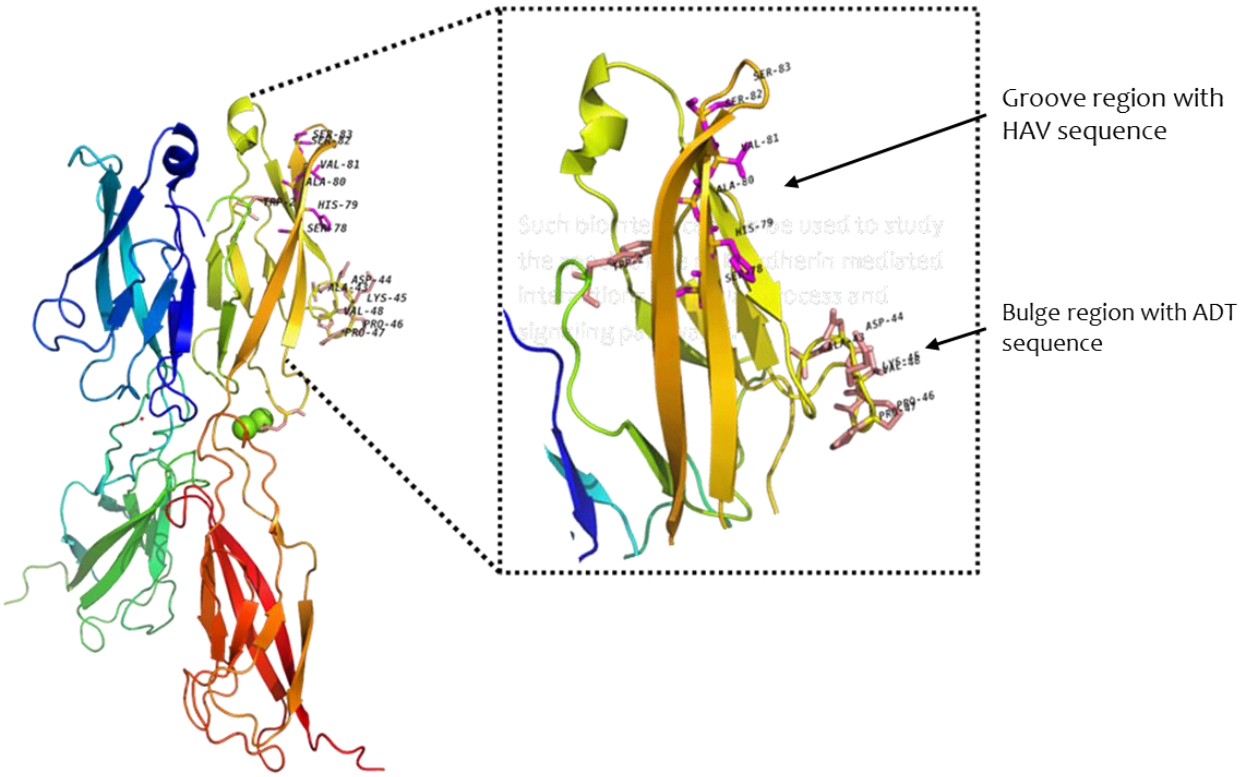

Fig. 2.1 *Crystal structure of E-cadherin dimer protein: Relevant amino acids in the groove (SHAVSS) and bulge binding (ADTPP) region are highlighted*[99] *(PDB code: 1FF5).*

2.1.1.2 N-cadherin peptidomimetic sequences

A few types of N-cadherin peptidomimetics were reported from the binding site of ECD1[100]. Three types of N-cadherin mimetic peptides based on the HAV sequence have been reported to have an antagonist function when used in solution: synthetic linear peptides, synthetic cyclic peptides and non-peptidyl peptidomimetics[100]. Flanking Asp and Ile amino acids in the sequence HAVDI determine N-cadherin specificity. The Asp and Ile contribute to the adhesion interface, with Ile elucidate 7.45% of the interface area[43]. The first peptides shown to be able to bind to extracellular domain of N-cadherin were linear peptides comprising the HAV motif[89]. The Ac-LRAHAVDING-NH2 decapeptide and INPISGQ present in the EC1 of human N-cadherin are able to block neurite out growth[101], myoblast fusion[102], and Schwann cell migration on astrocytes[103]. It was subsequently shown that synthetic cyclic peptides with the HAV motif act as N-cadherin antagonists[43]. The cyclic peptide, N-Ac-CHAVDIC-NH2 is able to disrupt a broad range of functions mediated by N-cadherin in solution[43]. However, a dimeric version of HAVDI motif (N-Ac-CHAVDINGHAVDIC-NH2) promotes neurite outgrowth from cultured cerebellar neurons[104]. Non-peptidyl peptidomimetics of N-cadherin have likewise been distinguished[105].

Recently, another class of N-cadherin antagonist has been identified and this linear peptide with a Trp residue at the second position from the N-terminal of the sequence (analogous to N-cadherin). Peptide, H-SWTLYTPSGQSK-NH2 inhibits the in vitro formation of endothelial cell tubes showing antiangiogenic characteristics[98]. The biological function of this peptidomimetics remains to be studied in depth.

The agonist activity of N-cadherin mimetic peptides when attached to biomaterials has been recently explored. It has been shown that incorporation of HAVDIGGGC peptide onto a methacrylate hyaluronic acid (MeHA) backbone mimics cadherin-cadherin binding and support early chondrogenesis of MSCs and cartilage-specific matrix production with culture[61]. Later HAVDI peptides were functionalized on hyaluronic acid (HA) hydrogels to impersonate the pro-osteogenic specialty in the endosteal space to advance the osteogenesis of hMSCs[62]. HAVDIGGGC peptide on the surface provides a binding pocket for W2 from the ECD1 of the N-cadherin protein on cell surface and which promotes cadherin mediated cell-cell adhesion. The previous studies on HADI peptides concludes that it is a potential candidate to mimic N-cadherin protein and promotes biological functions like neurite out growth[104], chondrogenesis[61] and osteogenesis of hMSCs[62].

2.1.2 Ru(II) polypyridyl complexes as photoremovable protecting groups of amines

Photoremovable protecting groups (PPGs) are a class of protecting groups typically used to temporally inhibit chemical or biological functionality of molecules. These groups are stably attached to the active site of the molecule, and can be removed by light exposure. PPGs are frequently used in biology and pharmacology studies to regulate the activity of bioefectors and drugs within the cell milieu. PPGs have to fulfill several conditions to be used for biological applications: (i) The PPG should present strong absorption at wavelengths >300 nm, where biological molecules show lower absorbance. (ii) The photolytic reaction should be clean and happen at high photolytic yield. (iii) PPGs must have good hydrolytic and enzymatic stability preceding and during photolysis. (iv) The photolysis byproducts must be biocompatible and inert at the irradiation wavelength. (v) PPGs should be inert towards biological system. (v) They should be affordable and feasible from a chemical synthesis point of view[76].

Ruthenium (II) complexes with polypyridyl-based ligands, $[Ru(ppy)_2L_2]^{2+}$, are interesting photoremovable groups to protect primary and secondary amines and nitriles, as well as

aromatic heterocycles[106] **(Fig. 2.2).** A broad range of bioactive molecules have been made photoactivatable with this chemistry, including neurotransmitters, enzyme inhibitors and peptides[107]. For example, γ-aminobutyric acid (GABA)[108,109], nicotine[110], the anti-tuberculosis compound isoniazid (INH), and metyrapone, a potent CYP11B1 inhibitor[111] have been protected with reported with bis-bipiridyl (bpy) ruthenium (II) complexes. The cytotoxic agent, 5-Cyanouracil (5-CNU) shown to inhibit pyrimidine catabolism *in vivo*, has also been derivatized with terpyridine (tpy) Ruthenium (II) complexes $[Ru(tpy)_3]$[112]. A Ru(II)tris(2-pyridylmethyl)amine complex functionalized with a nitrile group (Cbz-Leu-$NHCH_2CN$) containing two molecules of cathepsin K inhibitors was also developed[116]. The tripeptide Arg-Gly-His (RGH), containing $[Ru(bpy)_2]^{2+}$ complex at the His was used for controlling Ni(II)-dependent nuclease activity *in vitro*[113]. N-acetyl-methionine and biotin molecules were also protected with [Ru(tpy)(bpy)] complex[107]. Lately, [Ru(tpy)(biq)] (biq = 2,20-biquinoline) protected cytotoxic nicotinamide phosphoribosyl transferase (NAMPT) inhibitor was used for a photoactivated enzyme inhibition in hypoxic cancer cells[107].

In the octahedral $[Ru(bpy)_2L_2]^{2+}$ complexes, the biomolecule to be released occupies at least one of the coordination sites. The photorelease of biomolecule is optimized by modifying the characteristics of remaining five ligands. Two coordination positions are occupied by a planar dentate ligand, e.g. substituted 2,2-bipyridine or 1,10-phenanthroline which promotes metal to ligand charge transfer (MLCT). The $[Ru(bpy)_2]^{2+}$ is often selected because of its easily available starting material $[Ru(bpy)_2Cl_2]$. The physical and chemical properties of the phototrigger can be adjusted using the ligand at the fifth coordination site[114].

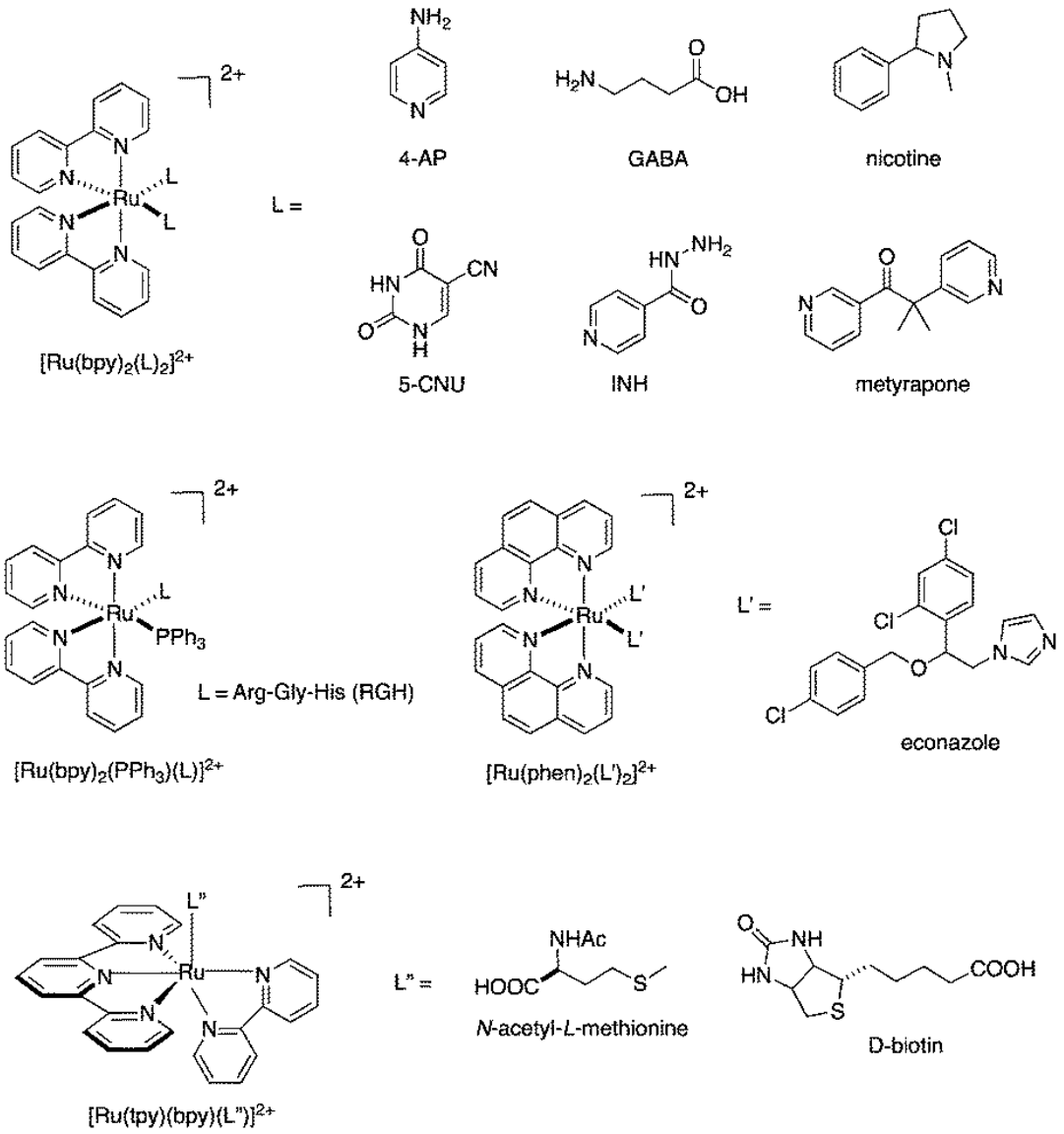

***Fig.* 2.2** *Chemical structures of Ru(II)-based PPGs and Ru(II) complex linked biomolecules*[107]*.*

Ru (II) complexes in aqueous condition are thermally stable. Ligand dissociation in Ru (II) complexes are obtained by the thermal population of ^{3}dd sates from a triplet metal to ligand charge transfer (^{3}MLCT) state upon light irradiation[107]**(Fig. 2.3).** The mechanism of photolysis reaction involves excitation of the complex's MLCT band leading to heterolytic cleavage of one of the ligands with a quantum efficiency of around 0.21, which is high compared to other photolytic reactions involved in PPG chemistry. Basicity of the ligand plays a key role in the quantum efficiency of photo cleavage. A lower basicity of the ligand shifts the MLCT band to higher energies, which promotes an easier occupation of the dissociative d-d sate. Phosphine ligands are usually non-photo cleavable and therefore, during the photocleavage of $[Ru(bpy)_2PPh_3L_2]^{2+}$ complexes where L=amine, the amine ligand is released[115–117].

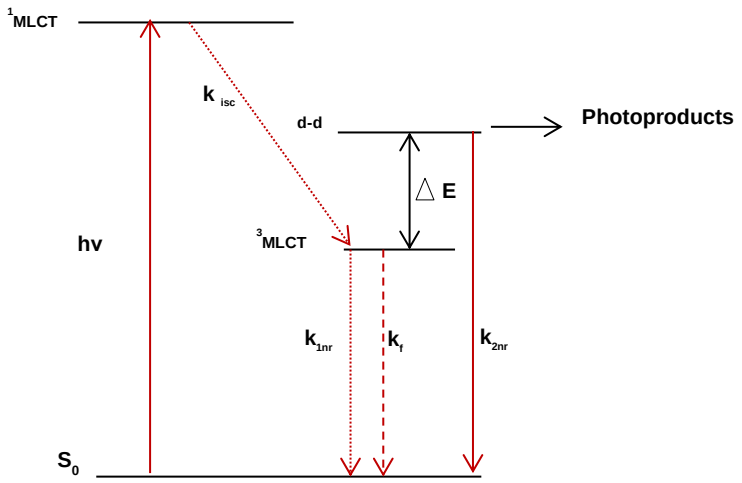

Fig. 2.3 *Simplified energy diagram of photochemical pathways in Ru(II) complex linked biomolecules. Photoproducts are released from the nonbonding d–d state*[110]*.*

Metal coordination complexes have several advantages to be used as photoremovable protecting groups. Metal complexes regularly shows absorption in the visible range due to a strong charge transfer as well as the bond energy of metal-ligand is much less than an organic σ- bond. Therefore, metal complexes based photoprotection enables the photo-release of biomolecules easy with light irradiation at higher wavelengths[107]. By controlling auxiliary ligands, photochemistry can be adjusted to achieve the release biomolecules over a wide spectral range from visible to near infrared wavelengths. Metal complexes are therefore useful chemical agents in biological studies. In this chapter, the $[Ru(bpy)_2PPh_3]^{2+}$ group will be used to protect the imidazole heteroaromatic ring of histidine.

2.2 Results and Discussion

2.2.1 Molecular design of photo-activatable N- and E-cadherin peptides

The literature search **(section 2.1.1.2)** lead to the peptide HAVDIGGGC as potentially suitable N-cadherin mimetic peptide. This sequence has been shown to have an agonist function for N-cadherins at cell membranes when attached to a biomaterial[57,61,118]. The HAVDIGGGC peptide contains the HAV tripeptide flanked by an Asp and an Ile residue at the N terminal, which account for the specificity to N-cadherin protein. The Cys residue at the C-terminus is introduced for covalent immobilization to thiol-binding surfaces. The three Gly residues are a flexible spacer between the active domain and the anchoring site that provide mobility and effective presentation of the peptide at the materials surface for cell binding. A

negative control peptide was also designed by shuffling the active HAVDI sequence between Gly residues, resulting in the AGVGDHIGC scrambled sequence. The two selected peptides are summarized in Table 2.1.

The selection of the E-cadherin mimetic peptide for this study was less straightforward. Four different sequences were found in the literature to act as antagonists for E-cadherin when added to the culture medium **(Section 2.1.1.1)**, but no results were found where the peptidomimetics were immobilized to biomaterials and used to interact with E-cadherin at the cell membrane. The sequence SHAVSSC containing the HAV tripeptide was selected due to its analogy to the N-cadherin mimetic peptide and the possibility to use a similar strategy for protection with a photoremovable group. In this sequence the HAV is flanked by three Ser residues which make this sequence specific for E-cadherin[89,96]. A Cys is also introduced as anchoring site for reaction with biomaterials. A variant with the tripeptide spacer GGG was also used. Two other E-cadherin peptidomimetics **(Table 2.1)** were also used for cell studies **(Chapter 4),** but no photoactivatable peptides were synthesized.

Table 2.1 *Sequences of E & N-cadherin mimetic peptides used in this thesis.*

	Peptide Sequence	
N-cadherin	Mimetic peptide	*****Ac-HAVDIGGGC[61]
	Scrambled peptide	Ac-AGVGDHIGC[61]
E-cadherin	Mimetic peptides	*****Ac-SHAVSSC[96] Ac-SHAVSSGGGC Ac-SHAVSSGGGK Ac-ADTPPVGGGK[96] Ac-SWELYYPLRANLGGGK[97]
	Scrambled peptides	Ac-HSVSASC[96] Ac-SGASGVGHSC Ac-SGASGVGHSK

***** Peptides have been selected for the synthesis of photoactivatable peptides.

In order to make photoactivatable variants of the cadherin peptidomimetics, a suitable position for the incorporation of a photolabile protecting group has to be selected. The selection of photo-activatable site depends on different parameters: (i) the particular

interactions at the binding complex between the extracellular domain 1 of cadherin and the peptide, (ii) the chemical reactivity of the side groups of the peptide sequence and therefore accessibility for introduction of a photolabile group; and (iii) the position of the amino acid in the sequence which can play a determinant role for the synthetic pathway. In the HAVDI sequence the Ala, Val and Ile amino acids do not allow any modifications since their side groups are aliphatic chains. Only the -COOH side group of the Asp and the imidazole group of the His residues can be reacted with a photocleavable protecting group. Since His is part of the generic HAV binding domain, common for all cadherins, and Asp only contributes to specificity for the N-cadherin peptidomimetic, the imidazole ring of the His residue was selected as protection site. Moreover, the His unit is the last one to be coupled during SPPS of the peptide, and this reduces the risk of hydrolysis of the photolabile protecting group during SPPS deprotection and coupling cycles.

The options to attach a PPG to Histidine are limited because of the low reactivity of the heterocyclic aromatic amine. Recently, bis-bipyridyl ruthenium complexes $[Ru(bpy)_2]^{2+}$ were explored as photolabile protecting groups for His[113]. Histidine was introduced as one ligand of the $[Ru(bpy)_2PPh_3]^{2+}$ and was cleaved at 455 nm with an uncaging quantum yield of $\Phi_{unc} \approx 0.06$[113]. The Ac-His$[Ru(bpy)_2PPh_3]^{2+}$)-OH complex was obtained in 4 steps with good yields. With these premises, the $[Ru(bpy)_2PPh_3]^{2+}$ complex was selected as suitable photolabile protecting group for the His unit in HAV in the cadherin-mimetic peptides for this work.

2.2.2 Synthesis of photoactivatable Histidine

The Ac-His($[Ru(bpy)_2PPh_3]^{2+}$)-OH complex was synthesized in four steps following a reported protocol **(Scheme 2.1)**[113]. Boc-His($[Ru(bpy)_2PPh_3]^{2+}$)-OH was synthesized from a *Cis*-bis(2,2'-bipyridine)dichloro ruthenium(II) complex, $[Ru(bpy)_2Cl_2]$. In a one pot reaction, firstly $[Ru(bpy)_2Cl_2]$ was reacted with triphenylphosphine (PPh_3) and then the intermediate was treated with Boc-His-OH. The Boc protected alpha amine in His (Boc-His-OH) was used as a reactant to facilitate selective substitution at the imidazole side chain. The substitution of the Cl^- ligands in the complex occurs based on the field strength of the particular ligand, which follows the order Cl^- < bpy (2,2'-bipyridine) < PPh3 according to the s*pectrochemical series*. The Cl^- ligand is substituted by PPh3 and Histidine ligands with higher field strength. In a second step, the Boc protecting group was removed from the complex in 50% TFA: DCM mixture, followed by acetylation of the amine group and precipitation with KPF_6. The residue was purified by reverse phase chromatography to afford the Ac-His($[Ru(bpy)_2PPh_3]^{2+}$)-OH building

block. The pure product was obtained as orange powder with 95% purity after HPLC purification. The final complex was obtained in 0.200 g scale and with 81% yield.

The chemical identification of the products and intermediate complexes was done by ESI-MS and ^{1}H-NMR. The formation of the intermediate complex **(1)** was confirmed by the signal corresponding to $[M-H]^+$ at 711.00 Da. The ^{1}H NMR of (**2**) showed a pair of doublets at 1.05 & 1.27 ppm corresponding to the *tert*-Butyl protons, which confirmed the insertion of Boc-His-OH into the complex. The deprotection of complex (**2**) resulted in the disappearance of the *tert*-Butyl singlet**.** The acetylation of (**3**) was confirmed by the appearance of a doublet at 1.58 ppm corresponding to three protons of acetyl CH_3 group. Each step of the synthesis was monitored by a shift in the analytical HPLC chromatogram (see experimental section). The ESI-MS of **4** showed $[M-H]^+$ peak at 872.00 Da. The unusual splitting of tert-butyl and acetyl protos were observed due to the formation different isomers of Ru Octahedral complex with chiral amino acid. Detailed analysis of chirality at octahedral centre is not explored in this these. The final complex **4** was soluble in PBS (pH 7.4) at a concentration of 1 mg/mL.

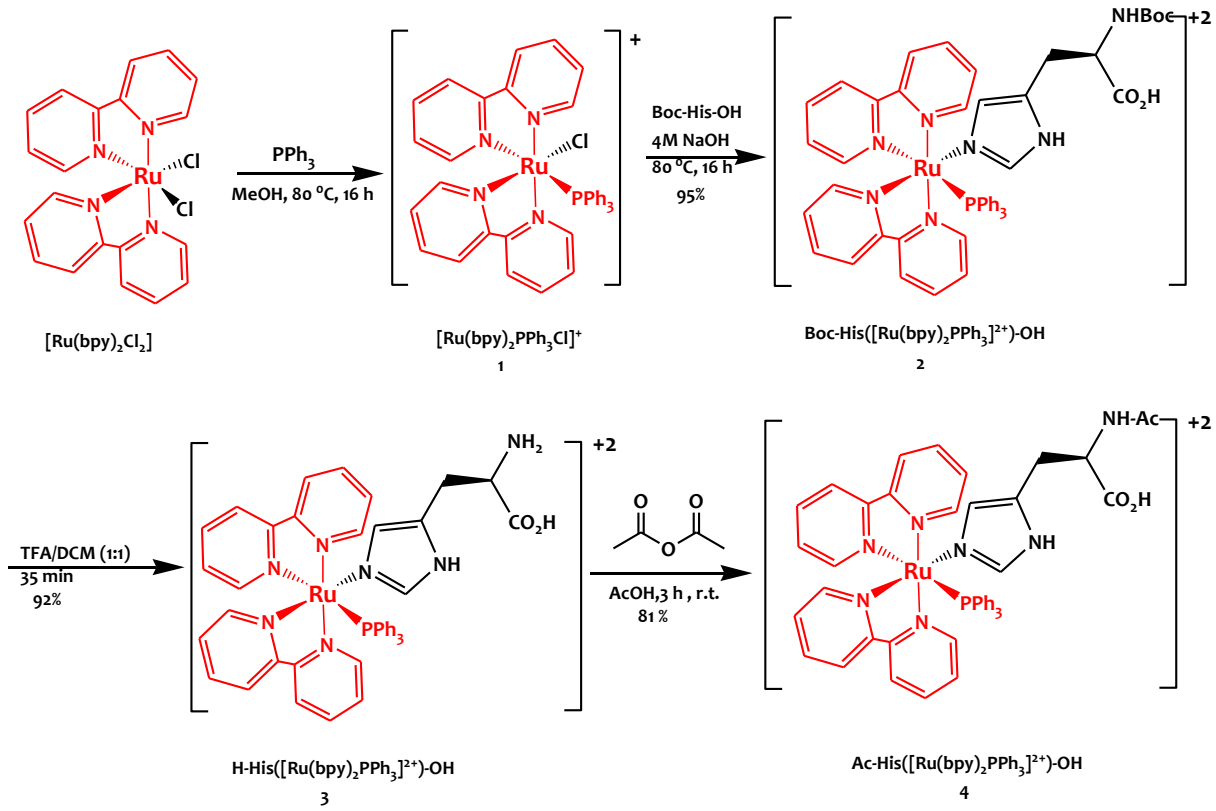

Scheme 2.1 *Synthesis of Ac-His($[Ru(bpy)_2PPh_3]^{2+}$)-OH (**4**)*

2.2.3 Synthesis of N-cadherin peptidomimetics

The N-cadherin mimetic peptide, HAVDIGGGC was synthesized by following standard protocol for Fmoc based solid-phase peptide synthesis (SPPS). The amino acids were sequentially coupled to a resin in a repeated manner during SPPS. The acid sensitive trityl-linker (CT) resin loaded with Cys(Trt)-OH was used for the synthesis. The HAVDIGGGC sequence was developed from C- to N- direction by successive steps of coupling of the Fmoc-protected amino acid with HBTU and HOBt as coupling agents, followed by Fmoc-deprotection under basic conditions (20% piperidine in DMF) **(Scheme 2.2)**. To avoid interference of the side groups of Asp, Cys and His amino acids with the Fmoc-based synthesis of the peptide, the carboxylic, thiol and imidazole side groups had to be protected. Acid-labile protecting groups were selected since these are stable towards the basic conditions needed for Fmoc-deprotection. *Tert*-butyl protecting group was used for COOH and the Trityl group was used to protect the SH and imidazole groups. Each coupling step was monitored by analytical HPLC and ESI-MS analysis. At the optimized conditions (amino acid (2 eq.), HBTU (2 eq.), HOBt (2 eq.), and DIEA (5.6 eq.) in DMF for 2 h at r.t.), coupling steps proceeded with >95% conversion. The peptide was cleaved from the resin with side chain protecting groups using acidic conditions (acetic acid, 2,2,2-triflouroethanol and DCM (3:1:6 v/v/v)) and the deprotection of the side chain protecting groups was performed using TFA, TIS, and H2O (95:2.5:2.5 v/v/v). The final peptide was obtained as white power after the lyophilization of collected pure fractions from preparative RP-HPLC and characterized by ESI-MS. The HAVDIGGGC peptide was obtained in 60% yield with >98% purity at 10 mg scale starting from 100 mg resin with a loading capacity of 0.039 mmol/100 mg. The scrambled peptide AGVGDHIGC was synthesized following a similar strategy. The final scrambled peptide AGVGDHIGC was obtained as white power after the lyophilization of collected fractions from preparative RP-HPLC and characterized by ESI-MS. The scrambled peptide AGVGDHIGC was obtained in 58% yield with >98% purity at 10 mg scale starting from 100 mg resin with a loading capacity of 0.039 mmol/100 mg. The peptides were soluble in PBS (pH 7.4) at a 1 mg/mL concentration.

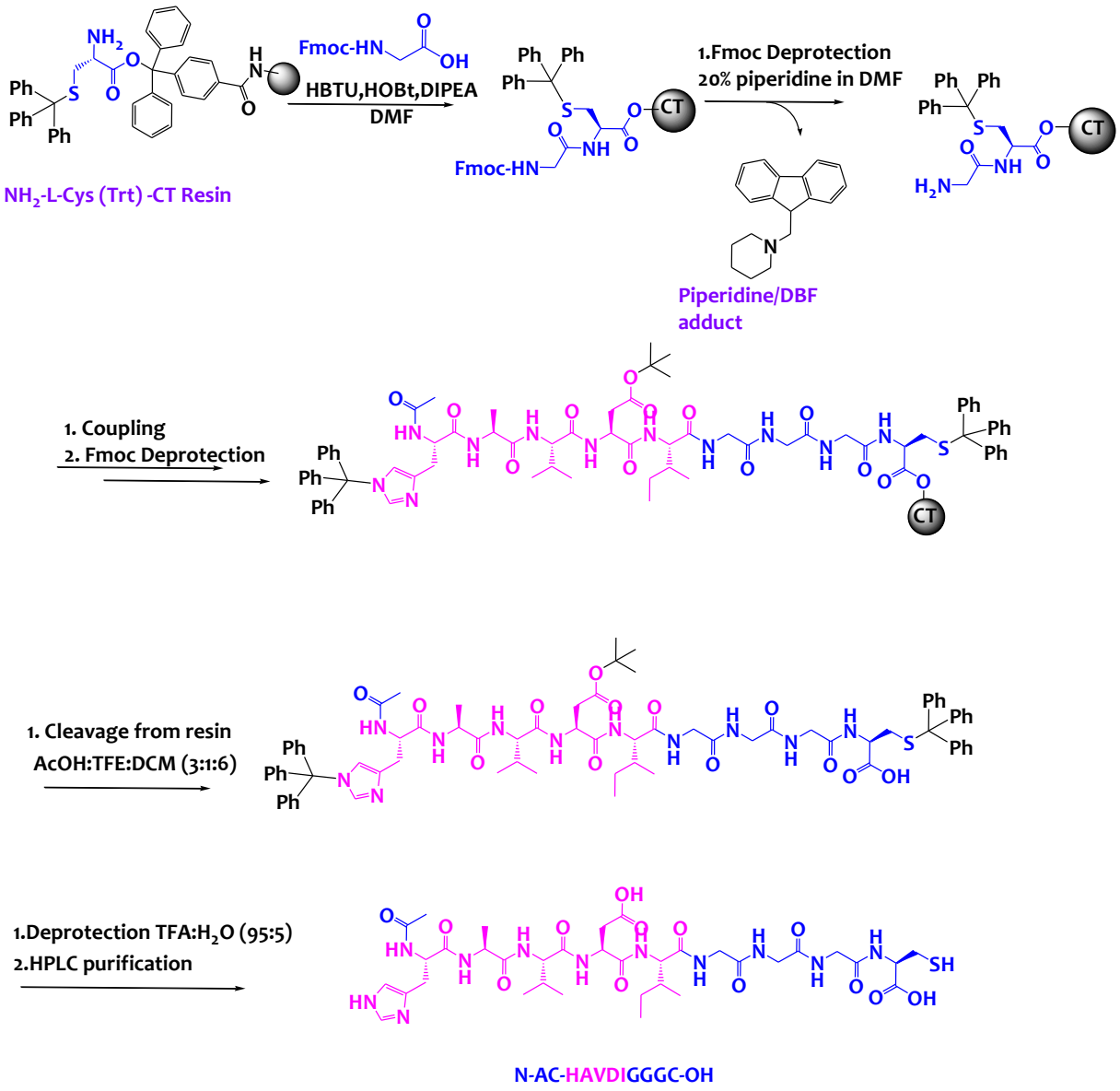

***Scheme* 2.2** *Synthesis of HAVDIGGGC by SPPS*

2.2.4 Synthesis of photoactivatable N & E-cadherin peptidomimetics

The photoactivatable Histidine (**4**) was incorporated into the HAVDIGGGC sequence during SPPS to render the photoactivatable peptide Ac-H[$Ru(bpy)_2PPh_3$]AVDIGGGC **(Scheme 2.3).** The synthesis protocol was the same as used for the native HAVDIGGGC sequence **(section 2.2.3).** The Ac-His([$Ru(bpy)_2PPh_3$]$^{2+}$)-OH amino acid was introduced at the last step of the SPPS. The Ru-complex remained stable at Fmoc-based SPPS coupling conditions. Mass analysis showed no changes in the complex during acidic resin cleavage and side chain deprotection conditions. The peptide was purified by RP-HPLC and characterized by mass spectroscopy. The peak corresponding to the peptide appeared at a retention time of 16 min using (5:95)

ACN:H2O eluent. The ESI-MS of the final photoactivatable N-cadherin showed $[M-H]^+$ peak at 1543.40 Da **(Fig. 2.8).**

Ac-H[Ru(bpy)$_2$PPh$_3$]AVDIGGGC was obtained at 20 mg scale with high purity (> 95%) and good an overall yield of 59%. The peptide was obtained as an orange colored solid. The photoactivatable N-cadherin peptide was soluble in water and PBS (7.4) at a 1 mg/mL concentration.

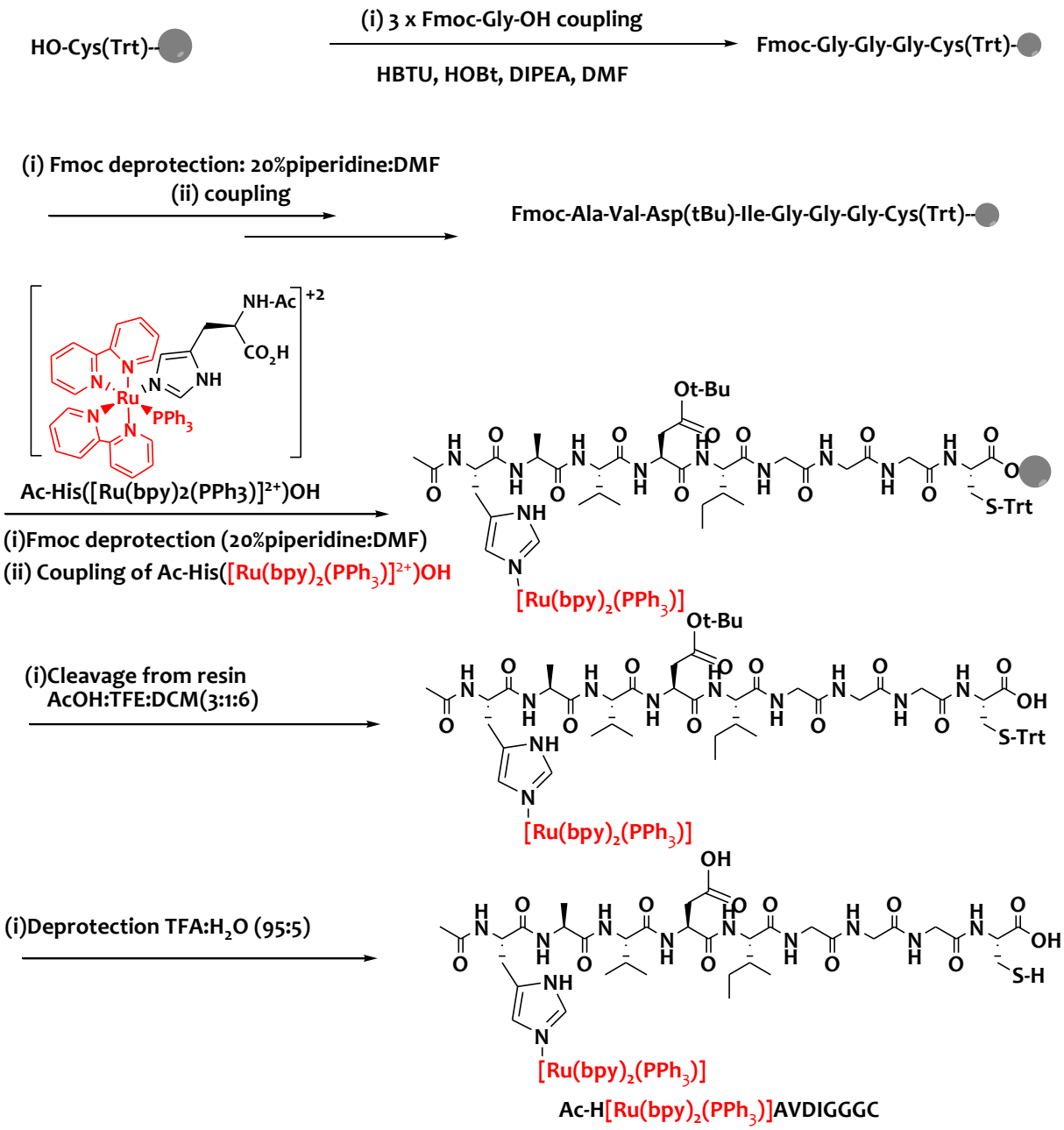

Scheme 2.3 *Synthesis of Ac-H[Ru(bpy)$_2$PPh$_3$]AVDIGGGC*

The photoactivatable E-cadherin mimetic peptide Ac-SH[Ru(bpy)$_2$PPh$_3$]AVSSC was also synthesized following the same protocol as described above. The RP-HPLC peak

corresponding to the peptide appeared at a retention time of 14 min using (5:95) H_2O:ACN solvent. The ESI-MS of the final photoactivatable E-cadherin showed $[M]^{2+}$ at 701.8 Da **(Fig. 2.9).** The final photoactivatable E-cadherin peptidomimetic, Ac-SH$[Ru(bpy)_2PPh_3]$AVSSC was obtained in high purity (> 96%), at 10 mg scale and reasonably good yields (48-52%). The peptide was obtained as an orange colored solid. The photoactivatable E-cadherin peptide was soluble in PBS and water at 2 mg/mL concentration.

2.2.5 Photochemical properties of N & E-cadherin peptidomimetics

The photolytic reaction of $[Ru(bpy)_2PPh_3]^{2+}$ complex from the Ac-H$[Ru(bpy)_2PPh_3]$AVDIGGGC peptide was followed by UV-Vis spectrophotometry. The UV spectra of a 0.5 mM Ac-H$[Ru(bpy)_2PPh_3]$AVDIGGGC solution in PBS at pH 7.4 before irradiation is shown in **Fig.2.4**. Two absorption maxima at 290 nm and 424 nm are appreciable. The absorption at 290 nm corresponds to the $\pi - \pi^*$ transitions of the bipyridines[119]. The maximum absorption at 424 nm corresponds to the MLCT band, which is characteristic of Ru polypyridine complexes[116]. The UV spectra were measured after irradiating the solution at increasing exposure times at 420 nm (2.7 mW/cm^2)). Visible changes in the UV spectrum occurred upon exposure. The absorption maximum at 424 nm was red shifted to 434 nm and showed a gradual increase in intensity with increasing irradiation time. The absorption maximum at 290 nm remained unchanged at irradiation times below 1 min, and showed a decay at longer exposure times **(Fig. 2.4 A)**.

The photolytic reaction is expected to yield $[Ru(bpy)_2PPh_3H_2O]^{2+}$ as a byproduct (**Scheme 2.4**). The red-shift of λ_{max} from ~424 to ~434 nm at pH 7.4 has been associated with the appearance of the hydroxo complex $[Ru(bpy)_2PPh_3H_2O]^{2+}$ in previous literature reports[116]. The uv-vis spectrum of the photoproduct was showed the characteristics of the spectrum of $[Ru(bpy)_2PPh_3H_2O]^{+2}$ complex which can be synthesized by refluxing the intermediate complex, $[Ru(bpy)_2PPh_3]^{2+}$ in water[116].

The chemical yield of the photolytic reaction was calculated from HPLC quantification of the irradiated solutions. In the HPLC elugram, the intensity of the Ac-H$[Ru(bpy)_2PPh_3]$AVDIGGGC peak at retention time 16 min is diminished and also a new peak has appeared at retention time of 14 min with increasing intensity **(Fig. 2.10).** This peak corresponded to free HAVDIGGGC according to mass analysis. A second peak at longer retention times (18 min) was also visible and corresponded to byproduct $[Ru(bpy)_2PPh_3H_2O]^{2+}$. After 5 min exposure at 420 nm, the HPLC analysis of the irradiated solution showed that 60%

of Ac-H[Ru(bpy)$_2$PPh$_3$]AVDIGGGC was photolyzed and 65% of HAVDIGGGC was formed **(Fig. 2.4B)**. After 20 min exposure the conversion ratio was 98%, confirming a high chemical yield of the photolytic reaction.

The photolysis analysis of the Ac-SH[Ru(bpy)$_2$PPh$_3$]AVSSC peptide showed similar features **(Fig. 2.11&12)**.

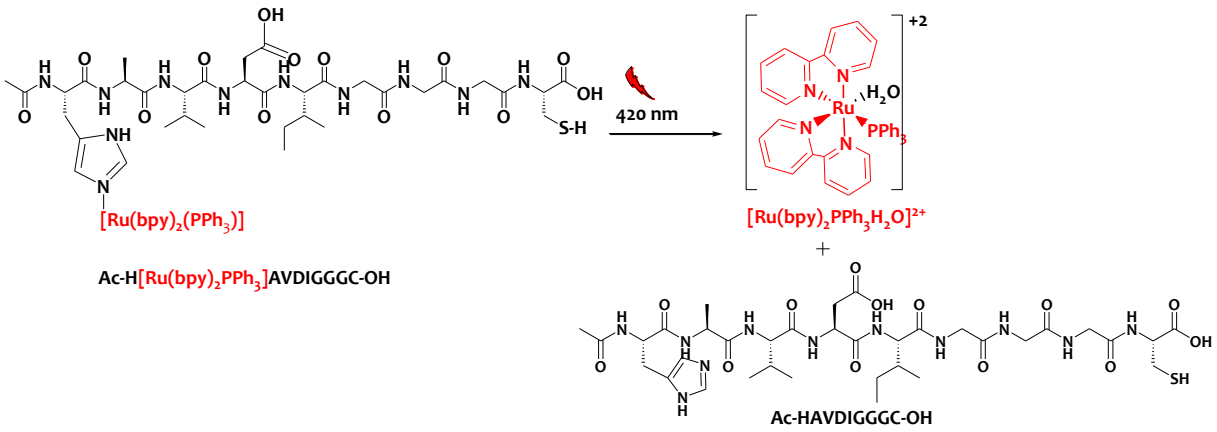

Scheme 2.4 *Photochemical reaction expected for Ac-H[Ru(bpy)$_2$PPh$_3$]AVDIGGGC*

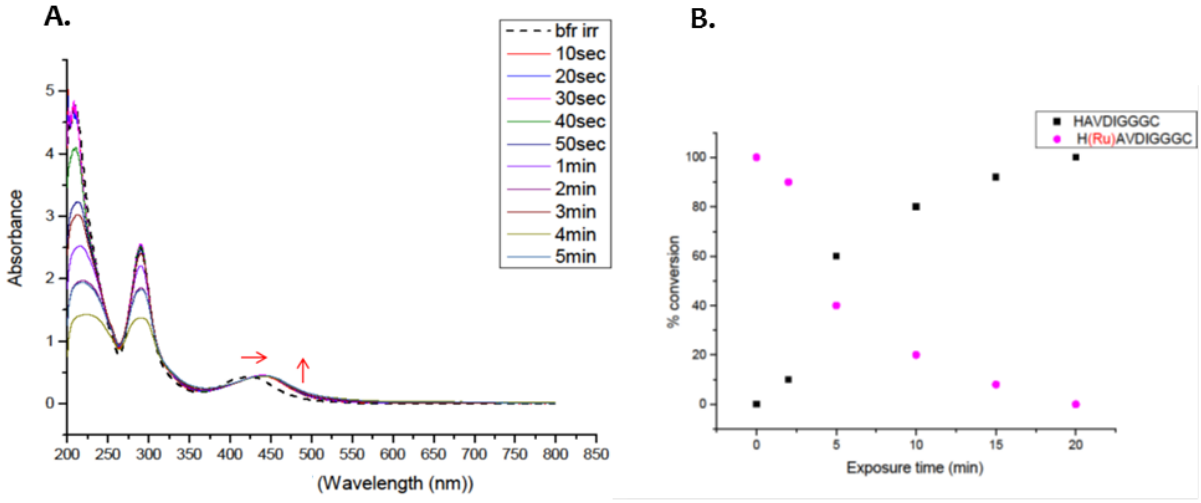

Fig. 2.4 (A) *UV-Vis spectra of Ac-H[Ru(bpy)$_2$PPh$_3$]AVDIGGGC solution (0.5 mM in PBS pH 7.4) after irradiation at 420 nm during increasing exposure times. (bfr irr: Before irradiation)* ***(B)*** *The conversion degree for the photolysis of Ac-H[Ru(bpy)$_2$PPh$_3$]AVDIGGGC*

At this point it is interesting to compare the photolysis of the Ac-H[Ru(bpy)$_2$PPh$_3$]AVDIGGGC peptides with the photolysis of reported photoactivatable peptides where the nitrobenzyl and nitroindolinyl ester derivatives were used as PPGs to

protect Asp and Lys residues. The Ru-complex absorbs in the visible spectrum and can be photocleaved with VIS light, which is expected to have lower risk of cell photodamage when irradiation in a biological system[109]. On the other hand, the sensitivity to VIS light requires the reactions and characterization steps to be performed in light protected conditions. The photochemical yield obtained for Ru -complex protected peptide in solution was around 98% in 20 min of exposure time.

2.3 Conclusion

Two photo-activatable derivatives of N- and E-cadherin peptidomimetics containing the HAV domain were successfully synthesized. This was achieved by introducing a photoremovable protecting group at the imidazole ring of the His side chain, which is critical for *trans* EC1-EC1 interaction. The $[Ru(bpy)_2(PPh_3)]^{2+}$ was used as a photoremovable protecting group and His was introduced as one of the ligands. Which was synthesized in high purity and good yield. The photoactivatable His was introduced into Ac-H$[Ru(bpy)_2PPh_3]$AVDIGGGC and Ac-SH$[Ru(bpy)_2(PPh_3)]$AVSSC peptidomimetic by Fmoc based SPPS. The photoactivatable peptides exhibited good water solubility as well as very good photolytic properties in solution for their application in biological studies.

2.4 Experimental section

2.4.1 Materials and methods

Solvents and Reagents: Chemicals and solvents were purchased from Acros Organics, Alfa Aesar by Thermo Fisher Scientific and Merk/ MilliporeSigma. Amino acids, coupling reagents and loaded resins for SPPS were purchased from Carbolution Chemicals GmbH, Novabiochem and Iris Biotech GmbH. All the chemicals and solvents were used as purchased, unless otherwise specified.

Characterization methods: The reactions and couplings were monitored by an analytical HPLC, column (250 mm x 4.6 mm, C18) filled with Reprosil RP18 (5 µm grain size, 250 x 20 mm) from JASCO and the purified with a semi-preparative HPLC PU-4086 series (column 100 mm C18) provided with a diode array UV-Vis detection system and fraction collector. Agilent Technologies InfinityLab Liquid Chromatography/Mass Selective Detector (LC/MSD) was used to measure mass spectra. UV/VIS Spectra were record on a varian Cary 4000 UV/VIS spectrometer (Varian Inc. Palo Alto, USA). Samples were prepared in quartz cuvettes, which

were washed with isopropanol and Milli-Q water and then dried with N2 stream before measurement. ^{1}H-NMR spectra were recorded on a Bruker Avance 300 (300 MHz) and the measurements were performed at room temperature using TMS (δ= 0 ppm) as reference. The chemical shifts were expressed in parts per million.

2.4.2 Synthesis and characterization of Ru-His Complexes

H-His([$Ru(bpy)_2PPh_3]^{+2}$) was prepared according to literature starting from *cis*-Bis(2,2'-bipyridine)dichlororuthenium(II)hydrate[113].

a. Boc-His([$Ru(bpy)_2PPh_3]^{+2}$)-OH (2)

cis-Bis(2,2'-bipyridine)dichlororuthenium(II)hydrate (760 mg, 1.55 mmol, 1 eq.) was dissolved in a 100 mL Schlenk flask with deoxygenated MeOH (15 mL) and water (15 mL). The solution was stirred 10 min under Ar at 80 °C. Triphenylphosphine (406 mg, 1.55 mmol, 1 eq.) was added, and the resulting mixture was stirred 14 h at 80 °C, then allowed to reach r.t. A solution of Boc-His-OH (1.975 g, 7.74 mmol, 5 eq.) in 1.9 mL of NaOH 4 M was added, and the reaction stirred again 14 h at 80 °C. The crude reaction mixture was partly concentrated under reduced pressure, and the product was precipitated with KPF_6. Finally, orange solid was filtered, washed with water and freeze dried to give the desired product as orange solid (1.58 g, 95.15%).

^{1}H-NMR (300 MHz, D_2O): δ/ppm = 1.05 (d, 3H, CH3), 1.27 (d, 6H, 2 x CH3), 2.52-2.84 (m, 2H, CH2), 3.95-4.03 (m, 1H, CH), 6.1 (s, Ar-H), 6.3 (s, Ar-H), 6.83-7.11 (m, 15H, Ar-H), 7.18-7.23 (m, 3H, Ar-H), 7.28-7.41 (m, 3H, Ar-H), 7.63-7.70 (m, 1H, Ar-H), 7.78-8.04 (m, 6H, Ar-H), 8.29-8.35 (m, 2H, Ar-H), 8.62 (s, Ar-H), 8.97-8.98 (d, 1H, Ar-H); ESI-MS/LC/MSD: *m/z* calc. for Boc-His([$Ru(bpy)_2PPh_3]^{+2}$)-OH $(M-H)^+$ 930.25, found 930.00

b. H-His([$Ru(bpy)_2PPh_3]^{+2}$)-OH (3)

Boc-His([$Ru(bpy)_2PPh_3]^{+2}$)-OH (900 mg, 0.84 mmol) was dissolved in a 2 neck round bottom flask with 12 mL CH_2Cl_2 and cooled to 0 °C. Trifluoroacetic acid (12 mL) was added slowly in to the above mixture and continued stirring at 0 °C for 35 min and 35 min at r.t. The solvent was concentrated under reduced pressure, and the residue was purified by preparative HPLC. The fractions containing final product were freeze dried, and the product was isolated as light orange powder (814.3 mg, 92%)

^{1}H-NMR (300 MHz, D_2O): δ/ppm =2.77-2.92 (m, 2H, CH2), 3.64-3.72 (m, 1H, CH), 6.1(s, Ar-H), 6.40-6.47 (d, 1H, Ar-H), 6.76 (s, 1H, Ar-H), 6.93-7.21 (m, 15H, Ar-H), 7.27-7.40 (m, 6H, Ar-H), 7.68-7.73 (t, 1H, Ar-H), 7.78-8.07 (m, 6H, Ar-H), 8.27-8.30 (d, 1H, Ar-H), 8.36-8.39 (d, 1H, Ar-H), 8.62 (s, Ar-

H), 8.72-8.78 (d, 1H, Ar-H), 9.03-9.06 (d, 1H, Ar-H); ESI-MS/LC/MSD: *m/z* calc. for H-His([Ru(bpy)$_2$PPh$_3$]$^{+2}$)-OH (M-H)$^+$ 830.25, found 830.20.

c. Ac-His([Ru(bpy)$_2$PPh$_3$]$^{+2}$)-OH (4)

H-His([Ru(bpy)$_2$PPh$_3$]$^{+2}$)-OH (200 mg, 0.24 mmol) was suspended in Acetic acid (5 mL) in a 50 mL round bottom flask. Acetic anhydride (68.25 µL, 0.722 mmol) was added drop wise at 0 °C and stirred at r.t. for 2 h. The crude reaction mixture was concentrated under reduced pressure and the residue was purified by reverse phase chromatography. The fractions containing final product were freeze dried, and the product was isolated as an orange powder (256.78 mg, 81.5%).

^{1}H-NMR (300 MHz, D$_2$O): δ/ppm =1.62 (d, 3H, CH3), 2.51-2.62 (m, 2H, CH2), 2.74-2.85 (m, 1H, CH), 4.11-4.19 (m, 1H, CH), 5.98-6.01 (d, 1H, Ar-H), 6.48-6.52 (d, 1H, Ar-H), 6.66-6.78 (m, 13H, Ar-H), 6.95-7.08 (m, 4H, Ar-H), 7.05-7.08 (t, 1H, Ar-H), 7.17-7.23 (q, 1H, Ar-H), 7.29 (s, 2H, Ar-H), 7.57-7.62 (t, 1H, Ar-H), 7.75-7.85 (m, 3H, Ar-H), 7.92-7.95 (d, 2H, Ar-H), 8.20-8.40 (dd, 2H, Ar-H), 8.56-8.58 (d, 1H, Ar-H), 8.81-8.86 (t, 1H, Ar-H); ESI-MS/LC/MSD: *m/z* calc. for Ac-His([Ru(bpy)$_2$PPh$_3$]$^{+2}$)-OH (M-H)$^+$ 872.21, found 872.00.

2.4.3 Synthesis of peptides

The E-cadherin mimetic peptides were purchased from GeneCust, France and used without further purification.

General protocols (GP)

GP1 - Coupling of protected amino acids to the resin with HBTU

All the mimetic peptides were synthesized by following standard Fmoc based SPPS using a preloaded 2-Chlorotrityl chloride (CTC) resin (0,039 mmol /100 mg), 100-200 mesh, 1% DVB on a 10 mL syringe provided with a PE-frit (CEL- 053 and CEL-1016), (Roland Vetter LaborbedarfOHG, Ammerbuch, Germany). The resin was swollen in DMF for 15 min before starting the coupling steps. Next amino acids were sequentially added to the resin by following the coupling protocol. A pre activated solution of the protected amino acid (2 eq.), HBTU (2 eq.), HOBt (2 eq.), DIEA (5.6 eq.) in DMF (1 mL) was added to the resin-bound free amine and agitated for 2 h at r.t. on an automated shaker. The coupling mixture was drained and the resin was washed with DMF (5 x). After each coupling, the Fmoc was removed by treating the resin with 20% piperidine in DMF (v/v) for 5 min and the same step was repeated for another 10 min. After draining the solution, the resin was washed with DMF (5 x).

GP2 – Cleavage of peptide from 2-Chlorotrityl chloride (CTC) resin (100-200 mesh), 1% DVB

The protected linear peptide bound to the resin was treated with acetic acid, 2,2,2-triflouroethanol and DCM (3:1:6 v/v/v) for 30 min and the solution was collected. The procedure was repeated for three times. The solutions were collected and pooled together. The solvents were removed using rotary evaporation to get the crude peptide.

GP3 – Deprotection of side chain protecting group (Boc and tert-butyl ester groups)

The crude peptide was treated with TFA/DCM (3 mL: 3 mL, 1:1; v/v) and stirred for 30 min to remove the side chain protecting groups Trt and tert-butyl ester (0.1 g). The solvents were removed under reduced pressure to obtain the deprotected Cys, His, & Ser (Trt removal) or Asp (t-butyl ester removal) residues.

GP4 – HPLC purification of Peptides

The concentrated residue was dissolved in acetonitrile/water 1:1 (2 mL) and purified by semi preparative RP-HPLC using (ACN + 0.1% TFA) and (H_2O + 0.1% TFA) as eluents, gradient: 5% to 95% Acetonitrile for 40 min. The fractions containing >95% pure peptides were collected and pooled together. Acetonitrile was removed under reduced pressure and lyophilized to get pure peptide and stored at -20 °C. The peptides were characterized by ESI-MS and analytical HPLC.

2.4.4 Photolysis of the peptide in solution

The photolysis studies of photoactivatable peptide in solution were carried out by irradiating 0.5 mM peptide in PBS (pH 7.4) with a LUMOS 43 (Atlas Photonics Inc.) at 420 nm (I= 2.7 mW/cm^2) for 20 min. The percentage of conversion in solution was quantified by Analytical HPLC chromatogram and ESI-MS.

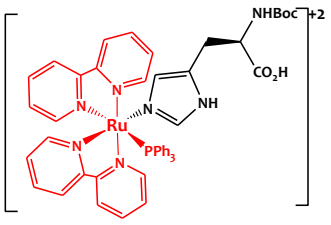

Boc-His([Ru(bpy)$_2$PPh$_3$]$^{2+}$)-OH

(A)

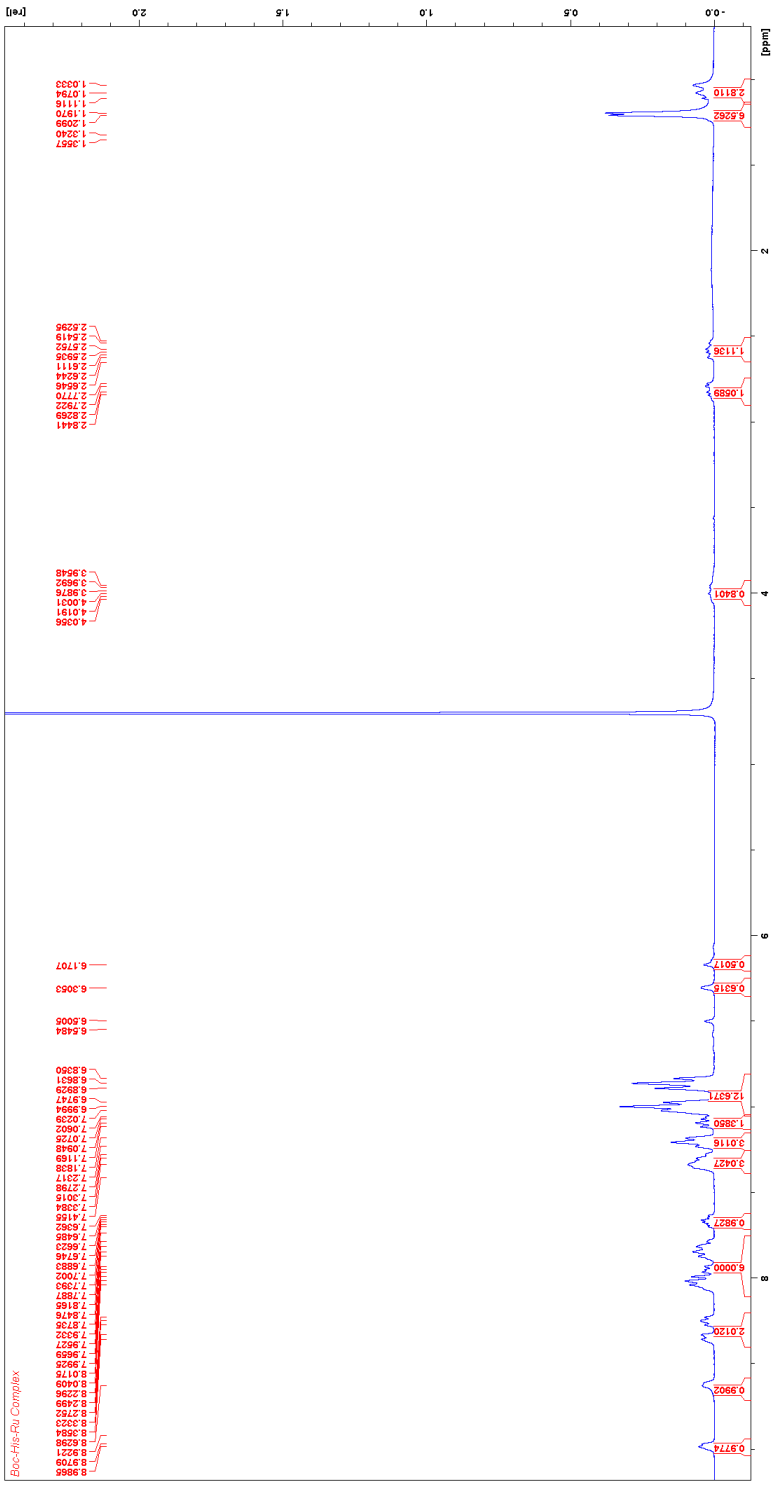

(B)

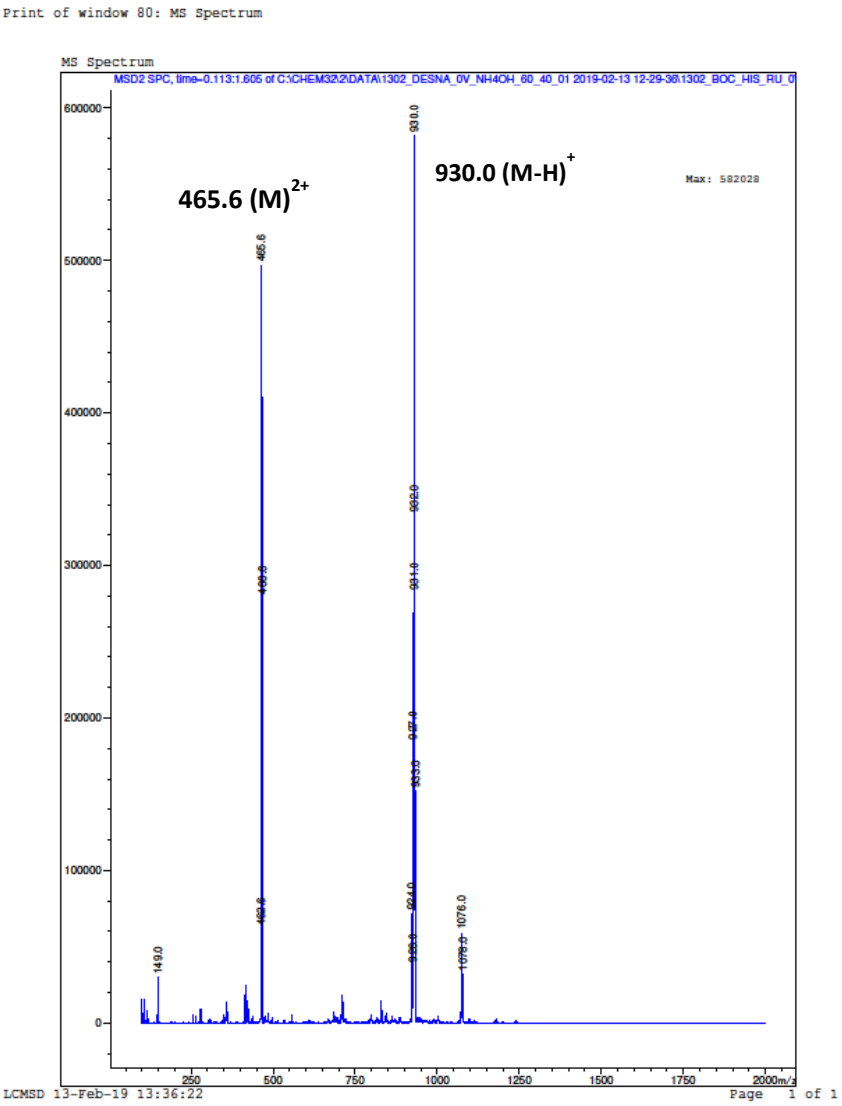

(C)

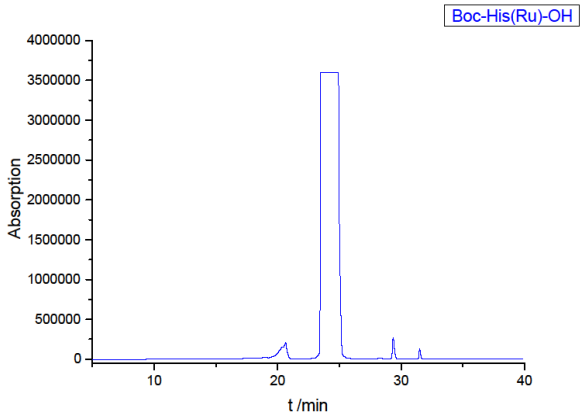

Fig. 2.5 Characterization of Boc-His([Ru(bpy)2PPh3]$^{+2}$)-OH (2) : *(A) ^{1}H NMR spectra (B) ESI-MS spectra (C) Analytical HPLC chromatogram*

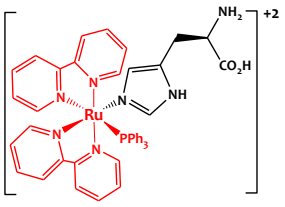

(A)

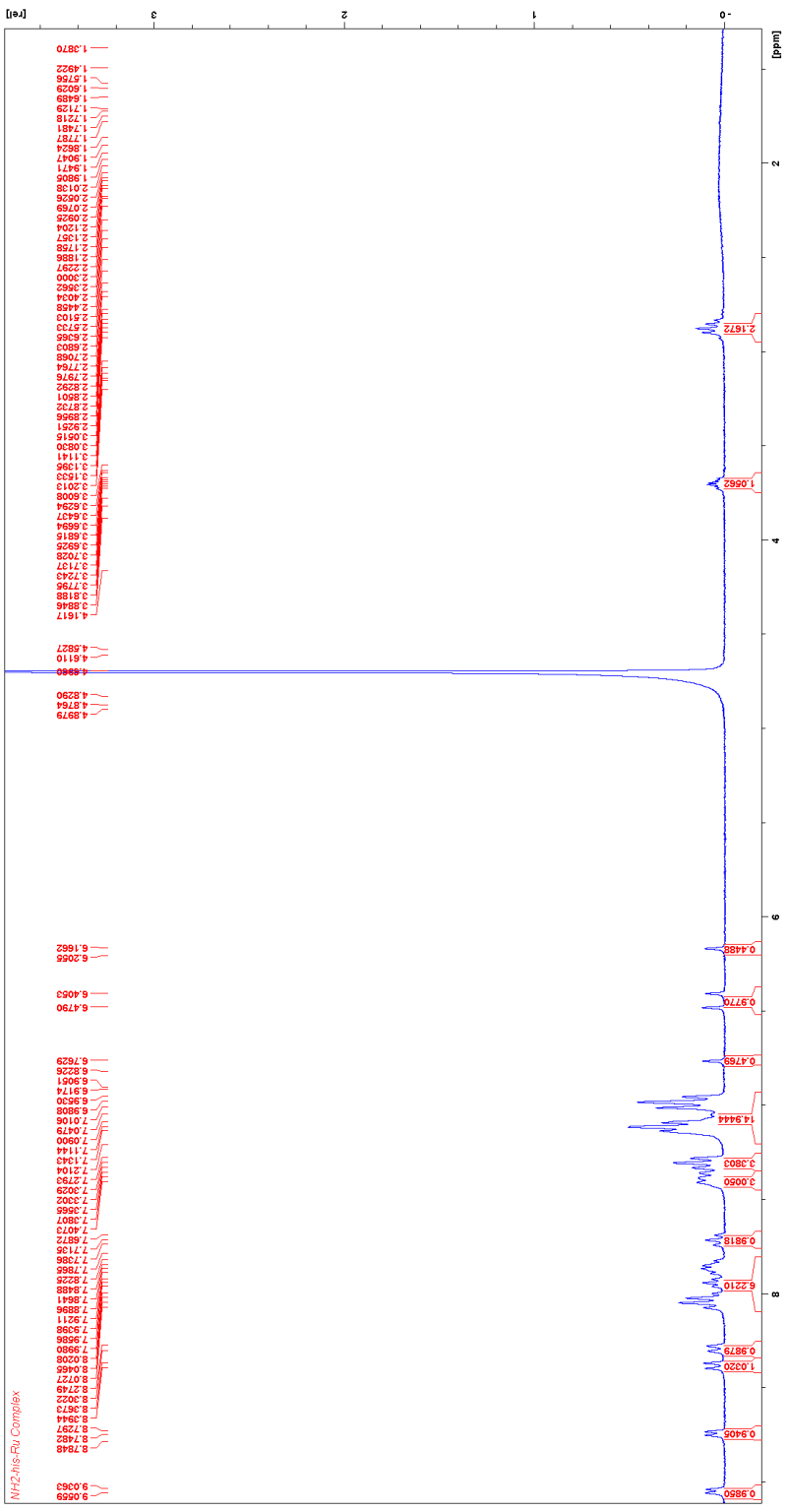

(B)

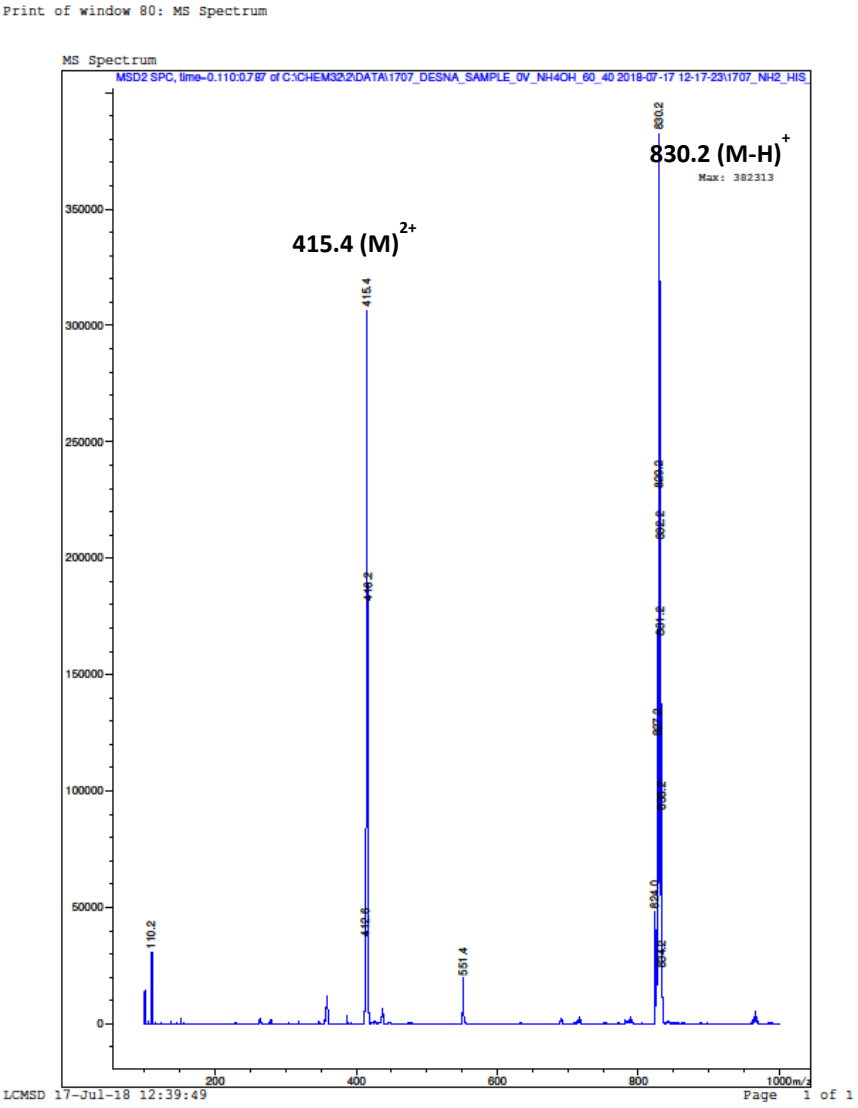

(C)

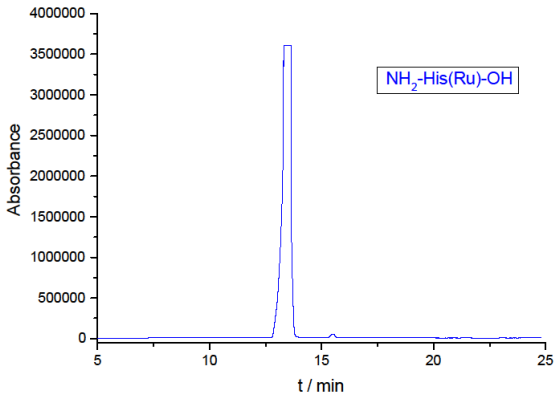

Fig. 2.6 Characterization of H-His([Ru(bpy)2PPh3]$^{+2}$)-OH (3) : *(A) ^{1}H NMR spectra (B) ESI-MS spectra (C) Analytical HPLC chromatogram*

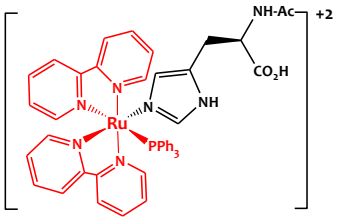

Ac-His([Ru(bpy)$_2$PPh$_3$]$^{2+}$)-OH

(A)

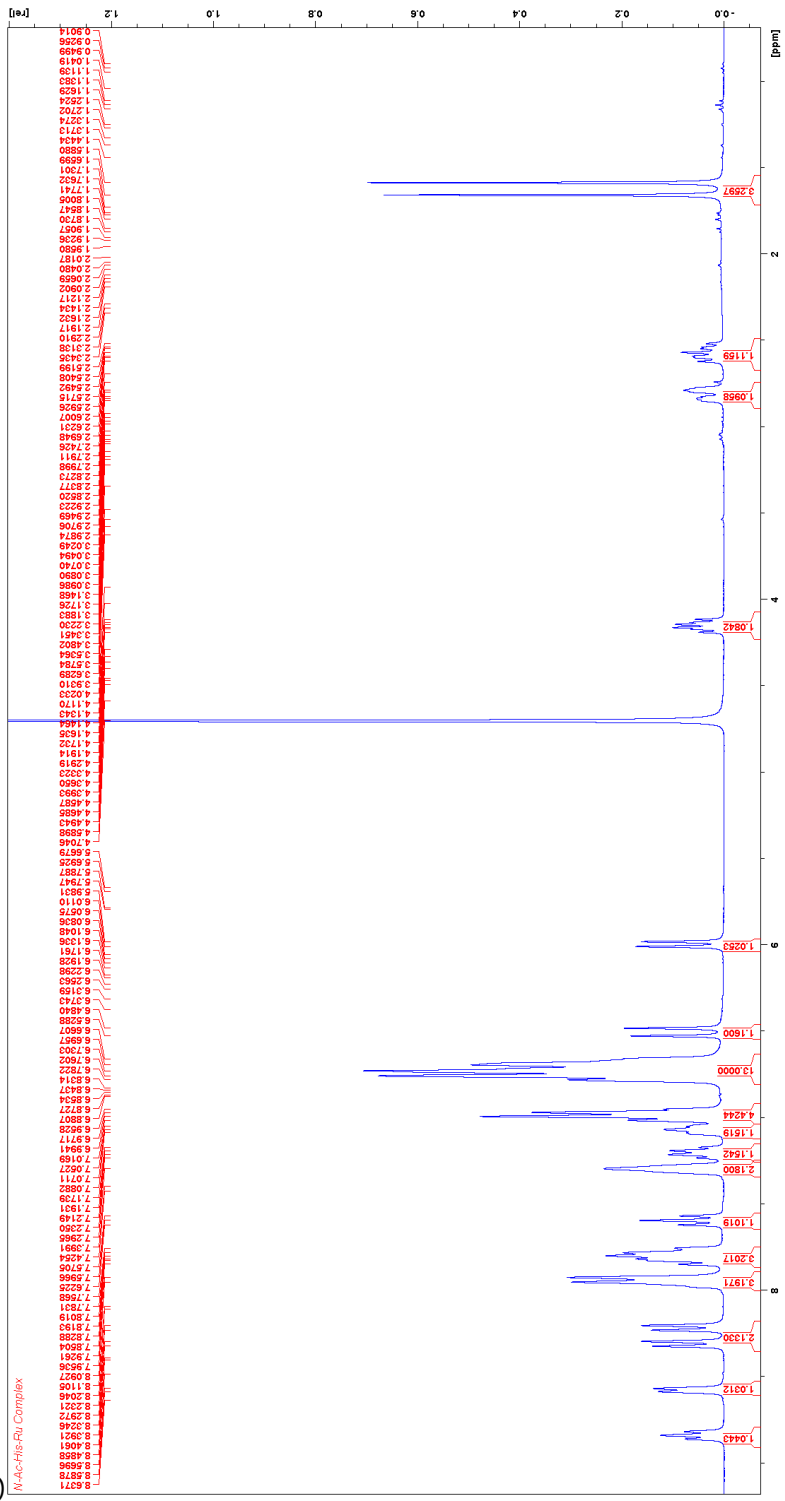

(B)

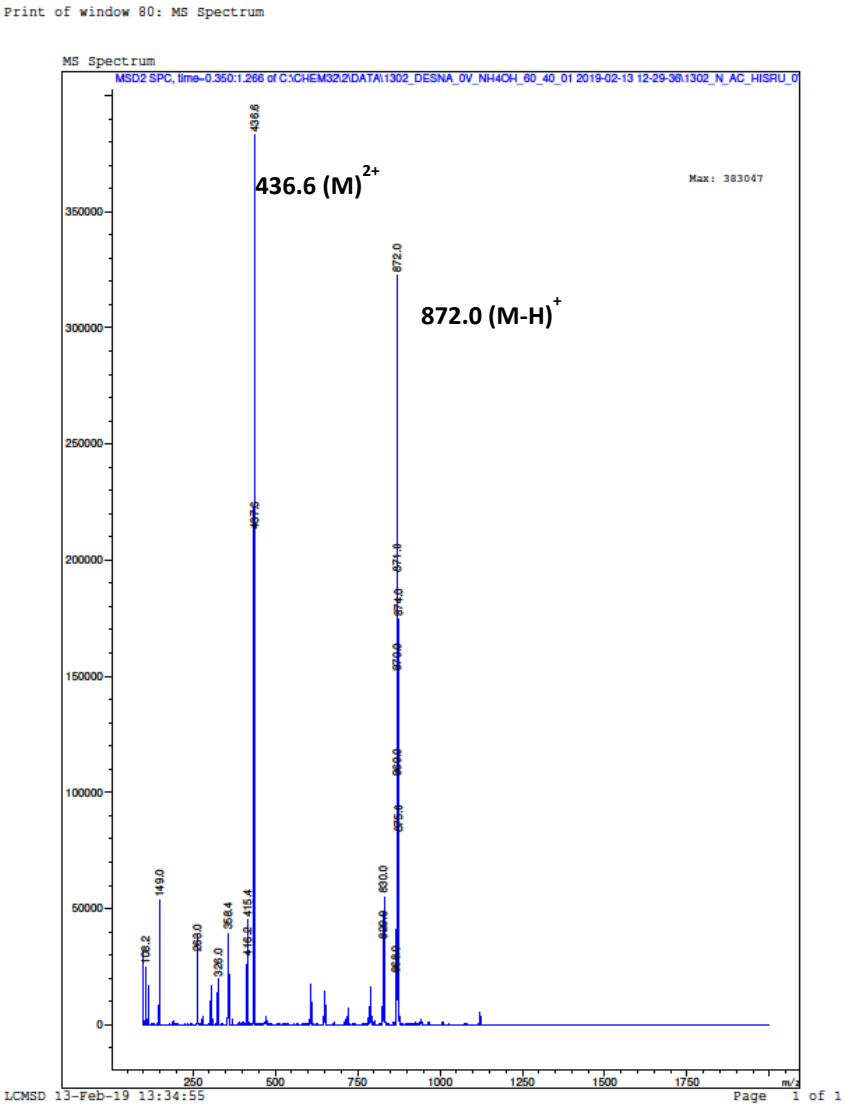

(C)

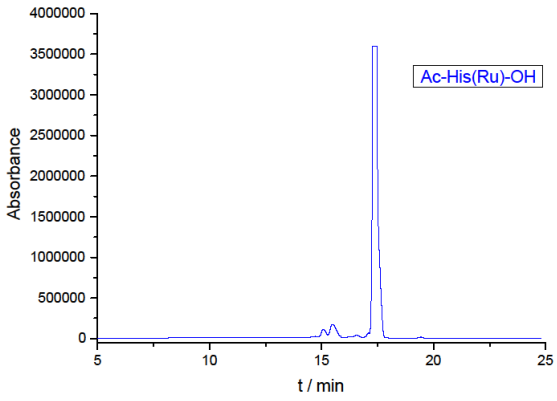

Fig. 2.7 Characterization of Ac-His([Ru(bpy)2PPh3]$^{+2}$)-OH (4): *(A) ^{1}H NMR spectra (B) ESI-MS spectra (C) Analytical HPLC chromatogram*

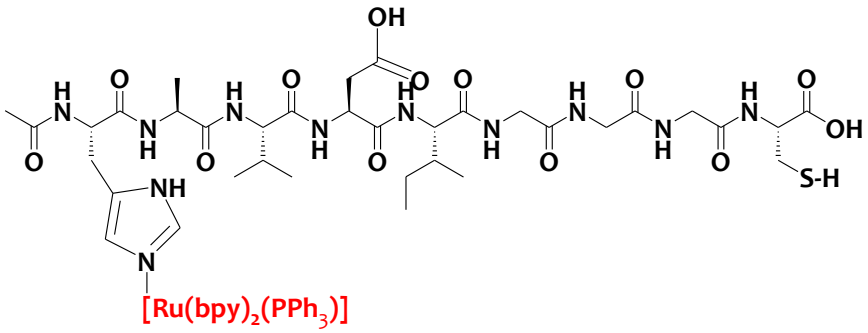

(A)

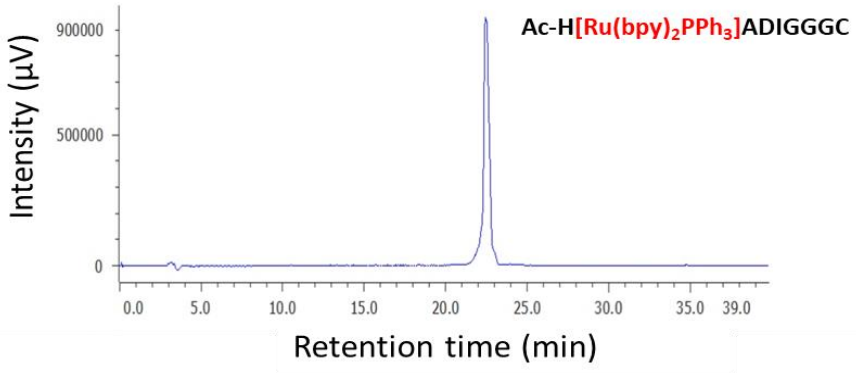

(B)

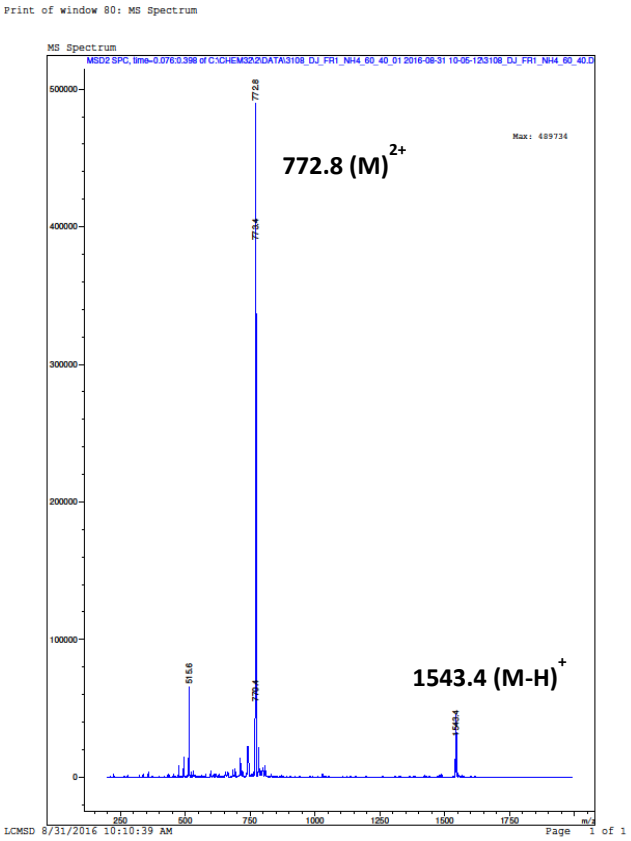

Fig. 2.8 Characterization of H(Ru(bpy)₂PPh₃)AVDIGGGC *(A) ESI-MS spectra (B) Analytical HPLC chromatogram*

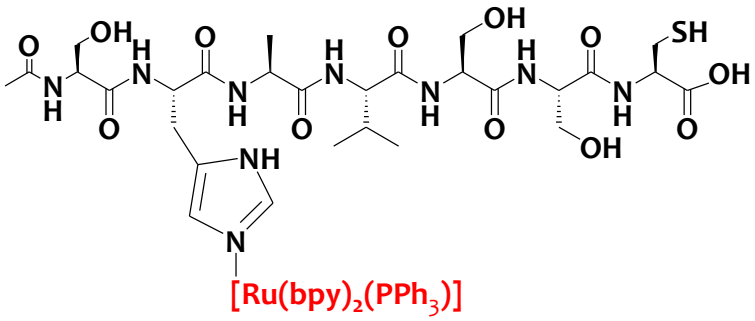

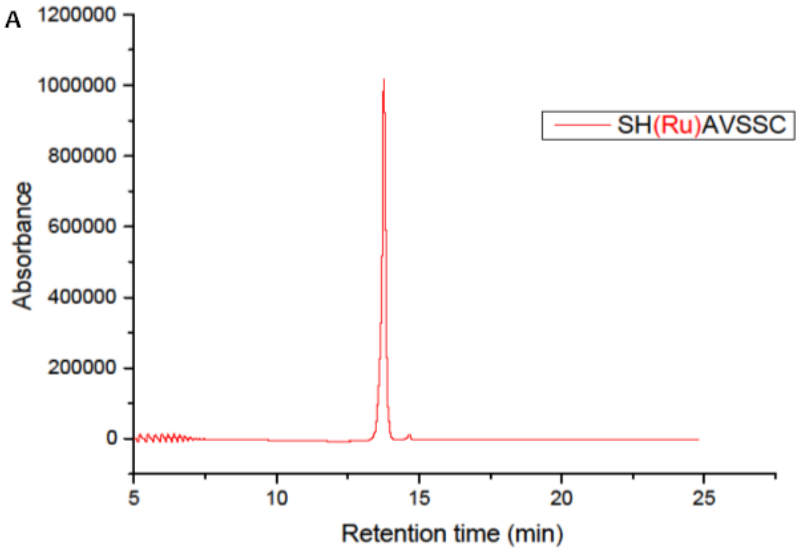

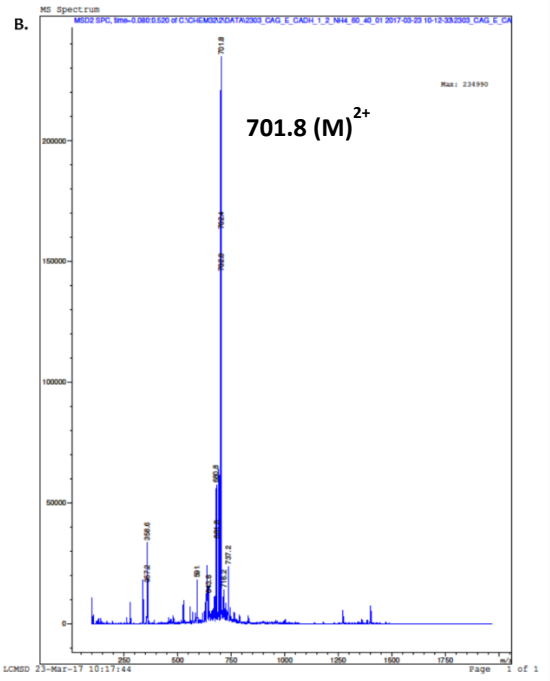

Fig. 2.9 Characterization of SH(Ru)AVSSC *(A) ESI-MS spectra (B) Analytical HPLC chromatogram*

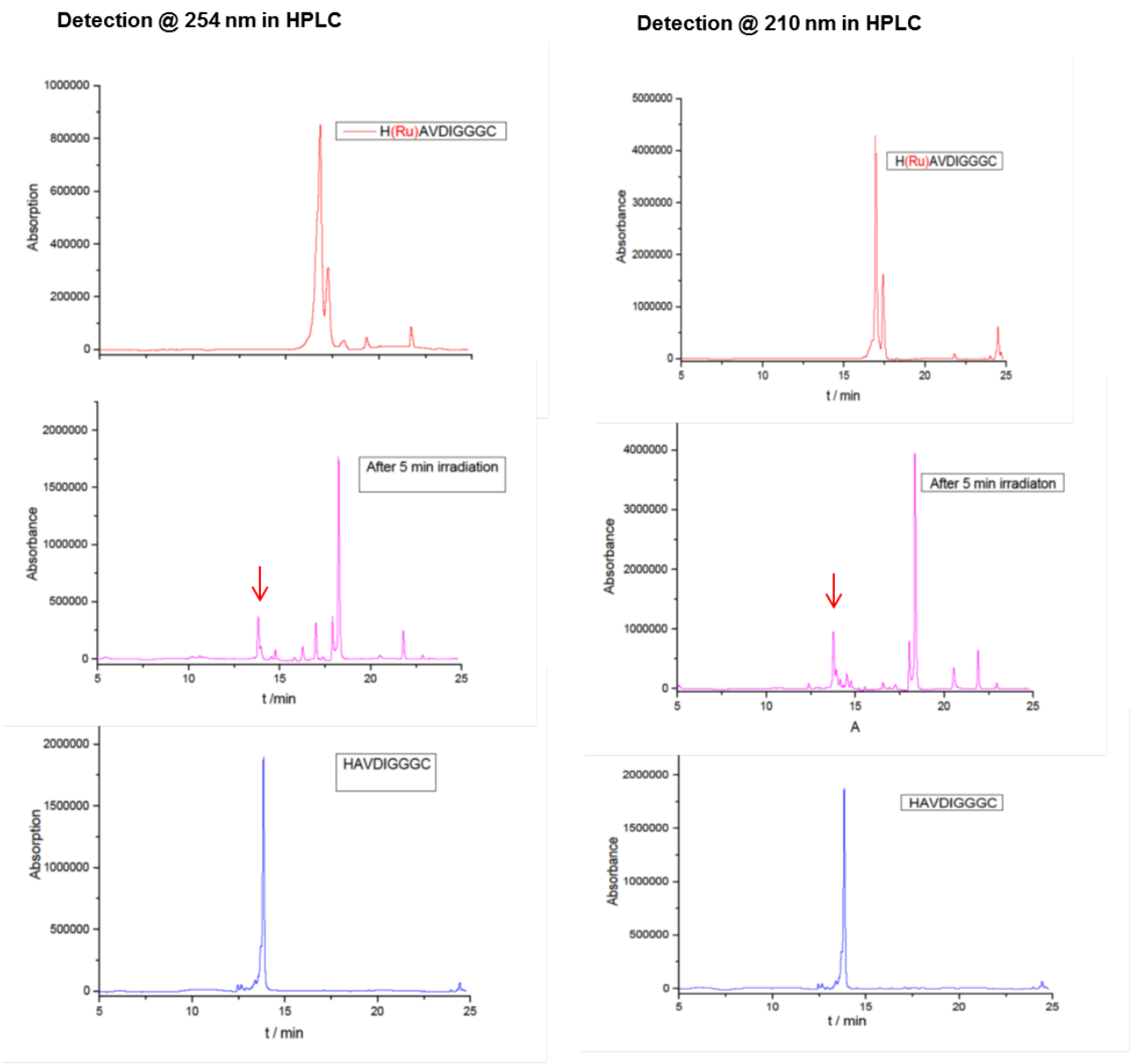

***Fig.* 2.10** *Analytical HPLC chromatograms of Ac-H[Ru(bpy)$_2$PPh$_3$]AVDIGGGC (0.5 mM) solution before and after irradiation at 420 nm for 5 min. The HPLC chromatogram is shown for 210 and 254 nm detection channels and HPLC chromatogram of HAVDIGGGC is shown as well.*

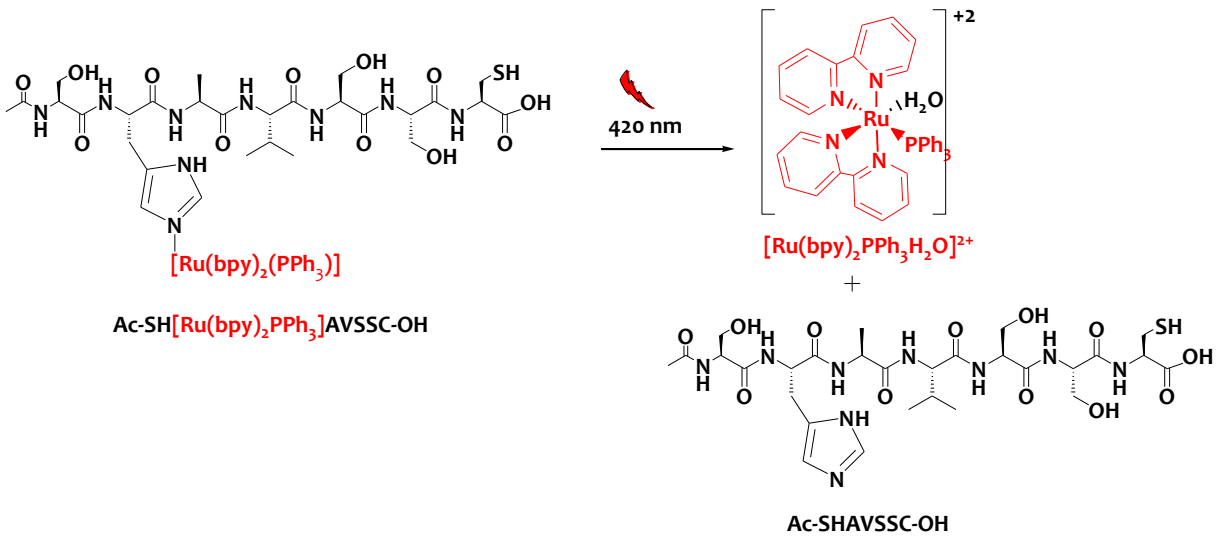

Scheme 2.5 Photochemical reaction expected for SH[Ru(bpy)$_2$PPh$_3$]AVSSC.

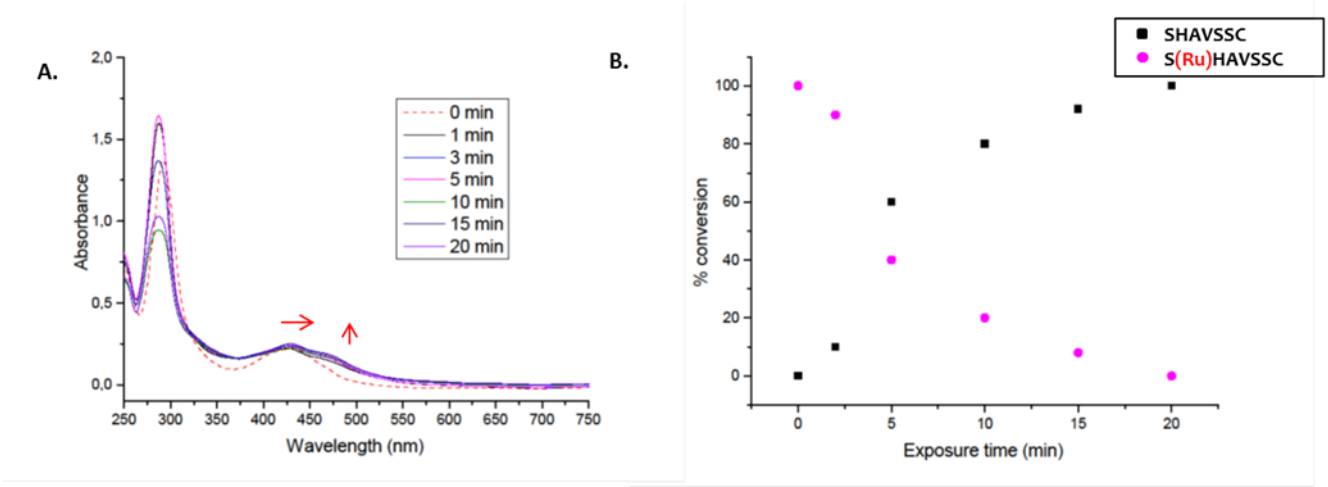

Fig. 2.11 *UV-Vis spectra of photolysis of SH[Ru(bpy)$_2$PPh$_3$]AVSSC (0.5 mM in PBS, pH 7.4) at 420 nm at increasing exposure times* ***(B)*** *Conversion degree of photolysis of SH[Ru(bpy)$_2$PPh$_3$]AVSSC.*

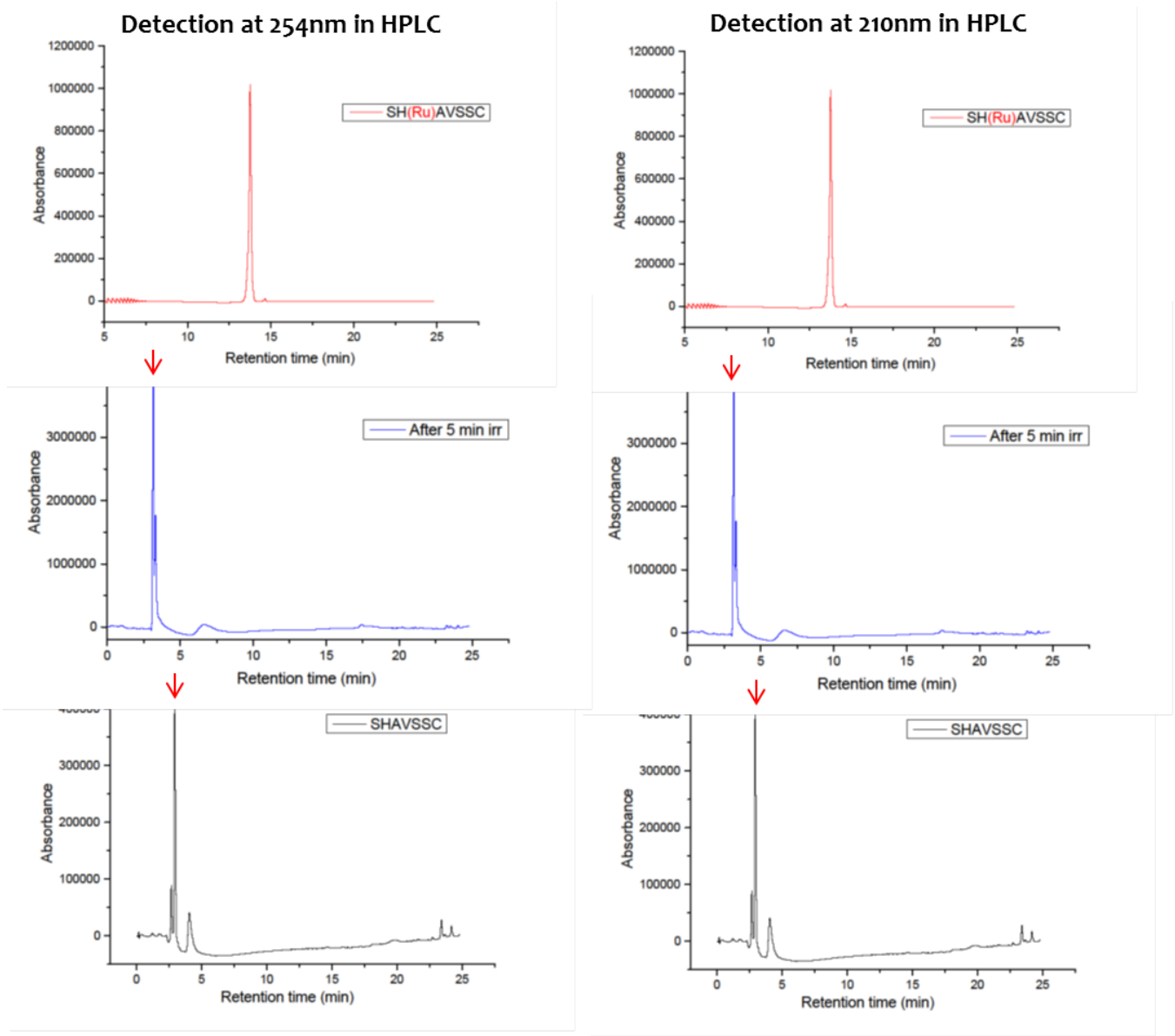

***Fig.* 2.12** *Analytical HPLC chromatograms of SH[Ru(bpy)$_2$PPh$_3$]AVSSC (0.5 mM solution), before and after irradiation at 420 nm for 5 min. The HPLC chromatogram is shown for 210 and 254 nm absorbance channels and HPLC chromatogram of SHAVSSC at different channels is also shown for comparison.*

Chapter 3

Biomimetic cell-cell biointerfaces with poly(acrylamide) hydrogels functionalized with cadherin ligands

In this chapter, copolymers of AAm, AA and phenyl oxadiazole methylsulfone acrylate will be used to synthesize hydrogels to which matrix-adhesive proteins and cadherin peptidomimetics bearing amine or thiol groups can be orthogonally coupled. 2D hydrogels with variable ligand type, ligand density and mechanical properties will be described. Model biointerfaces to study cell-matrix and cell-cell interactions are developed and characterized. Micropatterned hydrogels that allow reconstructing spatially differentiated cell-matrix and cell-cell interfaces in a cell culture will also be used. This model was developed by Dr. Aleeza Farrukh in the group and will be used in this thesis for testing the activity of the cadherin peptidomimetics in the next chapters.

3.1 Introduction

Poly(acrylamide), p(AAm), is a synthetic polymer that is inexpensive, simple to synthesize, transparent and cytocompatable. p(AAm) hydrogels can be prepared by radical polymerization of acrylamide monomer with a cross-linking agent bis-acrylamide and initiated by ammonium persulfate (APS) and tetramethylenediamine (TEMED)[120]. APS acts as a source of radicals and TEMED catalyzes the radical vinyl addition polymerization.

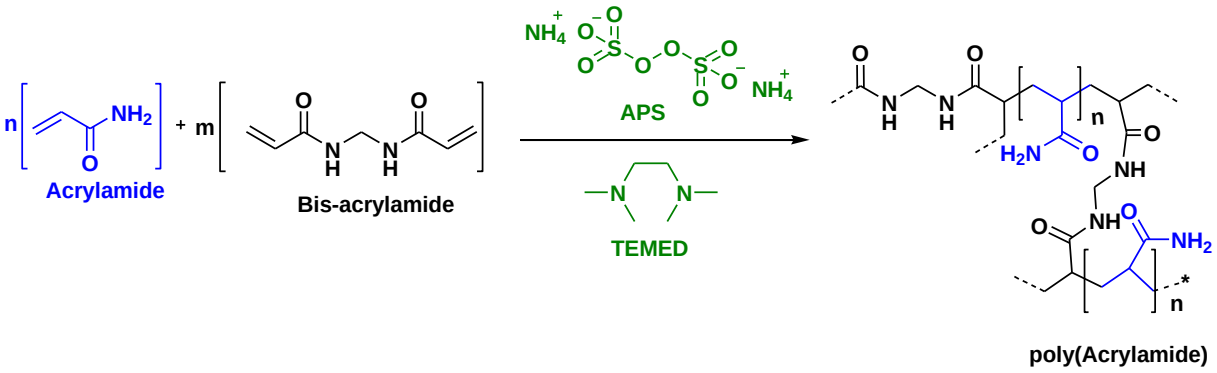

Fig. 3.1 *Mechanism of poly(acrylamide) hydrogel formation with Bis acrylamide cross-linking by radical polymerization* [121].

p(AAm) hydrogels are often used as cell culture materials for studying the response of cells to biochemical and mechanical properties of their microenvironment[122]. These gels can be prepared with mechanical properties similar to those of the physiological environment (0.1-100 kPa)[123] by simply varying the amount of bis-acrylamide crosslinker. Polyacrylamide hydrogels for cell culture are usually fabricated as thin films[59].

p(AAm) hydrogels are antifouling, i.e. they do not absorb proteins[124]. In order to allow interaction with cells, the hydrogels have to be functionalized with specific cell adhesive molecules (fibronectin, collagen or their peptidomimetics) to allow interaction with the membrane receptors at the cell membrane (typically integrins or cadherins)[124]. However, the amide group in p(AAm) is a rather inert functionality. Different strategies to functionalize p(AAm) hydrogels have been reported over the last years. One common method is by using the photoreactive heterobifunctional linker sulfosuccinimidyl-6-(4'-azido-2'-nitrophenyl-amino)hexanoate (sulfo-SANPAH) to couple a ligand covalently[125]. Photoactivation generates highly reactive intermediates from the aryl-azide unit of the bifunctional linker that react with the backbone of the p(AAm) hydrogel network through non-specific chemical reactions[126] (**Fig. 3.1A)**. The NHS activated carboxyl group on the other end of sulfo-SANPAH can form amide bonds with the free amines on cell adhesive molecules. Other methods for functionalization of p(AAm) hydrogels involve using gamma, UV radiation[127]. The major disadvantages of these methods are low reproducibility, multiple steps, long coupling times, and the involvement of toxic chemicals.

An alternative solution for the functionalization of p(AAm) hydrogels is the copolymerization of the acrylamide monomer with other comonomers containing reactive side groups. Acrylic acid (AA), N-(3-aminopropyl)-methacrylamide or N-hydroxethyl acrylamide

have been copolymerized with AAm for this purpose[128]. Recently, our group reported heteroaromatic methylsulfone acrylates (MS) as useful comonomers for the chemo-selective binding of thiol containing biomolecules to p(AAm) hydrogels. The radical polymerization reaction is not affected by MS monomers. MS monomers react with thiols by nucleophilic substitution reaction and form stable bioconjugates through covalent bonds[124,129] (**Fig. 3.1B**). Moreover, copolymerization of MS and AA comonomers in the same hydrogel allowed orthogonal immobilization of two types of ligands bearing thiol or amine groups on the same gel[129].

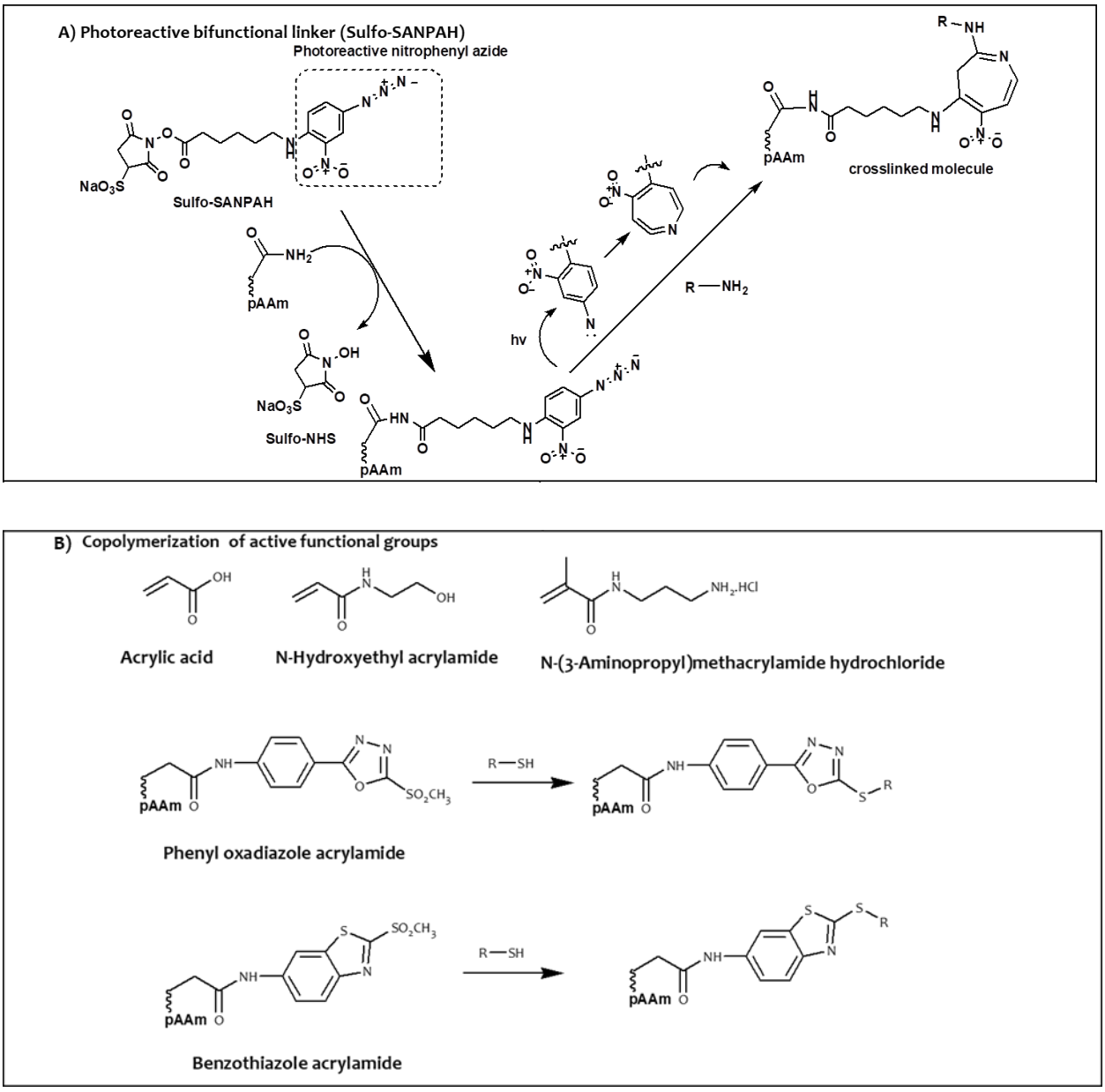

Fig. 3.1 *Different strategies for the functionalization of polyacrylamide hydrogels*[126,130].

The possibility to independently adjust the biochemical and mechanical properties of p(AAm) hydrogels makes them interesting models for the study of cell response to microenvironmental parameters. In fact, these gels have been widely implemented by cell biology groups as simplified models of the extracellular matrix to study cell response to changes in the composition and mechanical properties occurring in regenerative and pathological processes[121]. More recently, p(AAm) hydrogels functionalized with cadherins have been used to mimic the cell-cell biointerface[58]. In natural tissues, these two interfaces are segregated. In epithelial tissues, for example, cells build cell-cell interfaces with their neighbors laterally, and cell-matrix interfaces at the basal plane. This spatial segregation (called polarization in cell biology language) is difficult to mimic in a 2D hydrogel. In the group of Prof. Dr. del Campo, a 2.5D hydrogel model has been designed to mimic this situation. This system will be further explored in this thesis and tested with the cadherin ligands.

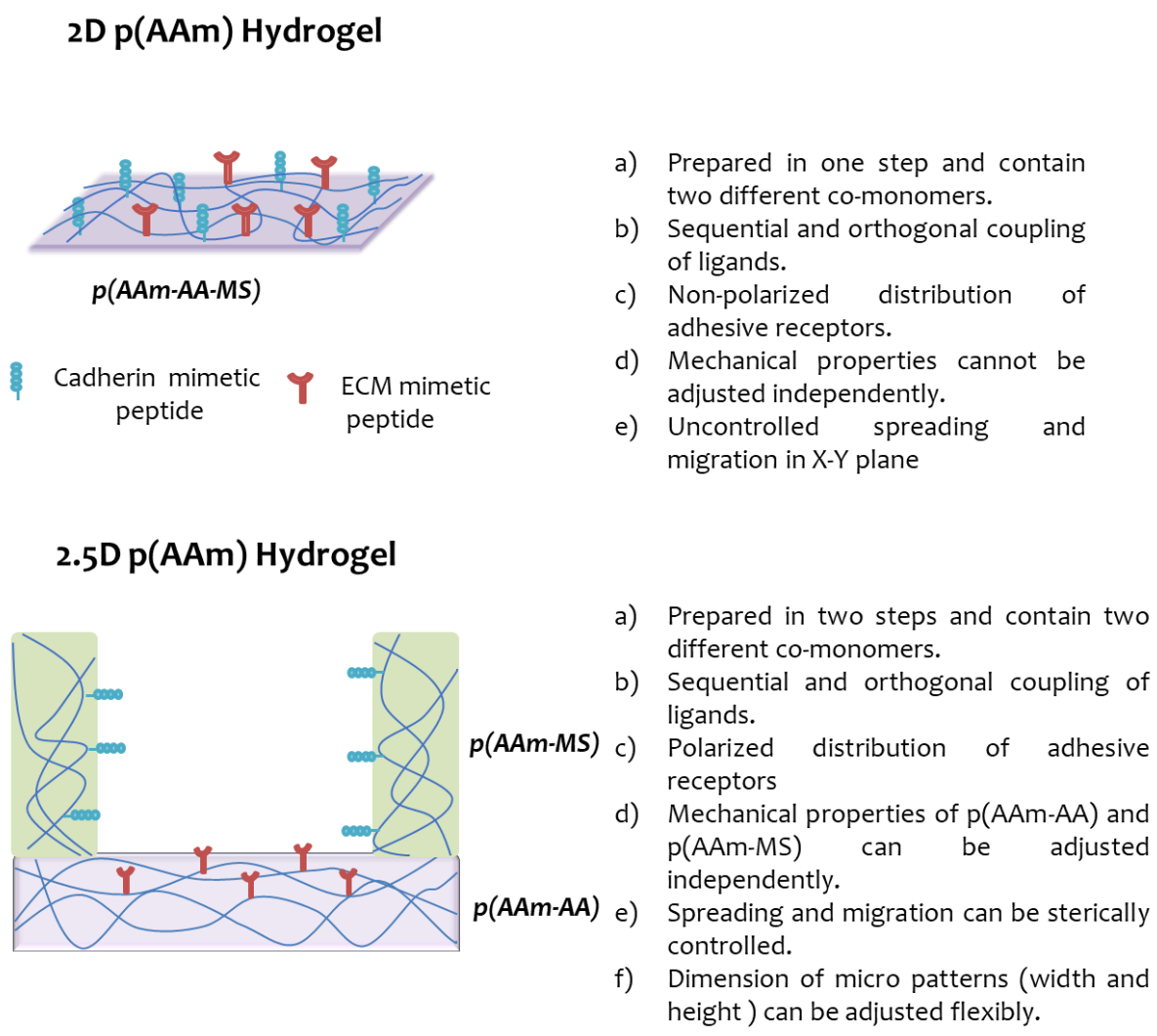

Fig. 3.2 *Schematic representation of 2D and 2.5D p(AAm) hydrogels*

3.2 Results and Discussion

3.2.1 Preparation of p(AAm-AA) and p(AAm-MS) hydrogel films with different mechanical properties

Thin films of p(AAm) hydrogel copolymerized with acrylic acid (AA) or -phenyl oxadiazole methylsulfonyl acrylate (MS) monomers were prepared by radical copolymerization following a reported protocol[129,131](**Fig. 3.3A&B**). Hydrogel films with Young's Moduli of 2, 10, 40, and 100 kPa were obtained by varying the amount of N,N′-methylene-bis-acrylamide crosslinker and acrylamide monomers. The thin films were supported by a coverslip, were transparent, and showed no topographic defects on the free surface. 2% (w/w) of MS or 10% (w/w) of AA were incorporated into the monomer mixtures. It is worth to mention that the MS comonomer cannot be introduced at higher concentrations because of its limited solubility in water. The MS monomer was dissolved in DMF and then added to the monomer mixtures. AA is fully soluble in water and can be introduced at any concentration. Introduction of the co-monomers to the AAm polymer network did not affect the polymerization reaction[124,129]. The radical polymerization is highly sensitive to oxygen. Therefore, for the preparation of the hydrogel films all the solutions were degassed and kept under inert atmosphere.

3.2.2 Preparation of bifunctional p(AAm-MS-AA) hydrogel films

Bifunctional hydrogels were prepared by copolymerizing AAm with MS and AA monomers following a reported protocol[129,131](**Fig. 3.3C**). The copolymerization of both ligands allows incorporation of both thiol and amine- containing ligands in the hydrogel. Reported work had demonstrated that the copolymerization didn't affect the physical properties of hydrogels significantly[124,129]. A concentration of 10 mol% of AA and 2 mol% MS comonomers was used. The bis-acrylamide crosslinker was added at different concentrations to obtain hydrogels with different mechanical properties. The hydrogels formed were transparent and without any topography defects. Details on the composition of the films are given in the experimental section.

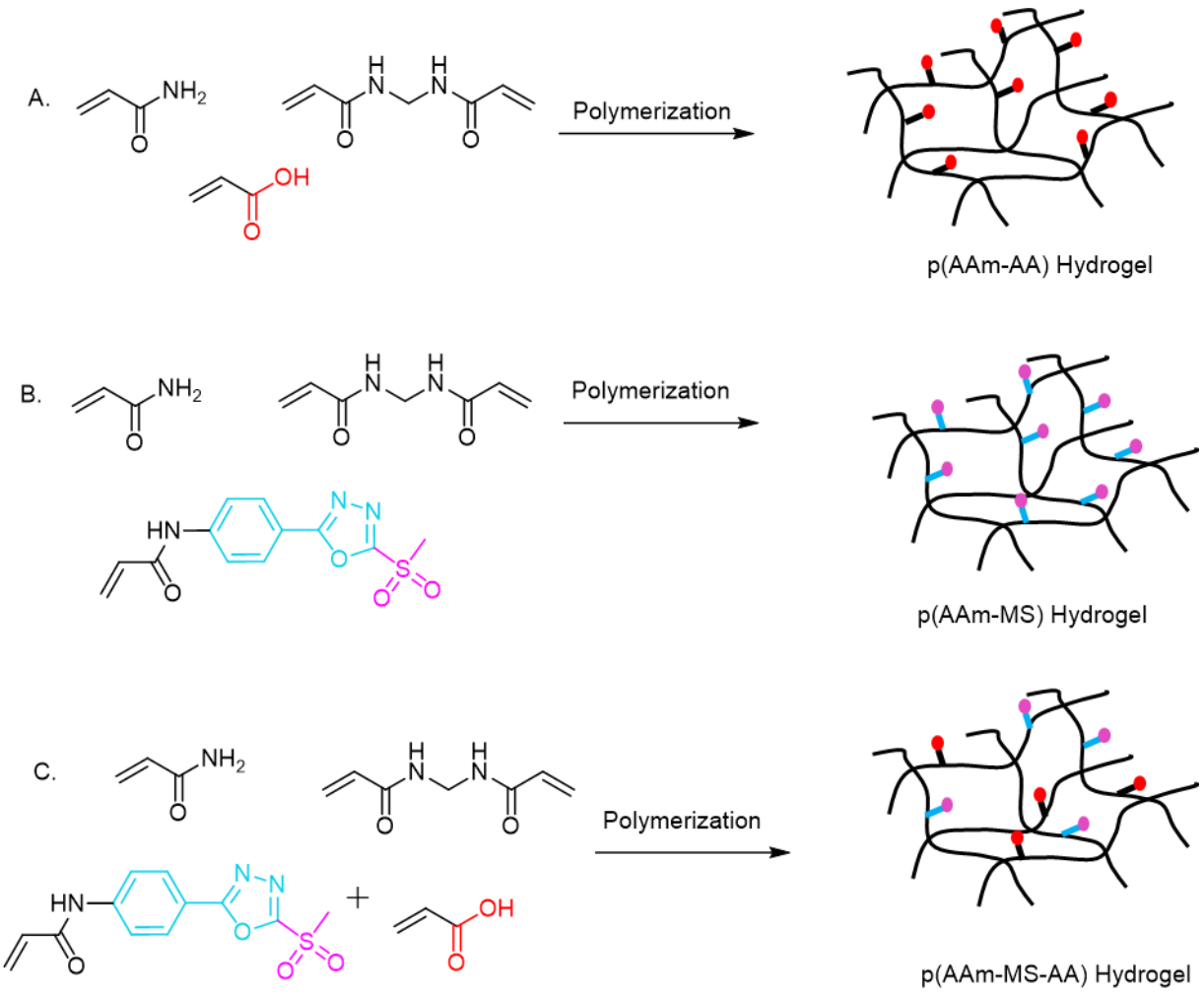

Fig. 3.3 *Schematic representation of the copolymerization of acrylamide and Bis-acrylamide with different comonomers (A) Copolymerization of p(AAm-AA) (B) Copolymerization of p(AAm-MS) (C) Copolymerization of p(AAm-MS-AA)*

3.2.3 Characterization of physical properties of p(AAm-AA) hydrogel films

The thickness, swelling degree and Young's modulus of the obtained p(AAm-AA) hydrogel films were tested. Established methodologies in the group were used for this purpose[129].

The thickness of p(AAm-AA) hydrogels was measured by confocal fluorescence microscopy after activation of the carboxylic groups with EDC/NHS chemistry and covalent coupling of the fluorescent dye pararosaniline. A z-stack across the hydrogel film allowed visualization of the gel thickness. Experiments were performed with films in both the dry and swollen states. The thickness of hydrogels in the dry state varied between 20 and 30 µm, and

increased with increasing monomer content. In the swollen state, the thickness of the films increased to 85-93 µm **(Table 3.1)**. It is important to note that the gel preparation protocols were optimized to get films with comparable swollen thickness[131]. This is an important parameter for the subsequent cell experiments. It has been reported that a film thickness >70 µm is necessary for cells not to detect the mechanical properties of the underlying glass substrate[132].

The homogeneity of the fluorescence across the film shows that the functionalization of hydrogel is homogeneous throughout the gel, meaning that the ligands are distributed evenly throughout the whole hydrogel from top to bottom. This implies that the functionalization of AA monomer with EDC/NHS chemistry was homogeneous and the coupled ligand distributed evenly throughout the gel film (**Fig. 3.4**).

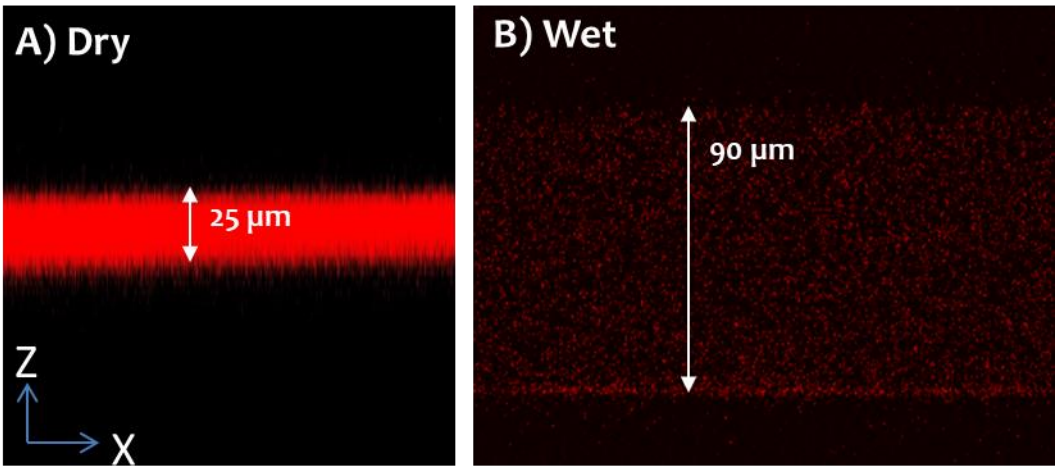

Fig. 3.4 *Representative z-stacks of fluorescence intensity of a 20 kPa p(AAm)-AA hydrogel after reaction with pararosaniline. A) Dry gel B) Swollen gel.*

The swelling ratio of the polymers, i.e. the capacity to hold water, was determined by gravimetry[59]. The hydrogel samples were prepared in an Eppendorf tube and the swelling ratio was determined by comparing the weight of the samples after soaking in water for 24 hours (Ws) and after drying for 24 h at 40 °C in a vacuum oven (W_d). The swelling ratio (SR) was calculated as $(\boldsymbol{Ws}-\boldsymbol{Wd})/\boldsymbol{Wd}$. **Table 3.1** shows that swelling ratios between 5.8 and 14.4 were obtained. The swelling ratio increased with the ratio of AAm monomer to bis-AAm crosslinker. The higher the crosslinking degree (e.g. the higher the bis-AAm crosslinker concentration), the lower the amount of water that the network can uptake.

The Young's modulus of the hydrogels was calculated by rheology using a plate-plate rheometer. The hydrogel sample was surrounded with low viscosity mineral oil to avoid drying of the hydrogel during the measurement. The Young's modulus (E) was calculated from the experimentally determined shear modulus (G´) from: $\boldsymbol{E=2G'\ x\ (1+\nu)}$, where $\boldsymbol{\nu}$ is the Poisson ratio. The mechanical properties of a swollen hydrogel is similar to rubber-like materials, having Poisson ratio as $\boldsymbol{\nu}$ = 0.5[133,134]. In this thesis hydrogels were always used in swollen form for biological experiments. Hence the passion ratio was taken as 0.5. The obtained values for the Young's modulus of the p(AAm-AA) hydrogels were 3, 13, 21, 40 and 101 kPa, very close to the previously reported values for gels with similar compositions[131]. The Young's modulus of hydrogels increased with increasing crosslinker concentration.

The obtained results for the p(AAm-AA) hydrogels were in agreement with previously reported data[131]. p(AAm-MS) hydrogels were also obtained following an established method in the group and used without further characterization[129].

Table 3.1 *Physical properties of p(AAm-AA) hydrogels*

Volume of monomers solution (µL) 2% of acrylamide		7.5	6	12	18	18
Bis-acrylamide/acrylamide ratio		0.8 %	3.3 %	1.6 %	1.1 %	5.5%
Young's modulus E (kPa)	**obtained**	3.0 (2±1.0)	13.1 (10±3.1)	21.2 (20±1.2)	39.8 (40±0.2)	101.3 (100±1.3)
Swelling ratio		14.4 ± 1.5	13.5 ± 1.2	11.33± 1.6	9.4±1.1	5.8±1.2
Thickness (µm)	**Dry**	20	22.5	25	27.5	30
	Wet	92	91	90	91	89

3.2.4 Functionalization of p(AAm-AA) and p(AAm-MS) hydrogels with cadherin peptidomimetics

The p(AAm-AA) or p(AAm-MS) hydrogels were functionalized with photoactivatable E-cadherin or N-cadherin mimetic peptides containing N-terminal Lys or Cys residues **(Chapter 2, Table2.1)** following a previously reported procedure[129]. The immobilization of the peptides to the hydrogels occurred by reaction of the $-NH_2$ amine of the N-terminus with -COOH groups of the AA monomer after activation of the carboxylic groups as NHS esters or by reaction of -SH side group of Cys with the MS moieties. **(Fig. 3.5)**. In order to test the coupling conditions for effective binding of the peptides to the hydrogel network, and to quantify the peptide density

after functionalization, I took advantage of the strong UV-Vis absorbance of the Ru-modified peptides and characterized the hydrogels by UV spectroscopy after the coupling reaction. For initial studies the chromophore, Pararosaniline hydrochloride was also used to avoid consumption of the amine bearing peptide. The coupling and quantification methodologies were adapted from previous studies[129].

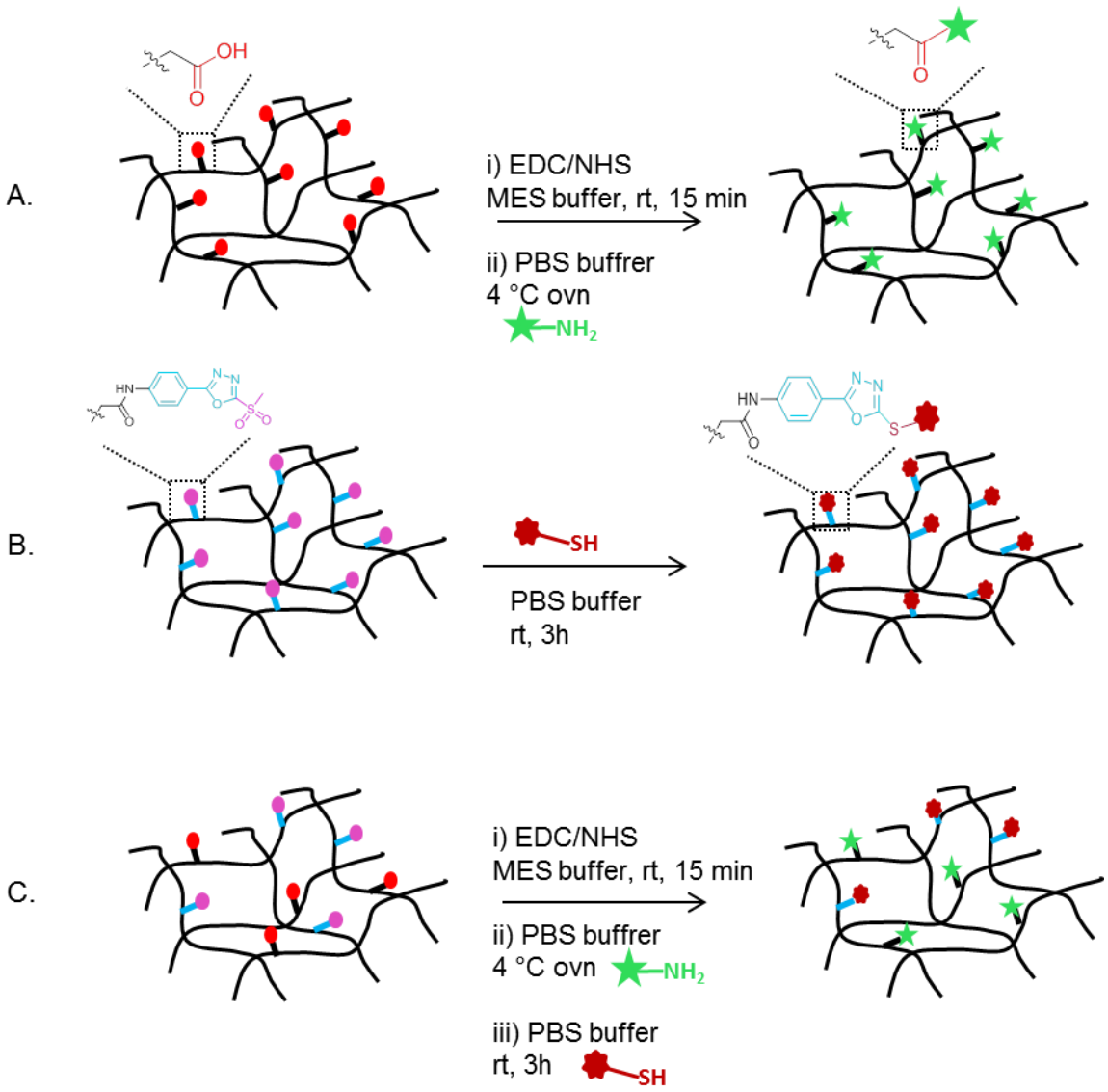

Fig. 3.5 *Bio-functionalization reactions on the hydrogels. (A) Conjugation of p(AAm-AA) with amine containing molecules. (B) Reaction of p(AAm-MS) with thiol containing molecules. (C) Sequential coupling of amine and thiol containing molecules to p(AAm-AA-MS) hydrogel*[129].

Fig. 3.6A&B show exemplary UV spectra of p(AAm-AA) hydrogels after reaction with pararosaniline, and of p(AAm-MS) hydrogels after reaction with the Cys terminated peptide H[Ru(bpy)$_2$PPh$_3$]AVDIGGGC and washing with water to remove unreacted compounds. **Fig. 3.6C** shows the UV spectra of p(AAm-AA) hydrogels having different stiffness functionalized

with pararosaniline of particular initial concentration and which resulted in similar absorbance. The spectra show absorption maxima at λ_{max} 560 nm and 425 nm respectively, consistent with the expected absorbance maxima of the pararosaniline and Ru complex. This result confirms the presence of the ligands in the network. Increasing incubation concentrations of the chromophore from 0.1 mg/mL to 1 mg/mL resulted in increasing absorbance values. Note that 1 mg/mL is the solubility limit for some of the peptidomimetics in this thesis.

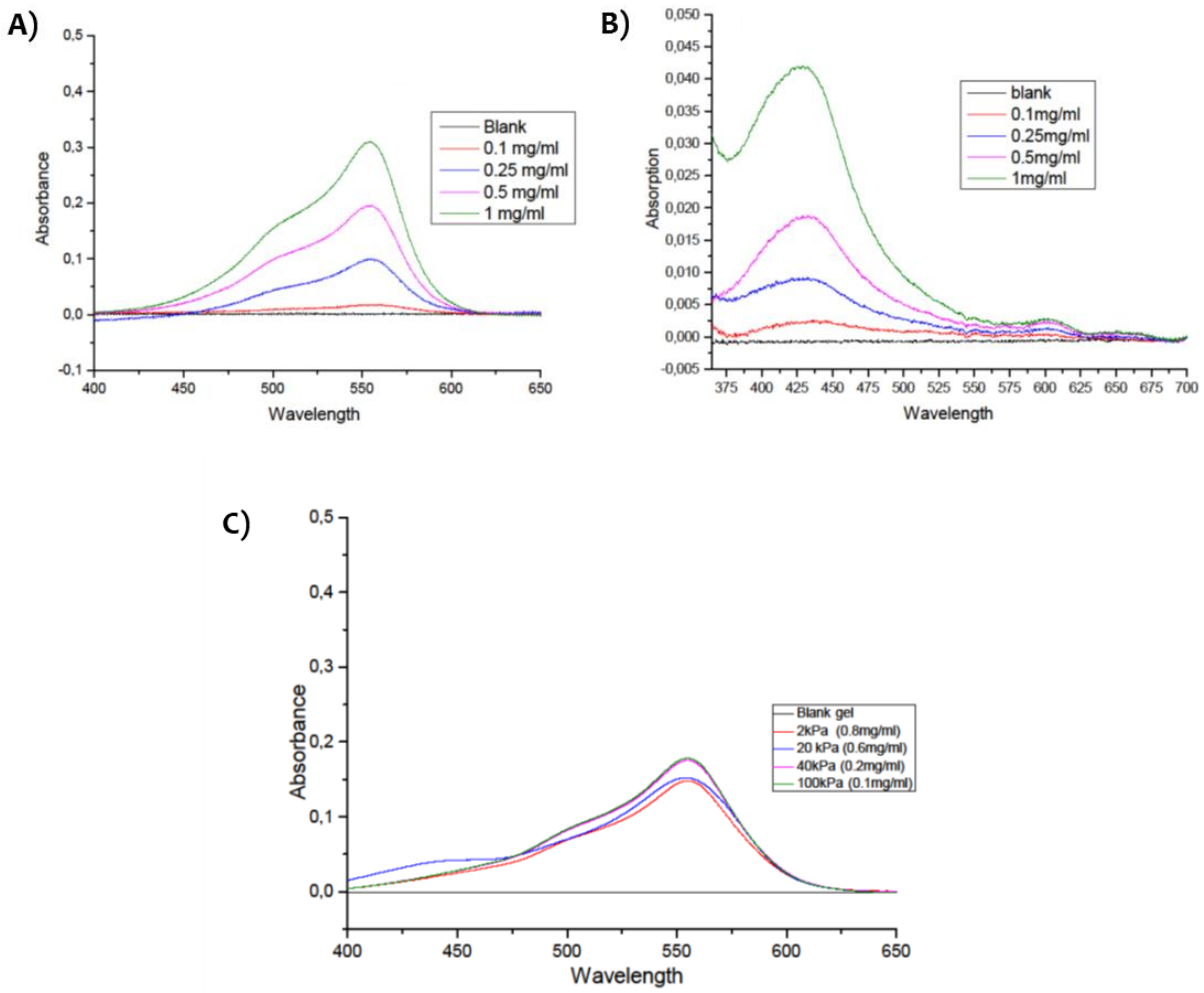

Fig. 3.6 *UV-Vis spectra of hydrogels after incubation with reactive molecules at different concentrations. A) 100kPa p(AAm-AA) hydrogels functionalized with pararosaniline base. B) 10kPa p(AAM-MS) hydrogels functionalized with H[Ru(bpy)$_2$PPh$_3$]AVDIGGGC. C) p(AAm-AA) hydrogels of different stiffness functionalized with pararosaniline base.*

The concentration of peptide in the hydrogel was calculated from the absorbance values by applying the Beer-Lambert law, $C = A/l\varepsilon$, where C is the concentration of the chromophore, A is the absorbance value at λ_{max}, l is the path length and ε is the molar extinction

coefficient at $\lambda_{max.}$ The reported values for extinction coefficients at respective λ_{max} of Pararosaniline and $[Ru(bpy)_2PPh_3]^{2+}$ complex are $3.0x10^4$ and 6400 $M^{-1}cm^{-1}$ respectively[113,135]. In this experiment the path length corresponds to the thickness of the swollen hydrogel film, which was 90 µm as determined by fluorescence confocal microscopy **(section 3.2.3). Table 3.1** shows that the calculated ligand density in each hydrogel increased with increasing concentration of incubating solution. The binding efficiency of chromophores to two different monomers were then calculated by; Binding Efficiency (%) = C in gel / C in solution x 100. Coupling of the peptide to the MS monomer showed > 80% binding efficiency for concentrations above 0.1 mg/mL. At the maximum tested concentration of 1 mg/mL, a binding efficiency of 98% was observed to the p(AAm-MS) hydrogel network. Binding efficiency of pararosaniline to p(AAm-AA) hydrogels was lower. A maximum of 78% was obtained by coupling 1 mg/mL solution to AA monomer. The obtained values for binding efficiency were in agreement with previously reported data with other peptides[124,129]. The final concentration of pararosaniline on p(AAm-AA) substrates of different hydrogels were adjusted to the concentration on 100 kPa hydrogel by adjusting the concentration of incubating solution. This was important for stiffness-based cell experiments. These experiments provide information on the expected ligand density on the hydrogels, available for recognition by cells.

Table: 3.1 *Binding efficiency of the peptide, H[Ru(bpy)$_2$PPh$_3$]AVDIGGGC and pararosaniline on p(AAm-MS)and p(AAm-AA) hydrogels respectively.*

Concentration of peptide in solution		Concentration of peptide in p(AAm-MS)	Binding efficiency in p(AAm-MS)	Concentration of pararoaniline in solution		Concentration of pararoaniline in p(AAm-AA)	Binding efficiency in p(AAm-AA)
mg/ml	*(mM)*	*(mM)*	*(%)*	*mg/ml*	*(mM)*	*(mM)*	*(%)*
0.1	0.06	0.05	82	0.1	0.30	0.21	68
0.25	0.16	0.14	87	0.25	0.77	0.54	71
0.5	0.32	0.29	92	0.5	1.50	1.10	73
1	0.64	0.63	98	1	3.09	2.41	78

3.2.5 Functionalization of p(AAm-AA) and p(AAm-MS) gels with cadherin proteins

After providing that the p(AAm-AA) and p(AAm-MS) hydrogels could be effectively functionalized with amine and thiol-bearing species, the gels were modified with commercially available recombinant E- and N-cadherin protein fragments and used as positive controls for the mimetic peptides in the cell experiments. The coupling of the proteins to the hydrogels

was performed by direct covalent coupling of the protein, or by using molecular recognition motifs.

In the direct covalent coupling, the activated carboxylic or MS groups on the hydrogels were coupled to the amines at the side chains of Lys residues or to the thiol groups at the side chain of Cys residues in the protein chain. Lys residues are very abundant in protein sequences. Both E- and N-cadherin proteins contain 8 Cys residues in their primary structure[136,137]. The covalent coupling of proteins has several advantages over non-covalent alternatives: the protein is stably attached to the gel, and the protein density can be regulated by the incubation concentration, as demonstrated with the peptides in the previous section. This methodology has, however, also some disadvantages. Lys and Cys residues are spread along the sequence of the protein and binding can occur at any (or many) of the residues. This can affect the functionality of the protein. In addition, the protein is immobilized in a non-oriented fashion, and the binding site for the cells may not be exposed.

The coupling protocol for N-cadherin protein to p(AAm-MS) hydrogel through Cys was previously developed in the group, and was used for this thesis without further modification (manuscript in preparation). For the modification of p(AAm-MS) and p(AAm-AA) hydrogel surfaces with E-cadherin protein different strategies were developed. Firstly, E-cadherin protein was directly coupled to p(AAm-MS) and p(AAm-AA) hydrogels through Cys and Lys respectively. And quantification of E-cadherin density on the immobilized surface was performed by staining with anti-E cadherin antibody and measuring fluorescent intensity by confocal microscopy. To ensure maximal binding of E-cadherin, excess amounts of E-cadherin protein were used for functionalization. At the same incubation concentration of E-cadherin, p(AAm-MS) gels showed higher fluorescence intensity than p(AAm-AA) hydrogels. This result indicates that coupling E-cadherin through Cys/MS chemistry was more efficient than coupling through Lys/AA chemistry, despite there being a lower concentration of MS groups (2.2 % mol/mol) in p(AAm-MS) than AA groups (10 % mol/mol) in p(AAm-AA). Taking into account that the number of Lys amino acids in the E-cadherin protein is higher than the Cys residues, this result indicates that either the SH/MS reaction is more efficient or the Cys residues are less shielded for reaction than the Lys in the protein structure (**Fig. 3.7**).

As an alternative coupling method, molecular recognition motifs were immobilized on the hydrogel and used to bind to affinity tags at the N or C terminus of cadherin domains. In particular, commercially available Fc tagged cadherins were used. The Fc domain has a strong affinity towards Protein A/G ($K_d \sim 10$ nM), which was immobilized on the gel. Protein A/G has

six Fc binding domains, four from Protein A and two from protein G. Compared to covalent binding, Fc-Protein A/G coupling is advantageous as it binds the protein to the surface in an oriented fashion[138]. The disadvantages of the method are the high production cost and the sensitivity to pH of the Protein A/G. It is important to point out that Fc-Protein A/G interaction has been used to immobilize E-cadherin protein to p(AAm-SulfoSANPAH) gels[87]. For the studies in this thesis, p(AAm-AA) hydrogels were used to immobilize Protein A/G via Lys residues, since the protein does not contain Cys residues in its sequence. The fluorescent intensity was measured by confocal microscopy. A higher amount of E-cadherin was observed on Protein A/G functionalized p(AAm-AA) hydrogel surfaces compared with the direct, Lys-mediated, covalent coupling of E-cadherin (**Fig. 3.7**).

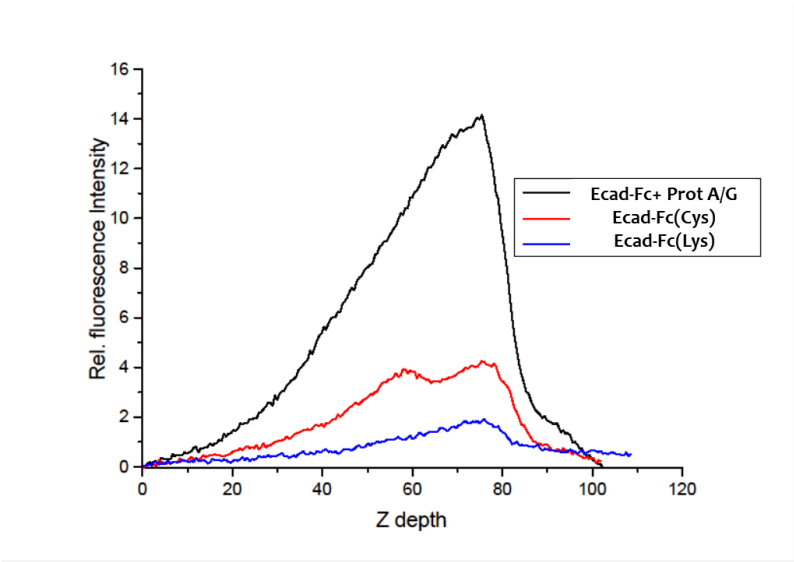

Fig. 3.7 *Relative fluorescence intensity of anti-E cadherin on the p(AAm) hydrogels modified with E- cadherin by different coupling methods.*

An alternative strategy to bind Fc-tagged proteins to surfaces is by using affinity peptides for the Fc domain[138]. These affinity peptides are used in antibody purification chromatography. Compared to Protein A/G, short affinity peptides are of smaller size and their immobilization on the gel is expected to be easier and more quantitative. Among the reported Fc affinity ligands, the 13mer DCAWHLGELVWCT-NH2 cyclic peptide (K_d = 16 nm) was selected for its reported high binding affinity[138]. This peptide is much smaller than compared to Protein A/G and its binding to Fc domain is only two-fold weaker. For immobilization to the gel, the peptide was extended with a flexible GGG spacer and an N-terminal Lys residue for binding to AA in the hydrogel. The peptide (DCAWHLGELVWCTGGGK-NH2) was immobilized on p(AAm-AA) hydrogels through the amine of the side chain Lys residue with previously NHS activated -COOH groups of the AA monomer in the hydrogel. This peptide was soluble in PBS (pH 7.4) at a 1

mg/mL concentration. Modification of the peptide with a terminal Cys was not convenient since the peptide contains two Cys for cyclisation. So, the coupling was not tested on p(AAM-MS) hydrogels. E-cadherin binding to 13mer peptide was tested directly by cell experiments **(Chapter 4, section 4.2.3).**

3.2.6. Photolysis of H[Ru(bpy)$_2$PPh$_3$]AVDIGGGC on p(AAm-MS) hydrogels

The photolysis of the photoactivatable N-cadherin peptide H[Ru(bpy)$_2$PPh$_3$]AVDIGGGC in the gel-immobilized state was analyzed by UV spectroscopy, and compared to the photolysis behavior in solution described in **Chapter 2**. Photolysis studies were performed to identify the minimum irradiation dose required to activate the peptides on the hydrogel, which is an important information for later experiments with living cells. p(AAm-MS) hydrogels functionalized with H[Ru(bpy)$_2$PPh$_3$]AVDIGGGC as described in **section 3.2.4** were irradiated at 420 nm for increasing times and washed with PBS to remove the photolysis by-product. A decrease in the absorbance at λ_{max} = 423 nm, which corresponds to the intact Ru complex, was observed with increasing irradiation doses **(Fig. 3.8)**. This result indicates that the chromophore is cleaved from the hydrogel by the light exposure and removed by the washing step.

The decay of the absorbance in the hydrogel can be used to estimate the yield of the photolysis reaction. The concentration of peptide in hydrogel was calculated from absorbance values obtained from the UV spectra by applying the Beer-Lambert law, $C = A/l\varepsilon$, as described above **(section 3.2.4)** and the photolysis yield was determined (**section 3.4.11.**). UV absorbance showed a clear decay just after 2 minutes of irradiation. A 52% yield was obtained for H[Ru(bpy)$_2$PPh$_3$]AVDIGGGC after 10 minutes of irradiation. The rate of photolysis on hydrogel was slower than in solution. 10 minutes exposure time was selected for the cell studies, since longer irradiation times were not compatible with cells (see **chapter 5, section 5.3**).

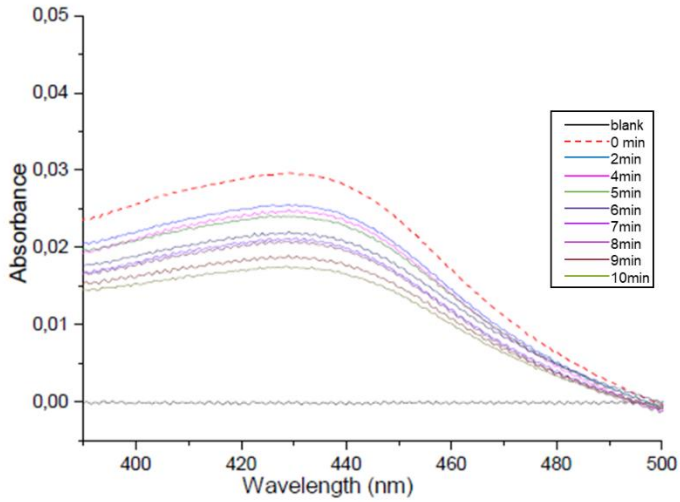

Fig. 3.8 *UV-Vis spectra of p(AAm-MS) hydrogels modified with H[Ru(bpy)$_2$PPh$_3$]AVDIGGGC peptide and exposed to 420 nm light at increasing exposure times.*

3.2.7 Fabrication of 2.5D hydrogel microenvironments

In del Campo's Lab at INM, micropatterned poly(acrylamide) hydrogels with channels that have different biofunctionalization on the bottom and on the walls were developed (manuscript in preparation). These micropatterns represent the polarized environment of epithelial cells, which are exposed to matrix proteins at the basal plane and cell adhesive proteins on the lateral plane. The micropatterned hydrogels consist of two hydrogel layers **(Fig.3.2)**. The bottom layer is a p(AAm-AA) thin film, which is topped with a soft-molded p(AAm-MS) layer using a PDMS stamp with microwalls or micropillars of defined dimensions (**Fig. 3.8A**). These constructs provide a micropatterned hydrogel with microchannels or microwells that can be derivatized with different cell adhesive ligands at the bottom or at the walls due to the orthogonality of the thiol/MS and amine/COOH-NHS reaction. Previous work by Dr. Aleeza Farrukh in the group has demonstrated the polarized functionalization and the response of C2C12 myofibroblasts to this environment. These results (unpublished) served as basis for the work in this thesis. All working protocols for the construction and derivatization of the 2.5D platform were up taken.

To fabricate the polarized microenvironments, a PDMS stamp was used to soft mold the patterned second hydrogel layer on top of the p(AAm-AA) film. Since the polymerization of the two layers is independent, the mechanical properties (as well as the comonomer type) of each layer can be adjusted independently. For this work, hydrogels with Young´s modulus

of 10kPa were used in both layers. This stiffness is similar to the stiffness of muscle tissue and has already been reported to support myogenic differentiation[139,140]. The geometry and dimensions of the PDMS stamp were selected based on previous studies. In particular, a stamp rendering hydrogel microchannels with 5 µm width, 5-8 µm height and 15 µm length was used. The microchannels were separated by walls of 50 µm width**.**

The copolymerization of AA in the bottom layer gel and MS in the top layer allowed site-specific positioning of amine or thiol containing ligands at the bottom or at the walls of the channels. In order to prove the selective biofunctionalization, the 2.5D hydrogels were incubated with Rhodamine-labeled polylysine (*Rh-PL-NH2*) and FITC-labeled PEG-SH. Confocal imaging revealed red fluorescence exclusively at the bottom layer, and green fluorescence exclusively at the top layer **(Fig. 3.8D&E).** This result confirms the localization of the comonomers in only one of the layers, and the orthogonality of the coupling reactions. Z-stack imaging across the bilayer allowed visualization of the thickness of the individual layers. The thickness of the swollen bottom layer was in the range of 50-65 µm, whereas the height of the walls of the channels in the top layer was 5-8 µm depending upon the composition of the Bis-acrylamide concentration in the precursor mixture.

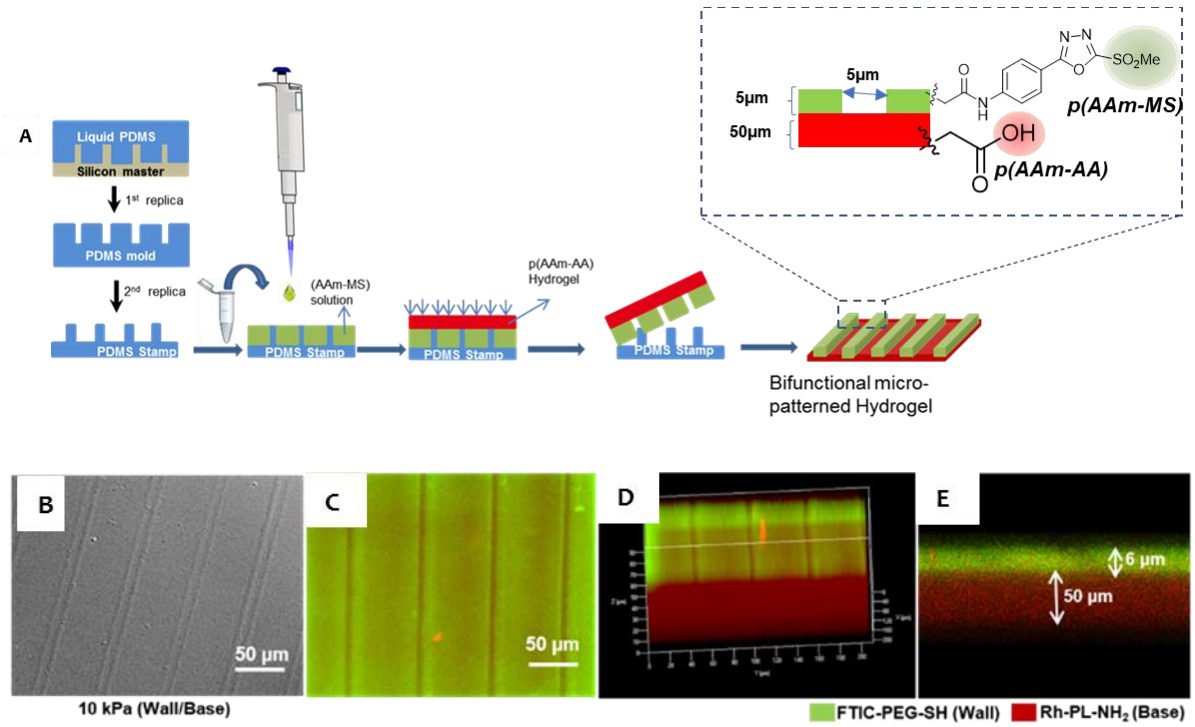

Fig. 3.9 *(A) Schematic representation of fabrication of bilayer hydrogels (B) Phase contrast image of a 2.5D hydrogel with 5 µm wide channels separated by 50 µm wide walls. (C) Confocal*

fluorescence image of the same 2.5D gel after reaction with Rh-PL-NH2 and FITC-labeled PEG-SH. (E) Confocal Z-stack from gel in (D) shows each fluorescent labeled Rh-PL-NH2 and FITC-PEG-SH reacted selectively with one of the layers, demonstrating the orthogonality of the coupling reaction. In (F) the section of the hydrogel reveals the thickness of the independent layers. (This experiment was performed in collaboration with Dr. Aleeza Farrukh).

The 2.5D hydrogels were used to investigate the effect of photoactivatable N-cadherin peptide in the myogenic differentiation of C2C12 mouse myoblast cell line in **chapter 5**. For that, the bottom layer, p(AAm-co-AA) was functionalized with ECM mimetic cyclo(RGDfK) peptide containing a Lys residue, and the p(AAm-co-MS) side walls were functionalized with N-cadherin mimetic peptides; HAVDIGGGC, H[Ru(bpy)$_2$PPh$_3$]AVDIGGGC, AGVGDHIGC or N-cadherin protein (CD2) through a Cys residue. The coupling was performed by using the same strategy used for 2D hydrogels **(section 3.2.4 &3.2.5).**

3.3 Conclusion

Copolymers of p(AAm) hydrogels that allowed amine and thiol bioconjugation were synthesized and characterized. Amine and thiol containing ligands were incorporated into hydrogel networks under physiological conditions. N-cadherin protein was successfully coupled to p(AAm) hydrogel through MS monomer. For the coupling of E-cadherin protein direct coupling to AA or MS were studied, but the obtained ligand density was much lower. Coupling of E-cadherin mediated by Protein A/G and Fc-binding peptides lead to improved ligand densities on hydrogel network. Photolysis studies of H[Ru(bpy)$_2$PPh$_3$]AVDIGGGC peptide on the hydrogels showed a light-regulated release of the protecting group, [Ru(bpy)$_2$PPh$_3$H$_2$O]. A bilayer micropatterned 2.5D hydrogel model based on polyacrylamide was fabricated for spatial segregation of cell-matrix and cell-cell interactions using integrin and cadherin specific peptidomimetics.

3.4 Experimental section

3.4.1 Materials and methods

Solvents and reagents: Acrylamide (AAm), N,N′-Methylenebis(acrylamide), Acrylic acid (AA), N,N,N′,N′-Tetramethylethylenediamine (TEMED), Ammonium persulfate (APS), N-(3-Dimethylaminopropyl)-N′-ethylcarbodiimide hydrochloride) (EDC), N-Hydroxysuccinimide (NHS), Pararosaniline hydrochloride and 2-(N-Morpholino)ethanesulfonic acid (MES) were purchased from Sigma-Aldrich Chemie GmbH and solvents were purchased from Sigma-Aldrich

Chemie GmbH and were used without further purification. The Methylsulfone acrylates (MS) was synthesized by following the reported protocol without modification[124].

3.4.2 Preparation of APTMS functionalized coverslips

3-Acrylpropyl–trimethoxysilane (APTMS) functionalized coverslips were prepared by following the reported protocol[124,129,139,141]. 13 mm round coverslips were washed with EtOH and immersed in 0.5% APTMS solution in water: ethanol (5:95%, v/ v) for 4 h. The coverslips were washed with EtOH and water, then dried at 80 °C in a *vacuum* oven for 1 h.

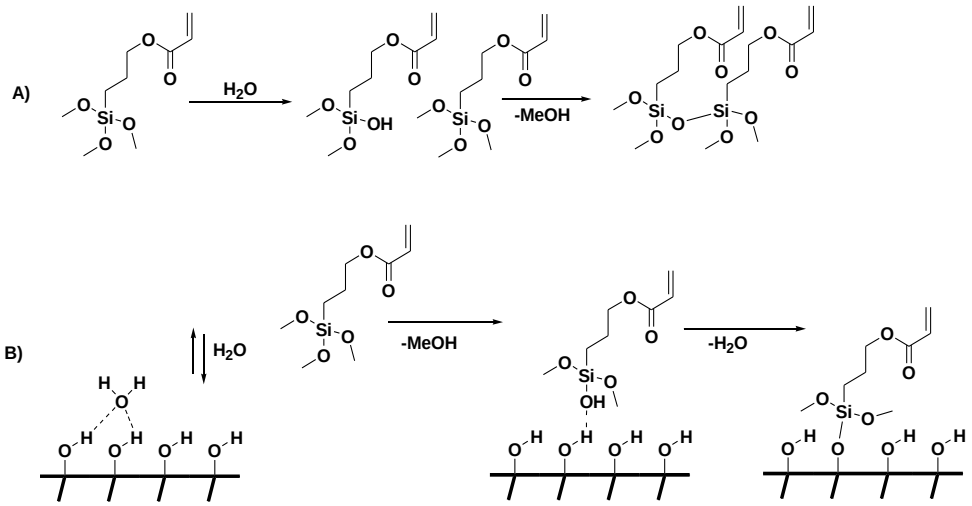

Fig. 3.10 *Modification of coverslips with APTMS (A) APTMS hydrolysis followed by condensation reaction in solution phase (B) APTMS hydrolysis followed by condensation on hydrated SiO_2 surface*

3.4.3 Preparation of Sigmacote-coated glass

Sigmacote-coated (it's a silanising agent that creates hydrophobic surface), glass slides were prepared by adapting a reported protocol[124,129,139,141]. 25x75 mm glass slides were washed with EtOH and dried with Nitrogen. Glass slides were immersed in commercial Sigmacote® solution and shaken for 30 min at r.t. The glass slides were washed with EtOH and water, then dried using vacuum.

3.4.4 Preparation of p(AAm-AA) hydrogel films

p(AAm-AA) hydrogels were prepared by following a reported protocol[124,129,139,141]. Briefly, acrylamide (7.5 - 18 wt %) was dissolved in PBS (pH 7.4) (1 mL). Acrylic acid (AA) (10% w/w to AAm), and N,N′-Methylenebis(acrylamide) (0.06 - 0.2% w/w) were added to the above

solution and 0.1 M NaOH aq. solution was used to adjust the pH to 8. Then oxygen was removed by degassing the monomer solution, and the initiator APS (10% w/w solution in water, 1/100 of total volume) and TEMED catalyst (1/1000 of total volume) were added. 10 µL of the monomer solution was pipetted on a glass slide coated with sigmacote and covered with an APTMS functionalized coverslip. The hydrogel formed in between the sigmacote-coated glass slide and covalently anchored to the APTMS functionalized coverslip. After 5 min, the hydrogel bound to the APTMS functionalized coverslip was removed from the Sigmacote glass slide in water and kept in PBS (pH 7.4) at 4 °C until further use.

3.4.5 Preparation of p(AAm-MS) hydrogels

p(AAm-MS) hydrogels were prepared following a reported protocol[124,129,139,141]. Briefly, Acrylamide (7.5 – 12% w/w) was dissolved in PBS (1 mL, pH 7.4). N,N′-Methylenebis(acrylamide) (0.06 – 0.2% w/w) was added to the above solution and oxygen was removed by degassing the monomer solution. Into this premixed solution Methylsulfone acrylate (MS) comonomer (2% w/w) dissolved in dimethylformamide (DMF) (125 µL), the radical initiator APS (10% w/w solution in water, 1/100 of total volume), and TEMED catalyst (1/1000 of total volume) were added. 10 µL of the monomer solution was pipetted on a glass slide coated with sigmacote and covered with an APTMS functionalized coverslip. The hydrogel formed in between the sigmacote-coated glass slide and covalently anchored to the APTMS functionalized coverslip. After 5 min, the hydrogel bound to the APTMS functionalized coverslip was removed from the Sigmacote glass slide in water and kept in PBS (pH 7.4) at 4 °C until further use.

3.4.6 Preparation of p(AAm-AA-MS) hydrogels

p(AAm-AA-MS) hydrogels were prepared by adapting a reported protocol [124,129,139,141]. Briefly, acrylamide (7.5 - 18% w/w) was dissolved in PBS (pH 7.4) (1 mL). Acrylic acid (AA) (10% w/w to AAm), and N,N′-Methylenebis(acrylamide) (0.06 - 0.2% w/w) were added to the above solution and 0.1 M NaOH aq. solution was used to adjust the pH to 8. Then oxygen was removed by degassing the monomer solution, into this premixed solution Methylsulfone acrylate (MS) comonomer (2% w/w) dissolved in DMF (125 µL), the radical initiator APS (10% solution in water, 1/100 of total volume), and TEMED catalyst (1/1000 of total volume) were added. 10 µL of the monomer solution was pipetted on a glass slide coated with sigmacote and covered with an APTMS functionalized coverslip. The hydrogel formed in between the sigmacote-coated glass slide and covalently anchored to the APTMS functionalized coverslip.

After 5 min, the hydrogel bound to the APTMS functionalized coverslip was removed from the Sigmacote glass slide in water and kept in PBS (pH 7.4) at 4 °C until further use.

3.4.7 Functionalization of p(AAm-AA) hydrogels with amine bearing molecules

The carboxylic groups of AA in the hydrogel were activated by using EDC/NHS chemistry. For that, the hydrogel was covered with 100 µL solution of 0.2 M EDC and 0.1 M NHS in 0.1 M MES buffer (containing 0.5 M NaCl) for 15 min. Afterwards the hydrogels were washed with water and incubated overnight at 4 °C with 30 µL solution of the desired molecule in PBS (pH 7.4) and washed 3 times with water and then incubated with 10 mg/mL BSA in PBS (pH 7.4) for 30 min to block the unreacted activated carboxylic acids.

For E-cadherin peptides: After activation, the gels were washed and incubated with different concentrations of peptide solution (0.1 mg/mL to 1 mg/mL) in PBS (pH 7.4) for overnight at 4 °C and washed with water (3x).

For Pararosaniline: After activation, the gels were washed and incubated with different concentrations of Pararosaniline solution (0.1 mg/mL to 1 mg/mL) in PBS (pH 7.4) for overnight at 4 °C and washed with water (3x).

For E-cadherin-FC protein: After activation, the gels were washed and incubated with 300 µg/mL Protein A/G in PBS (pH 7.4) for overnight at 4 °C and washed with water (3x). Then incubated with 150 µg/mL E-cadherin: Fc for 3 h at r.t.

For Fc-binding peptide: After activation the gels were washed and incubated with Fc-binding peptide in PBS (pH 7.4) for overnight at 4 °C and washed with water (3x). Then the hydrogels were incubated with E-cadherin-Fc for 3 h at r.t.

3.4.8 Functionalization of p(AAm-MS) hydrogels with thiol containing molecules

The coupling of thiol containing molecules to p(AAm-MS) hydrogels was done by directly incubating the hydrogel with 30 µL of the peptide/protein solution in PBS (pH 7.4) for 3 h at r.t. After coupling the hydrogels were washed with water (3x).

For N-cadherin peptides: The gels were washed and incubated with N-cadherin mimetic peptide solution (0.05 mg/mL) in PBS (pH 7.4) for 3 h at r.t.

3.4.9 Characterization of hydrogels by rheology

100 µl of hydrogel monomer mixture were polymerized between two Sigmacote functionalized coverslips (13 mm). The obtained hydrogel film was immersed in PBS and removed from the coverslips. The storage modulus (G´) of swollen hydrogels was measured by dynamic mechanical analysis (DMA) using a plate-plate geometry on a Discovery HR-3 (TA instruments) rheometer at 25 °C, and at frequency of 0.1 rad/sec with 0.5 % applied strain at 0.5 N force. The hydrogel samples were prepared between two 13 mm Sigmacote-coated coverslips and swollen in PBs for overnight. The hydrogel formed in between the coverslips was removed and brought in contact with the upper rheometer plate. The Young´s modulus (E) was calculated from the storage modulus (G´) by using the $E = 2G'(1+\nu)$. Where $\boldsymbol{\nu}$ is the Poisson ratio.

3.4.10 Characterization of the thickness of dry and swollen gels

The thickness of the dry and swollen hydrogel samples after labeling with a 0.1 mg/mL Pararosaniline was measured by confocal microscopy using a Zeiss-LSM 880 with Airyscan. A Z-stack fluorescence measurement was first performed on the dry gel. 100 µL PBS solution with Fe_3O_4 nanoparticles (~ 1 mg/mL, 250 nm size) was added on to the hydrogel and allowed to preswell for 5 min, then the thickness was measured again to get the swollen thickness. The nanoparticles remained at the surface of the hydrogel and facilitated identification of the top layer of the hydrogel in swollen state.

3.4.11 Photolysis studies on hydrogel films

Hydrogels functionalized with H[Ru(bpy)$_2$PPh$_3$]AVDIGGGC were irradiated at λ_{max} ,420nm (0.34 mW/m^2) using a Xe-lamp equipped with a monochromator (Polychrome V, TILL Photonics GmbH, Gräfelting, Germany). The hydrogels were irradiated for different time intervals and washed with PBS to remove photolysis by-products after each irradiation. UV-Vis spectrum was measured after each irradiation. The photolysis yield on hydrogel was calculated from the concentration of H[Ru(bpy)$_2$PPh$_3$]AVDIGGGC in hydrogel and which is calculated by using the UV-absorbance by Beer-Lambert law: $\boldsymbol{C=A/l\varepsilon}$.

$$\boldsymbol{Photolysis\ Yield\ \%} = \frac{\boldsymbol{Ci - Cf}}{\boldsymbol{Ci}}\ \boldsymbol{x\ 100}$$

Ci = initial concentration; Cf = final concentration

3.4.12 Preparation of PDMS stamp for soft molding p(AAm) hydrogels

The PDMS stamp for bifunctional micro patterned hydrogel was fabricated using a double soft lithography process[142–145]. An existing SU-8 photolithographic template containing channels with width of 50 µm, spacing of 5 µm and height of 5 µm was used for this purpose. The SU-8 template was first treated with oxygen plasma (100 W, 0.1 mbar) for 2 min and perfluorinated in a vacuum desiccator for 30 min using ~60 µL of 1H,1H,2H,2H-perfluorodecyltrichlorosilane, then baked in a vacuum oven for 1 h at 120 °C. The PDMS precursor, Silgard 184A (Dow Corning, 10:1 prepolymer/crosslinker ratio) was mixed for 10 min and degassed for another 30 min. The degassed mixture was poured onto the SU-8 template and cured in a vacuum oven for 1 h at 120 °C. The produced PDMS mold with desired pattern was used as a mold in the second step, soft replication. The PDMS mold was then perfluorinated using the same condition as mentioned above for the SU-8 template. The PDMS precursor was prepared as described above and poured onto the perfluorinated PDMS soft mold and cured in a vacuum oven for 1 h at 120 °C and then demolded. Micropatterned PDMS stamps with channels with width of 5 µm, spacing of 50 µm and heights of 5 µm were obtained. Stamps were cut into small squares (14 mm^2) and perfluorinated using the same condition as for PDMS template.

3.4.13 Preparation of bilayer hydrogels

p(AAm-AA) hydrogel films were prepared as described in **section3.4.3.** The remaining PBS layer on the hydrogel was gently removed with a filter paper and the gels were placed in a petri dish covered with aluminum foil and left for drying (30 min). Rapid drying of the hydrogel inside a fume hood, under vacuum, or with nitrogen gun resulted in cracks on the gel surface. The monomer solution for the top layer of the hydrogels was prepared as described in section 2.3. A drop (2 µL) of the co-monomer solution was placed on the middle of PDMS stamp and instantaneously covered by the dry p(AAm-AA) gel. A gentle pressure was applied to squeeze out the excess of AAm-MS solution. After 8 min the PDMS stamp was gently separated from the bilayer hydrogel and hydrogels were kept in PBS at 4 °C.

3.4.14 Functionalization of bilayer hydrogels

The bilayer hydrogels were orthogonally functionalized with peptides and proteins as described.

Firstly, the bottom layer, p(AAm-AA) gel was functionalized with cyclo[RGDfK] peptide. The carboxylic groups of AA in the hydrogel were activated by using EDC/NHS chemistry. For that, the hydrogel was covered with 100 µL solution of 0.2 M EDC and 0.1 M NHS in MES buffer (0.1 M, containing 0.5 M NaCl) for 15 min. Afterwards the hydrogels were washed with water and incubated overnight at 4 °C with 30 µL solution of the desired molecule in PBS (pH 7.4) and washed 3 times with water and then incubated with 10 mg/mL BSA in PBS (pH 7.4) for 30 min to block the unreacted activated carboxylic acids.

Secondly, the coupling of thiol containing molecules to p(AAm-MS) hydrogels was done by incubating the hydrogel with 30 µL of the peptide solution in PBS (pH 7.4) for 3 h at room temperature. After coupling the hydrogels were washed three times with water.

For N-cadherin peptides: the gels were washed and incubated with different concentrations of thiolated peptides [HAVDIGGGC, AGVGDHIGC and H[$Ru(bpy)_2PPh_3$]AVDIGGGC], peptide solution (0.05 mg/mL) in PBS (pH 7.4) for 3 h at r.t.

For cyclo(RGDfK) peptide: After activation, the gels were washed and incubated with 0.1 mg/mL of peptide solution in PBS (pH 7.4) for overnight at 4 °C and washed with water (3 x).

Chapter 4

Evaluation of the activity of hydrogel-immobilized E-cadherin mimetic peptide in epithelial cell cultures

In this chapter, E-cadherin mimetic peptides His-Ala-Val (HAV), Ala-Asp-Thr (ADT), and Ser-Trp-Glu-Leu (SWEL) are immobilized on polyacrylamide surfaces and the adhesion and spreading of epithelial cells are studied. The interaction of E-cadherin mimetic peptides immobilized on polyacrylamide surfaces with E-cadherin protein on cell membrane is compared to the interaction between surface immobilized E-cadherin protein and E-cadherin protein on the cell membrane. A novel strategy is developed to immobilize E-cadherin protein on p(AAm) surface using Fc-binding peptides. The effect of elastic modulus on cell attachment and spreading is studied as function of E-cadherin derivatization on p(AAm) hydrogels of different mechanical properties. E-cadherin interaction mediated plasma membrane protrusion and organization of actin cytoskeleton was explored on novel E-cadherin mimetic hydrogels.

4.1 Introduction

Cell-cell interactions mediated by E-cadherin play a significant role in biological processes during development, wound healing and in tissue homeostasis[146]. E-cadherin adhesion complexes regulate signaling by linking to the actin cytoskeleton and other proteins (catenin, vinculin) at their cytoplasmic domains[147,148]. Previous studies of cells on E-cadherin surfaces shows that the establishment of cell-cell contacts reorganizes the actin cytoskeleton and is closely regulated by actin nucleating protein and Rho GTPases activity. Cell-cell adhesion is involved the lateral expansion of lamellipodia activity induced by Rac1 and ARP2/3 [149,150].

In order to study cadherin mediated cell-cell interactions, surfaces decorated with cadherin protein or fragments are used as models of the cell membrane. Such surfaces are used as culture substrates to which cells can establish cadherin-mediated contacts[51]. The

immobilization of cadherin on a synthetic interface allows the observation of cadherin-specific processes, isolated from other possible interactions at the natural cell-cell interface[51]. For example, polystyrene surfaces coated with E-cadherin induced spreading of embryonic stem cells and enhanced proliferation and paracrine function of MSCs[52]. Self-assembled monolayers (SAM) of thiols bearing benzylguanine (BG) groups at the end are covalently coupled to SNAP-tag attached extracellular domain of E-cadherin protein shows the effect of receptor density and specific contribution of individual extracellular domains. E-cadherin protein fragment containing five extracellular domains (EC1-5) efficiently promoted cell adhesion and spreading. Whereas, E-cadherin protein fragment consist of first and second outer-most extracellular domains (EC1-2) was not effectively promoted cell adhesion[54]. These results indicate that in the absence of integrin mediated cell adhesion all five extracellular domains in E-cadherin protein are required to facilitate cell adhesion and spreading.

E-cadherin mediated cell adhesion has been demonstrated to be sensitive to mechanical cues[58]. E-cadherin responds dynamically to changes in tension at cellular junctions[151]. The response of cells to external forces applied directly to cadherin using functionalized beads has been extensively studied[152–154]. More recently, the response of E-cadherin homophilic interactions to mechanics was investigated using polyacrylamide gels of different stiffness functionalized with extracellular domain of E-cadherin through a protein-substrate linker sulfo-SANPAH. Findings showed significant changes in morphology and membrane dynamics of Madin-Darby Canine Kidney (MDCK) cells cultured on hydrogels with varying Young's modulus between 30 kPa and 60 kPa[58].

Most of the experiments with E-cadherin coated surfaces have used the extracellular domain of E-cadherin protein for surface functionalization. This is in contrast with the extensive use of peptidomimetics preferred by the scientific community working with other adhesive ligands[68,74]. In contrast to the full-length proteins, peptidomimetics have high stability, can be easily synthesized and chemically modified. E-cadherin peptidomimetics have been used in solution to interfere with cell-cell contacts and modulate intercellular junctions in cell cultures in order to increase blood-brain barrier (BBB) permeability and enhance drug absorption[92–94]. For this purpose, E-cadherin peptides containing the evolutionary conserved tripeptide His-Ala-Val flanked by Ser residues from the groove region of EC1 domain, and the Ala-Asp-Thr sequence from the bulge region of EC1 domain have been used (**section 2.1.1.1**). Recently reported E-cadherin mimetic Ser-Trp-Glu-Leu peptide has been used to understand the structural and signaling role of E-cadherin in mouse embryonic stem cells (mESCs)[97]. No reports

have been found where E-cadherin peptidomimetics were used to study cell-cell interactions on model surfaces. In this chapter this possibility is explored. Model biointerfaces containing immobilized E-cadherin peptides on a poly(acrylamide) hydrogel are developed and the interaction of these surfaces with MDCK cells was tested. Lamellipodia activity, cell adhesion and spreading were studied as function of E-cadherin peptide concentration and stiffness.

4.2 Results and Discussion

4.2.1 Response of MDCK epithelial cells to hydrogels modified with E-cadherin peptidomimetics from the groove region (containing SHAVSS sequence)

E-cadherin mimetic peptides were reacted with p(AAm-MS) and p(AAm-AA) hydrogels as described in chapter 3 and used as a model bio-interface to study cell-cell interactions. Out of the different E-cadherin peptidometic sequences identified in the literature search (**section 1.6.1.1),** this section reports on studies with peptides containing the sequence SHAVSS**.** For coupling to the hydrogel, the functional sequence was extended with a Cys or Lys residue at the C-terminal end to allow anchoring to the p(AAm-MS) or p(AAm-AA) hydrogels respectively. In addition, a GGG flexible spacer was introduced in between the functional sequence and anchoring site to allow for more flexibility and facilitate orientation of the immobilized peptide for binding. For these studies MDCK cells were used as a model epithelial cell system. MDCKs have been shown to form adhesive structures with surfaces modified with E-cadherin and their cell-cell adhesion dynamics has been extensively studied[46]. Based on recently reported data on rigidity sensing of epithelial cells[58], hydrogels with Young's modulus of 100 kPa were used for the experiments.

SHAVSSC (HAV6)

Reported results had shown that the SHAVSS peptide inhibits E-cadherin mediated cell-cell adhesion in cultures of MDCK cells when applied to the cell culture medium at 1 mM

concentration for 2 h[91–93]. To determine whether this peptide can establish E-cadherin mediated cell-cell interactions on a model biointerface, MDCK cells were seeded on p(AAm-MS) hydrogels modified with SHAVSSC at different concentrations (0.001 - 2.0 mg/mL incubation concentration). The hydrogel surface was blocked with 1% BSA before cell seeding to avoid nonspecific attachment of cells. This step was necessary to reduce nonspecific attachment of the cells to the hydrogel and lead to higher contrast in the experiments. Cell culture on hydrogels functionalized with the integrin binding peptide cyclo(RGDfC) at 0.01 mg/mL incubation concentration were run in parallel as a positive control to observe MDCK attachment and spreading levels.

Fig. 4.1 shows MDCK cells on HAV6 modified hydrogels after 24 h of culture**.** Isolated clusters (3-5 cells) of MDCK cells were found on the HAV6 surfaces. Cells had a rounded morphology on all substrates, independently of the ligand concentration, indicating that they did not significantly interact with the peptide at the surface. Similar morphology was observed on the unmodified p(AAm-MS) surface blocked with BSA. In contrast, cells spread and formed large colonies on cyclo(RGDfC) modified hydrogels, indicating that they recognized and bound to the integrin-binding peptide. Note that, this type of cells have been reported to spread and form colonies on p(AAm) hydrogels modified with E-cadherin protein fragment[58]. Altogether, these results indicate that the SHAVSSC peptide is not sufficient to establish E-cadherin-E-cadherin adhesions and the model biointerface.

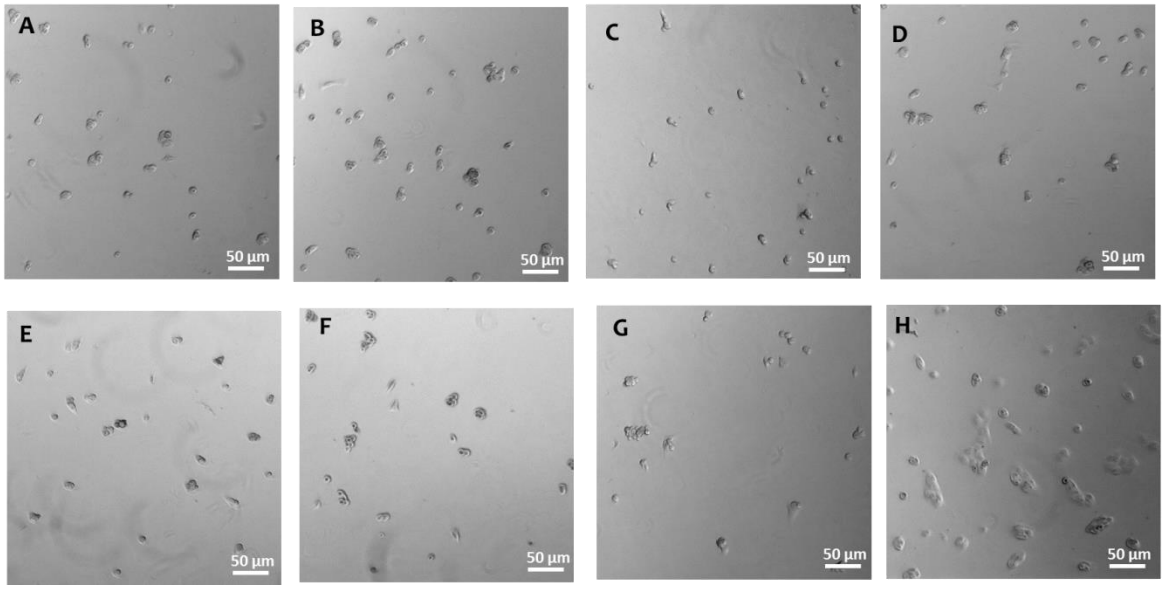

Fig. 4.1 *Bright field images of MDCK cells cultured on 100kPa pAAm-MS hydrogels functionalized with (A) 0.001 mg/mL HAV6, (B) 0.01 mg/mL, (C) 0.1 mg/mL HAV6, (D) 1 mg/mL HAV6, (E) 2 mg/mL HAV6, (F) 5 mg /mL HAV6, (G) 1% BSA, and (H) cyclo(RGDfC) 0.01 mg/mL for 24 h.*

One possible reason for the lack of spreading could be an insufficient concentration of the E-cadherin peptidomimetic on the surface. In order to rule out this possibility, parallel trials were performed on NEXTERION® Slide AL slides. These are commercial glass slides coated with a reactive poly(ethyleneglycol) layer containing aldehyde groups at high concentration. The HAV6 peptide with cysteine was coupled to the NEXTERION® Slide AL using a bifunctional amine-maleimide (N-(2-Aminoethyl)maleimide) linker. The NEXTERION slides were incubated with different concentration of HAV6 peptide (from 0.001 mg/mL to 2.0 mg/mL) and seeded with MDCK cells. MDCK cells showed similar features as observed in the hydrogels (**Fig. 4.13**). The cells formed clusters in solution and cell attachment was even less than on p(AAm) hydrogels. Cells on control substrates modified with cyclo(RGDfC) showed attachment and spreading. This observation indicates that the cells could not create a stable interaction mediated by E-cadherin with this surface type either. Most likely the short HAV6 peptide does not seem to be enough to support formation of E-cadherin mediated cell-hydrogel contacts.

SHAVSSGGGK (HAV10)

A longer peptide sequence was designed to increase the accessibility of the immobilized ligand to the membrane receptor at the cell surface. Compared to the short HAV6 peptide sequence, the HAV10 (SHAVSSGGGK) sequence contains a flexible GGG sequence between the active sequence (SHAVSS) and the anchoring site (Lys, K). The GGG spacer provides mobility and separates the active sequence from the surface. This could facilitate the access of the peptide to the membrane cadherin. And the coupling chemistry has been changed from MS/Cys to AA/Lys. The HAV10 peptide was coupled to p(AAm-AA) hydrogels of 100 kPa stiffness. A blocking step with 1% BSA protein to avoid nonspecific attachment of cells was also included.

The morphology of MDCK cells on HAV10 modified hydrogel surfaces after 24 h of culture is shown in **Fig. 4.2** MDCK cells showed a flattened morphology, they attached and spread on the surface, and they formed colonies with 8-10 cells. These features indicate that cells recognize the HAV10 peptide on the surface. The number of colonies (**Fig. 4.2G**) increased with HAV10 concentration up to 0.05 mg/mL, but decreased at higher concentrations. Cells on HAV10 surfaces incubated with peptide concentrations >0.05 mg/mL formed cell clusters without spreading and they were removed from surfaces during washing, which is an indication of lower interaction with the surface. Hydrogels not functionalized with the peptide failed to support cell attachment, indicating that the attachment and spreading is a

consequence of specific interaction with the surface peptide. These results indicate that the introduction of the GGG spacer on the peptide sequence, and the consequent increased mobility and reduced steric hindering from the surface, could be favorable for the interaction of HAV peptides to the E-cadherin on the cell membrane. However, it should be noted that the concentration of HAV6 and HAV10 peptides on the hydrogel surfaces could be different, since different coupling chemistries were used. This fact hinders a conclusive statement about the benefit of the flexible spacer for binding. The biphasic response of cell adhesion and spreading on low-to high concentrations of HAV10 found in these experiments could be explained as follows: a higher concentration of HAV10 ligand may cause accumulation of the membrane E cadherin protein at the hydrogel surface. As a result, the cell-cell contact between neighboring cells in the colony is weakened and cells separate from each other. Intermediate concentrations of HAV10 sequence allow binding to the hydrogel surface and stabilization of small colonies in parallel. **Fig: 4.2** (H) showed immunofluorescent image of a representative colony of MDCK expressing Ecad:dsRed on the 0.05 mg/mL HAV10 functionalized surface. Cells responded to this HAV10 functionalized substrate with formation of small colonies characterized by an extended lamellipodium. This morphology is characteristic for specific cell adhesion triggered by homophilic binding of E-cadherin[58]. A detailed analysis of cell morphology is given in **section 4.2.5**.

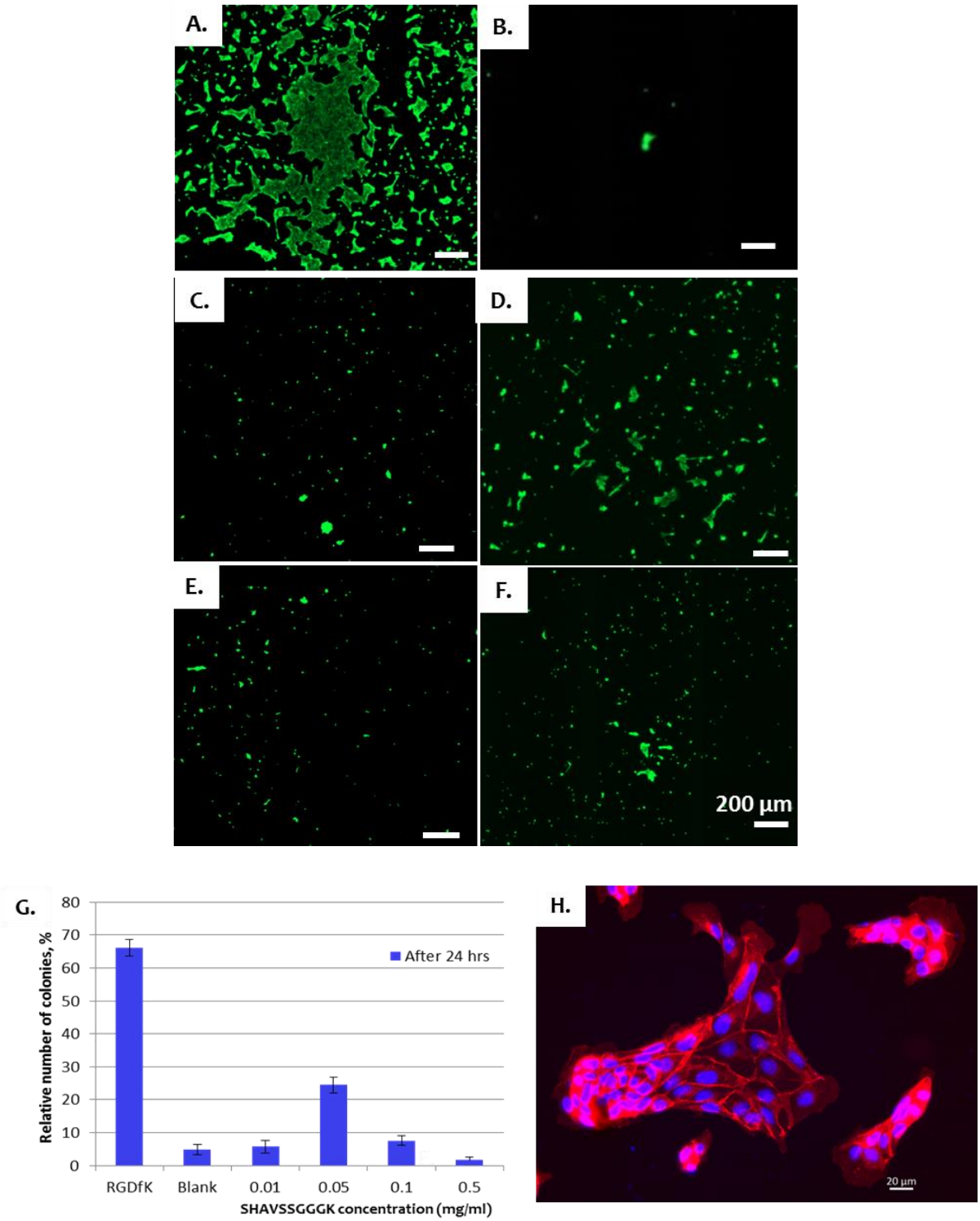

Fig. 4.2 *Representative fluorescence images of MDCK cells cultured on p(AAm-AA) hydrogels functionalized with different concentration of HAV10 peptide for 24 h; (A) 0,01 mg/mL cyclo(RGDfK), (B) 1% BSA (C) 0.01 mg/mL (D)0.05 mg/mL, (E) 0.1 mg/mL, and (F) 0.5 mg/mL. (G) Quantification of the number of colonies of MDCK cells cultured on cyclo(RGDfK) and HAV10 functionalized surfaces for 24 h (H) Representative fluorescent immunofluorescence image of*

MDCK cells expressing Ecad:dsRed on 0.05 mg/mL HAV10 functionalized surface. F-actin (green), E-cadherin (red), and nuclei (blue)

4.2.2 Response of MDCK epithelial cells to hydrogels modified with E-cadherin mimetic peptides from the bulge region: ADTPPVGGGK (ADT) and SWELYYPLRANLGGGK (SWEL)

Similar experiments were performed with E-cadherin peptidomimetics from the bulge region of the EC1 domain, ADT and SWEL. Both ADT (1 mM) and SWEL (0.01 mM) peptides have been demonstrated to block E-cadherin protein binding activity in MDCK and mESCs cell cultures respectively[91,96,97]. These peptides were modified with a GGG spacer and a K anchoring site, since this had been proven eventually beneficial for cell attachment in the previous studies. p(AAm-AA) hydrogels of 100 kPa stiffness were used for these studies. A peptide incubation concentration of 0.05 mg/mL was selected based on the experience from HAV10 peptide.

The morphology of MDCK cells on ADT and SWEL modified hydrogels after 24 h of culture is shown in **Fig. 4.3** MDCK cells showed a flattened morphology, they attached and spread on the surface and formed small colonies (8-10 cells), similar to the morphology observed on HAV10 modified surfaces. These features indicate that cells recognize the ADT and SWEL peptides on the surface. Interestingly, the number of colonies on HAV10, ADT and SWEL are similar (**Fig. 4.3C**).

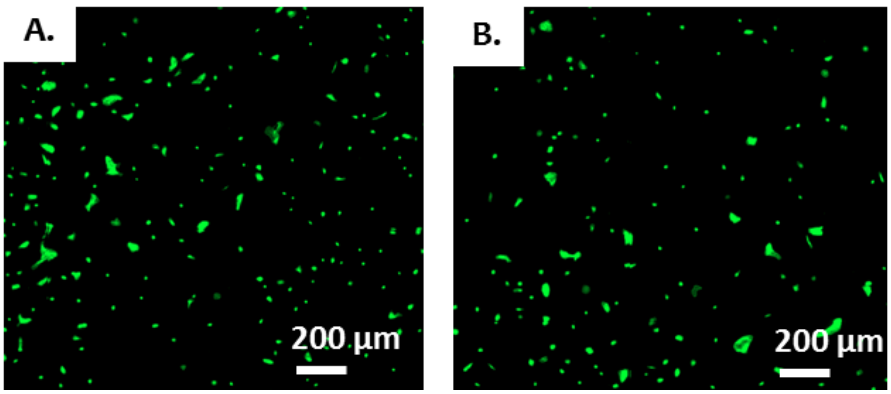

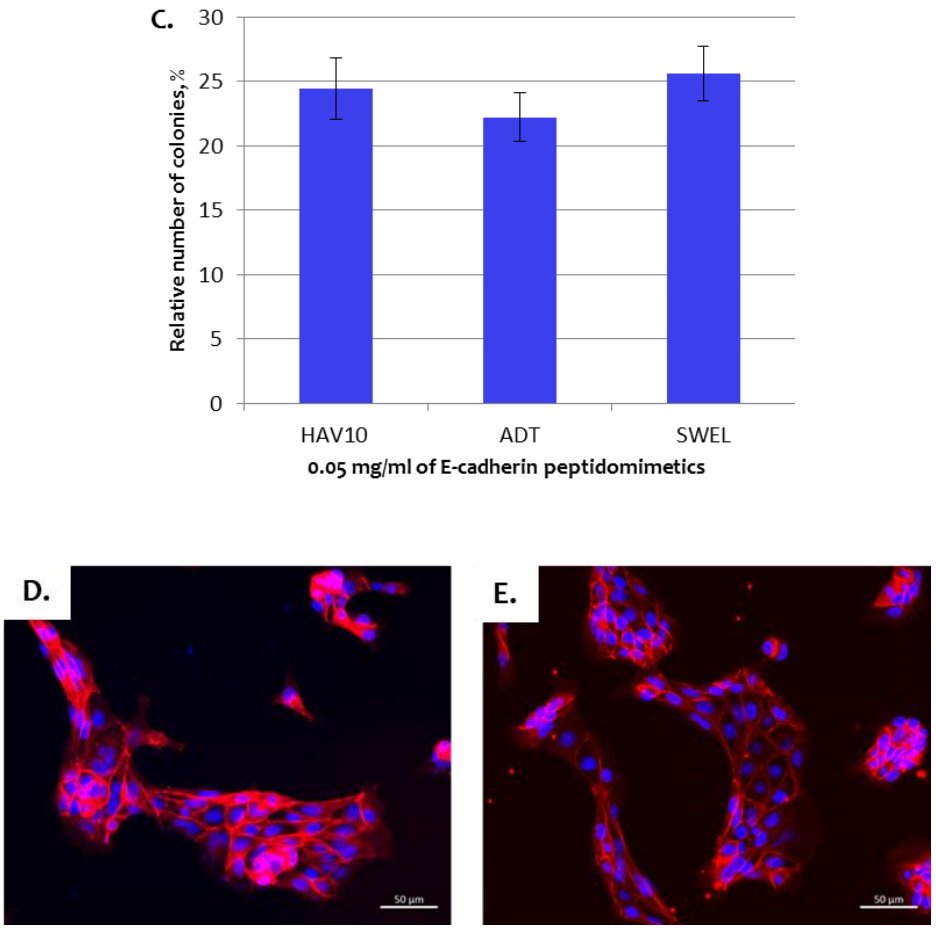

Fig. 4.3 *(A, B) Representative fluorescence images of MDCK cells cultured for 24 h on p(AAm-AA) hydrogels functionalized with (A) ADT and (B) SWEL at 0.05 mg/mL incubation concentration. (C) Quantification of the number of colonies of MDCK cells cultured on ADT and SWEL functionalized surfaces. (D, E) Representative immunofluorescence image of MDCK expressing Ecad:dsRed on (D) ADT and (E) SWEL functionalized surface. F-actin (green), E-cadherin (red), and nuclei (blue).*

4.2.3 Response of MDCK epithelial cells to hydrogels modified with E-cadherin protein

In order to compare the cell behavior induced by the peptidomimetics with the behavior induced by native E-cadherin protein, similar experiments were performed on hydrogels functionalized recombinant E-cadherin-Fc (Ecad-Fc) protein fragment. The protein was coupled to the hydrogel by three different strategies: (i) oriented immobilization via Protein A/G linker on the hydrogel through Lys residues, and direct covalent coupling of Ecad-Fc via (ii) Cys or (iii) Lys residues (**section 3.4**).

MDCK cells were cultured on the substrates functionalized with Ecad-Fc and blocked with BSA. Cells were mostly rounded and formed small clusters on all surfaces **(Fig. 4.4)**. These results were similar to those obtained from HAV6 peptide functionalized substrates and indicate that cells are not able to recognize E-cadherin protein on the hydrogel surface. This result was surprising, since previously reported data on Ecad-Fc protein functionalized on p(AAm) gels surfaces modified with sulfoSANPAH induced spreading and attachment of MDCK cells[58]. The different immobilization strategies could lead to different protein densities at the surface. In order to check this point, Ecad-Fc protein binding on the p(AAm) hydrogels was quantified by staining with anti-Ecad antibody. The fluorescent intensity was measured by confocal microscopy. The highest fluorescence intensity was observed on the hydrogel with Protein A/G mediated binding of Ecad-Fc, followed by the Cys and Lys-mediated coupling (**chapter 3, Fig. 3.7**). The values were not directly comparable to previously reported data on sulfoSANPAH. The difference in cell attachment and spreading may be due to the difference coupling strategy. The covalent coupling of Protein A/G through Lys residues might not be as efficient as coupling through sulfoSANPAH. Also, here we have to consider that the functionalization using photoreactive sulfoSANPAH bind to p(AAm) network through non-specific chemical reactions. The free radicals generated during the reaction can also react to Protein A/G in a nonspecifically and makes it difficult to control the exact surface density of protein and can also lead to unspecific attachment of cells.

Based on this data, no conclusive reason can be provided for the contradiction between our results and the previously studies[58]. One can speculate in two directions: different protein density on the surface, or loss of functionality of the hydrogel bound Ecad-Fc depending on the immobilization method. Covalent binding of the protein to the surface leads to random orientation of the protein. In the worst case, the binding site for membrane E-cadherin protein might be pointing towards the hydrogel surface and would not be accessible for the cell. This is applicable to the covalent strategies in this study, and also to the sulfo-SANPAH immobilization method. Non-covalent Protein A/G-Fc interaction might lead to leakage of the E-cadherin on the hydrogel surface, or not be stable enough to retain the bound membrane cadherins from the cells once spreading occurs and forces are exerted on the cell-hydrogel adhesion complexes.

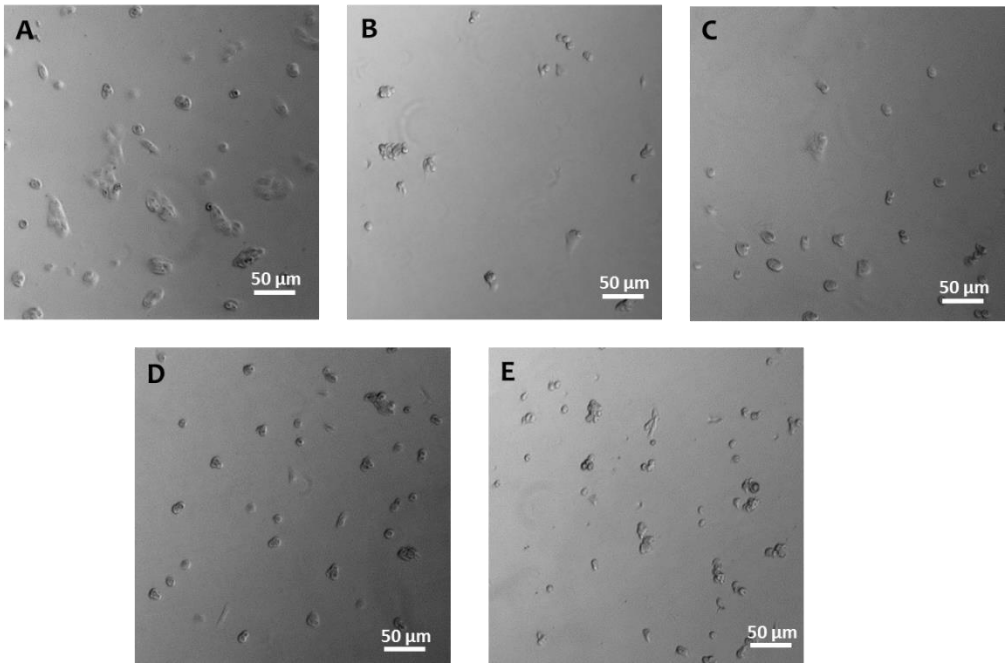

Fig. 4.4 *Bright field images of MDCK cells cultured on p(AAm) hydrogels functionalized with (A) 0.01 mg/mL RGDfK (B) 1% BSA (C) 0.3 mg/mL Protein A/G – 0.15 mg/mL Ecad-Fc protein (D) 0.15 mg/mL Ecad-Fc coupling through Lys and (E) 0.15 mg/mL Ecad-Fc coupling through Cys for 5 h.*

In an attempt to increase the concentration of E-cadherin at the surface while retaining the oriented exposure, the high affinity Fc binding peptide cyclic(NH2-DCAWHLGELVWCT-OH) modified with a GGGK sequence at the C-terminus was used for the immobilization of the Ecad-Fc protein[138]. In this case MCDK cells attached, spread and formed colonies on the Ecad-Fc protein gels **(Fig. 4.4).** Cells remained attached to the surface after washing, as a clear sign that of stronger interaction between cells and the Ecad-Fc protein modified hydrogel. In the control experiments with hydrogels modified only with Fc binding peptide poor cell adhesion was observed. These results indicate that Ecad-Fc protein immobilization via high affinity Fc-binding peptides increased either the protein concentration or the accessibility of the Ecad-Fc protein on the surface, and resulted in more stable cell attachment and spreading. This can be either the surface density of Fc-binding peptide on p(AAm) network coupled via Lys is more than proteinA/G or the affinity of Ecad-Fc protein to Fc-binding peptide is much better than to proteinA/G.

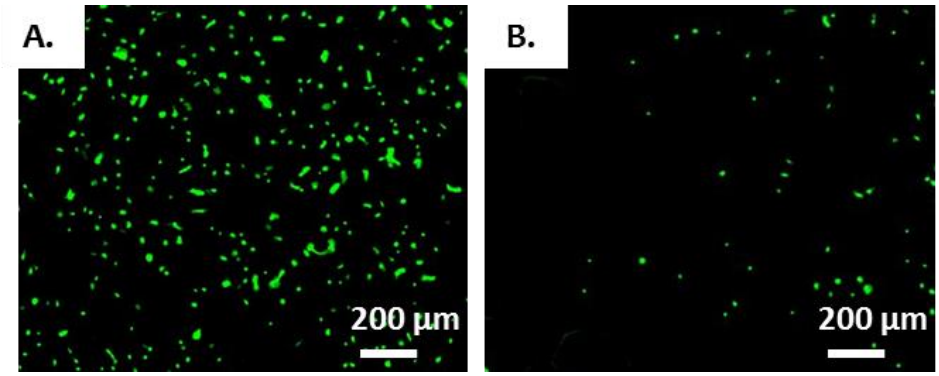

Fig. 4.5 *MDCK cells cultured on p(AAm)-AA hydrogels functionalized with (A) 0.3 mg/mL Fc-peptide- 0.15 mg/mL Ecad-Fc protein (B) Fc-binding peptide alone for 24 h, F-actin (Green).*

4.2.4 Specificity of the response of MDCK epithelial cells to hydrogels modified with HAV10 and Ecad-Fc

The specificity of the binding of cells to the HAV10 and Ecad-Fc modified hydrogels via recognition of the binding ligands by E-cadherin receptors at the cell membrane was tested in a series of experiments. First, p(AAm-AA) hydrogels were functionalized with a scrambled HAVC10 sequence (SGASGVGHSK or ScrbHAV10), in which the functional sequence is disordered. Hydrogels were modified at 0.05 mg/mL incubation concentration, as selected based on the results obtained in section 4.2.5. Results were compared with those obtained on HAV10 and Ecad-Fc protein immobilized via Fc binding peptide. The morphology and attachment of MCDK cells on the surfaces was monitored before and after washing. Cells on Scrb HAV10 modified hydrogels did not attach to the substrate, appear clustered and were easily washed out from the surface with PBS (**Fig. 4.6)**, while good cell attachment, spreading and colony formation was observed on HAV10 and Ecad-Fc surfaces. This result demonstrates that the interaction of cells with HAV10 modified surfaces is specific to the HAV10 sequence.

To further confirm that the interaction between MDCKs and the HAV10 peptide or the E cadherin protein is E-cadherin specific, cell adhesion experiments were carried out with two different types of fibroblast cells which do not express E-cadherin protein: L929 and MEFs. These two fibroblast cell lines express N-cadherin protein on their cell membrane. These cells were unable to attach or spread on HAV10, ScrbHAV10 and Ecad-Fc modified hydrogels (**SI, Fig. 4.14 & Fig. 4.15).** Cells remained floating on the medium, or they clustered together and were removed during washing with PBS. These cells were able to attach to cyclo(RGDfK) surfaces as

positive control. These results indicate that the attachment of MDCK cells to the E-cadherin mimetic surfaces is specific through E-cadherin protein.

Taken together, all the presented results show that HAV10 peptide sequence acts as an E-cadherin mimetic sequence and can be recognized by E-cadherin protein from the cell membrane on p(AAm-AA) hydrogels. Thus, hydrogels modified with this peptidomimetic can potentially be used as platforms to reconstruct the cell-cell interface and study E-cadherin mediated cellular processes.

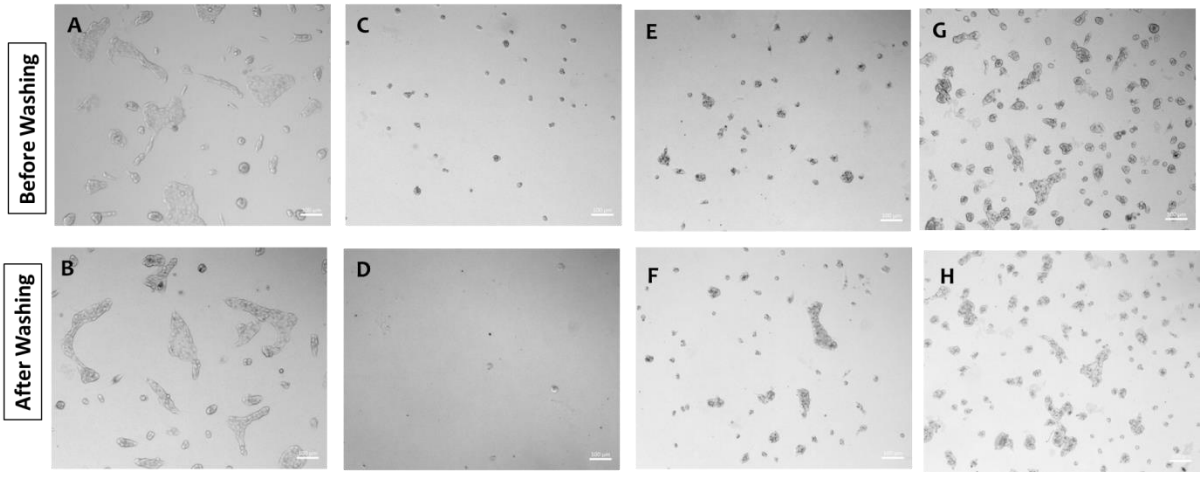

Fig. 4.6 *Bright field images of MDCK cells cultured 100 kPa p(AAm) hydrogels functionalized with 0,05 mg/mL (A&B) cyclo(RGDfK), (C&D) ScrbHAV10, (E&F) HAV10, and (G&H) Ecad-Fc protein for 24 h, Scale bar:100* μm.

4.2.5 Response of MCDK cells to HAV10 modified gels with different rigidity

E-cadherin dependent adhesion of MDCK epithelial cells to hydrogels modified with Ecad-Fc protein has been shown to be sensitive to the hydrogel stiffness[58]. The rigidity sensing by cadherin during cell adhesion was studied on mechanically tunable p(AAm) hydrogels functionalized with Ecad-Fc protein and found that the changes in Young's modulus produced noticeable differences in cell morphology, actin organization, and membrane dynamics[58].This section describes experiments to evaluate if HAV10 modified hydrogels can elicit similar rigidity responses of MDCK cells.

The behavior of MDCK cells on p(AAm-AA) gels with Young's modulus 2, 20, 40, and 100 kPa modified with HAV10 was studied. To make sure the effect was completely depending on

rigidity, the concentration of HAV10 peptide on p(AAm-AA) gels kept same. For this purpose, 2, 20, and 40 kPa hydrogels were incubated with different peptide concentrations than 100 kPa p(AAm-AA) gels (**chapter 3, section 3.2.4**). This biomaterial optimization step is crucial, since both ligand density and rigidity are known to affect cellular attachment[155,156]. Experiments on (0.15 mg/mL) Ecad-Fc and (0.01 mg/mL) cyclo(RGDfK) modified hydrogels were also performed for comparison.

The morphology of MDCK cells on HAV10 functionalized hydrogels with different stiffness after 24 h of culture is shown in **Fig. 4.7.** Cells attached and spread to 100 kPa hydrogels. On 40 kPa hydrogels cells showed weaker attachment and smaller spreading areas, and they formed small colonies of rounded shapes. Softer substrates did not support attachment of MDCK cells. These results show that mechanical factors regulate the formation of E-cadherin contacts via HAV10 peptidomimetic. The attachment and spreading behavior were similar to that observed on Ecad-Fc functionalized surfaces (**Fig. 4.8).** The number of cells attached to E-cadherin substrates after washing increased with increasing substrate rigidity. Ecad-Fc functionalized hydrogels with Young's modulus 100 kPa showed good cell attachment and spreading, and also supported the formation of small cell colonies. Cell spreading on Ecad-Fc functionalized 40 kPa substrates was lower, though cells did not form clusters significantly. Cells on softer substrates (2 or 20 kPa) showed low attachment, formed globular clusters and were largely removed during washing. This behavior has been also reported by other authors[58]. Taken together, these results indicate that there is a threshold stiffness facilitating E-cadherin mediated cell adhesion between 20 and 40 kPa. In addition, the increased cell spreading seen on 100 kPa compared to 40 kPa suggests that cells are able to activate cell spreading pathways through E-cadherin mediated substrate stiffness sensing.

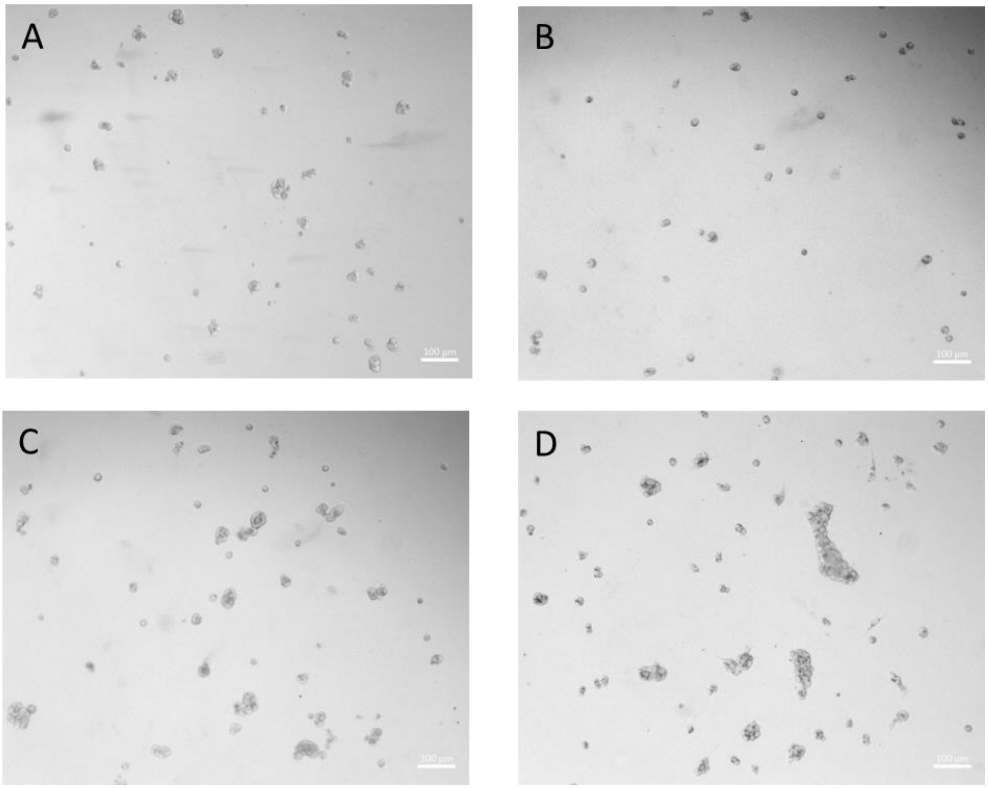

Fig. 4.7 Bright field images of MDCK cells cultured on HAV10 substrates with different stiffness; (A) 2 kPa (B) 20 kPa (C) 40 kPa (D) 100 kPa; Scale bar 100 µm.

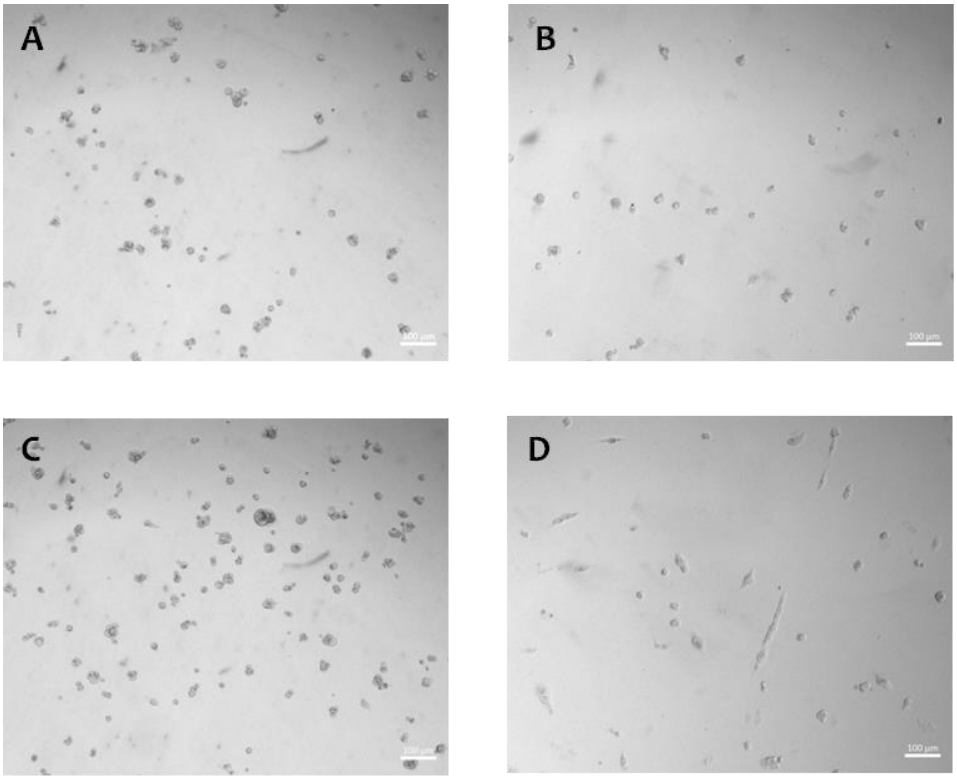

Fig. 4.8 *Bright field images of MDCK cells cultured on Ecad-Fc substrates with different stiffness; (A) 2 kPa (B) 20 kPa (C) 40 kPa (D) 100 kPa; Scale bar 100* µm

In contrast, MDCK cells adhered to 0.01 mg/mL cyclo(RGDfK) functionalized substrates showed strong attachment, large spreading and colony formation on all hydrogels, regardless their Young's modulus (**Fig.4.9).** The RGD-integrin adhesion site does not seem to respond to the rigidity of the underlying surface at the range of ligand density and stiffness tested. In contrast, the stiffness of the E-cadherin mimicking substrates within the same experimental window affected cell morphology and spreading.

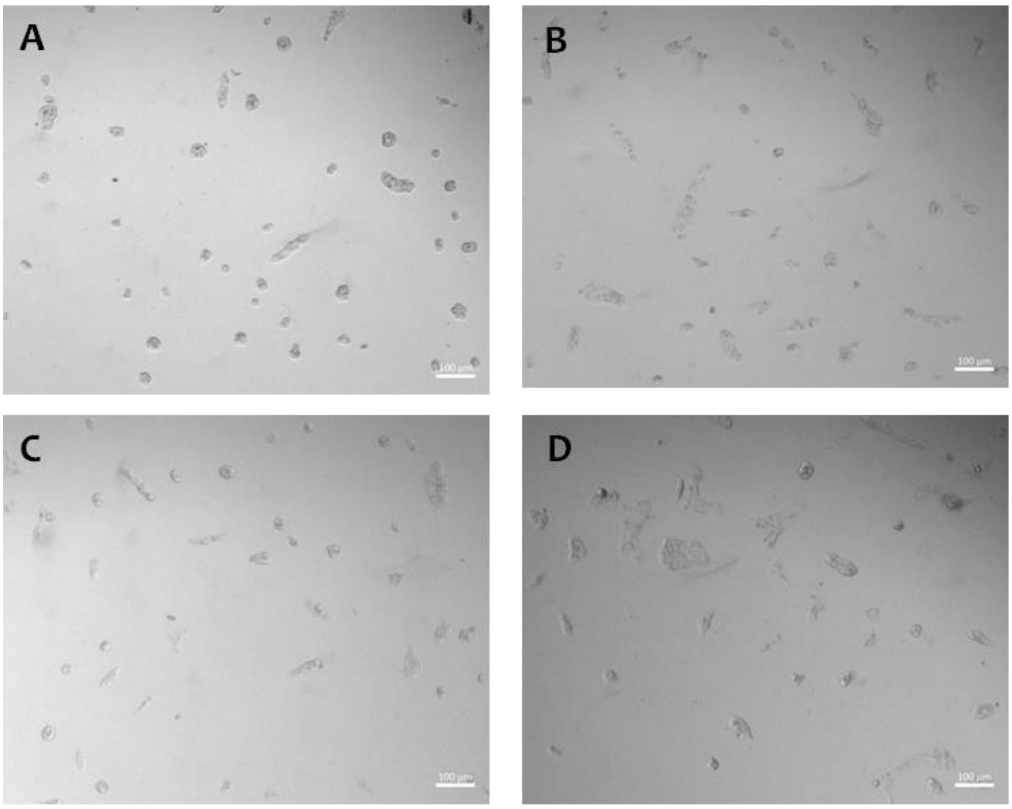

Fig. 4.9 *Bright field images of MDCK cells cultured on cyclo(RGDfK) substrates with different stiffness; (A) 2 kPa (B) 20 kPa (C) 40 kPa (D) 100 kPa; scale bar 100* µm.

4.2.6 E-cadherin and HAV10 functionalized gels induce plasma membrane protrusion and organization of actin cytoskeleton in MDCK cells

In order to visualize the localization of the membrane receptors and the organization of the cytoskeletal structures in cells attached to Ecad-Fc or HAV10 modified hydrogels, MDCK cells stably expressing E-cadherin:DsRed were seeded on the substrates, cultured for 24 h, fixed and fluorescently stained for F-actin, and paxillin (which is associated to integrin based focal adhesions) and imaged by immunofluorescence microscopy.

First, MDCK cells adhered to Ecad-Fc coated hydrogels were imaged (**Fig. 4.10A**). The fluorescence microscopy images confirmed that cells flattened, spread, and formed small colonies. Adhesion of cells to the E-cadherin mimetic surfaces were observed along with the spreading of large lamellipodium and the reorganization of its actin cytoskeleton. For comparison, cells grown on cyclo(RGDfK) exhibited a compact shape without any lamellipodium extensions (**Fig. 4.10E**). The actin cytoskeleton of cells showed circular network of filaments around the nucleus, along with radial cables directed towards the lamellipodium.

At the end of the radial F actin bundles, the E-cadherin staining revealed the formation of broad lamellipodia, i.e. protrusion-like membrane structures at the edge of the cell. These protrusions extended beyond the visible cortical F-actin ring. Actin formed small microspikes (branched actin network) in the extended lamellipodia. This extension of cadherin interaction is related to actin nucleation as previously observed and new actin arrangement could initiate the formation of lamellipodium protrusions[53]. Previous reports have demonstrated that Arp2/3 nucleates the formation of actin microspikes found in lamellipodia, and contributes to the cell spread and formation of lamellipodia[58,157,158]. Paxillin staining was observed throughout the cytoplasm but no focal adhesions were observed at the end of actin bundles. E-cadherin appeared concentrated at the cell-cell interfaces within the cell colonies, and no cadherin plaques were observed. The protrusions of lamellipodium can be considered as a preferential site for new cell-cell contacts. These observations were comparable to the previously reported results of cell adhesion on N-cadherin protein coated surfaces[53].

Similar results were obtained on hydrogels functionalized with HAV10 (**Fig. 4.10B**). This indicates that HAV10 mediated attachment of MDCK cells is E-cadherin specific and does not activate integrin-engagement. The colonies on HAV10 hydrogels were not as flat as on Ecad-Fc modifications. Extended, large lamellipodia protrusions raffled around the entire cell periphery is a characteristic of cells on E-cadherin hydrogels[58].

MDCKs on hydrogels functionalized with ADT and SWEL peptides also showed similar features (**Fig. 4.10C**). Lamellipodia protrusion and formation of actin microspikes were observed. However, in this case paxillin staining showed focal adhesions at the end of the extended actin microspikes. It suggests that binding to ADT and SWEL peptides is not exclusive for cadherins, and also integrins can bind and form focal adhesions with them.

Cells on cyclo(RGDfK) substrates showed different features (**Fig. 4.10D**). Cells flattened and spread extensively, and they showed no/less broad lamellipodia like protrusions. Cells

adhered on cyclo(RGDfK) substrates showed a circumferential ring of F-actin and clear enrichment of paxillin at the end of the F-actin belt and particularly over the edges of the cell . Integrin specific paxillin staining was predominant on these substrates. E-cadherin staining was diffused and concentrated on junctions between cells.

In order to quantify the different features of the cells on the E-cadherin mimetic peptides, the length of protrusions was measured (**Fig. 4.11).** Cells adhered to an Ecad-Fc protein and on the E-cadherin peptidomimetics showed long lamellipodia around the entire periphery of the colony. The length of protrusions on SWEL peptide were shorter. Cells adhered to cyclo(RGDfK) showed less lamellipodium extensions.

Provided the difference between HAV10 and cyclo(RGDfK) functionalized hydrogels in cell spreading and plasma membrane protrusions, single cell morphology was also studied to eliminate interference with native cell-cell adhesions in larger cell colonies. Single cells adhered to HAV10 (**Fig. 4.12A)** hydrogels had large lamellipodia protrusions extended beyond the cortical F-actin ring. Actin forms small microspikes of branched actin network in the extended lamellipodia. E-cadherin mainly concentrated at the edges of the cell to form cadherin specific cell-cell adhesion between adjacent cells. And paxillin was diffused throughout the cytoplasm and didn't show focal adhesion clusters at the end of actin fiber. However, cells on ECM mimetic cyclo(RGDfK) (**Fig. 4.12B)** hydrogels show clear enrichment of focal adhesion clusters at the end of F-actin and around the cell periphery. E-cadherin was distributed in the whole cytoplasm.

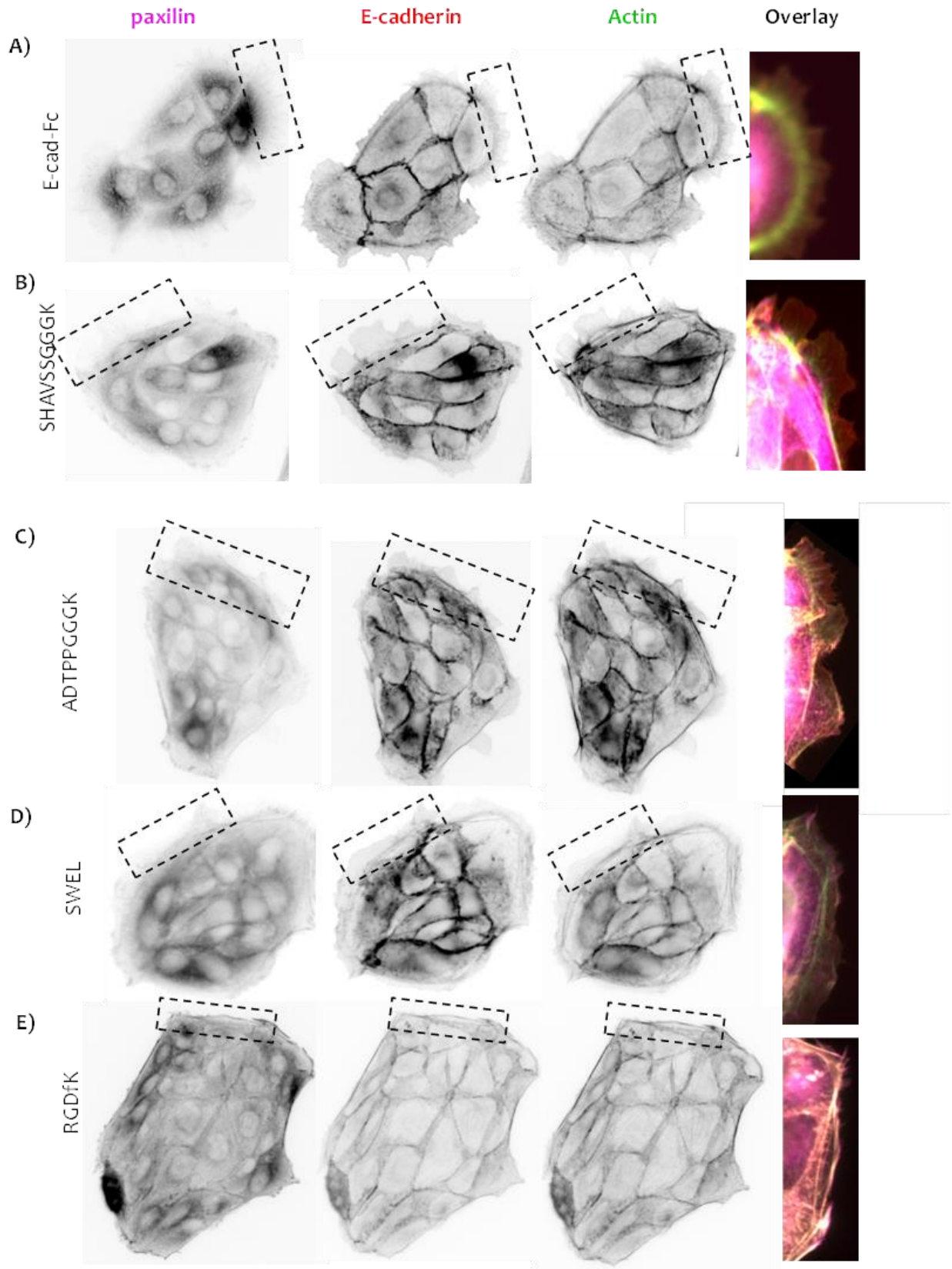

Fig. 4.10 *Immunofluorescence images of MCDK cells on hydrogels functionalized with (A)Ecad-Fc protein (B) HAV10 (C) ADT10 (D) SWEL (E)* cyclo(RGDfK) *peptides for 24 h. F-actin (Green), E-cadherin (Red), and paxillin (Magenta)*

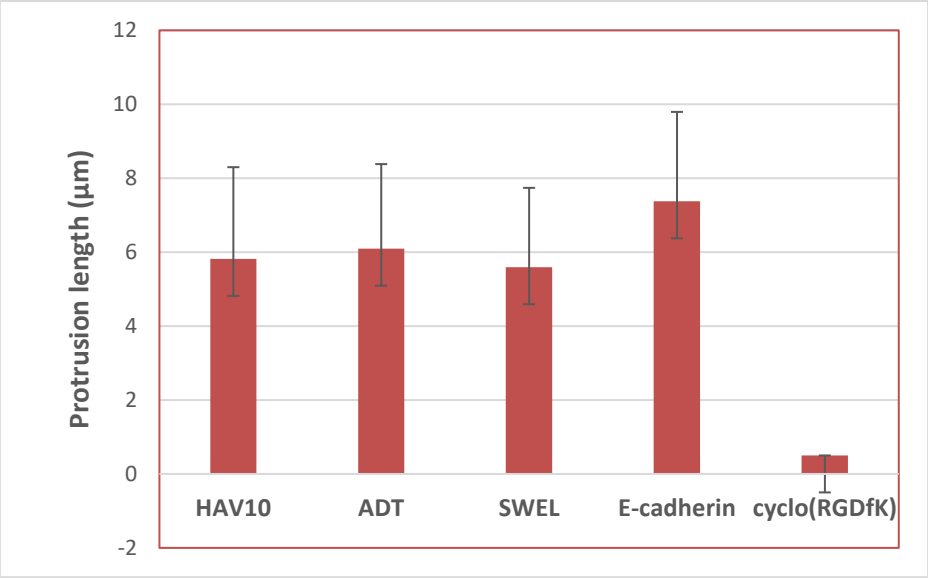

Fig. 4.11 *Quantification of protrusion length of MCDK cells on hydrogels functionalized with (A) Ecad-Fc protein (B) HAV10 (C) ADT10 (D) SWEL (E) cyclo(RGDfK) peptides for 24 h.*

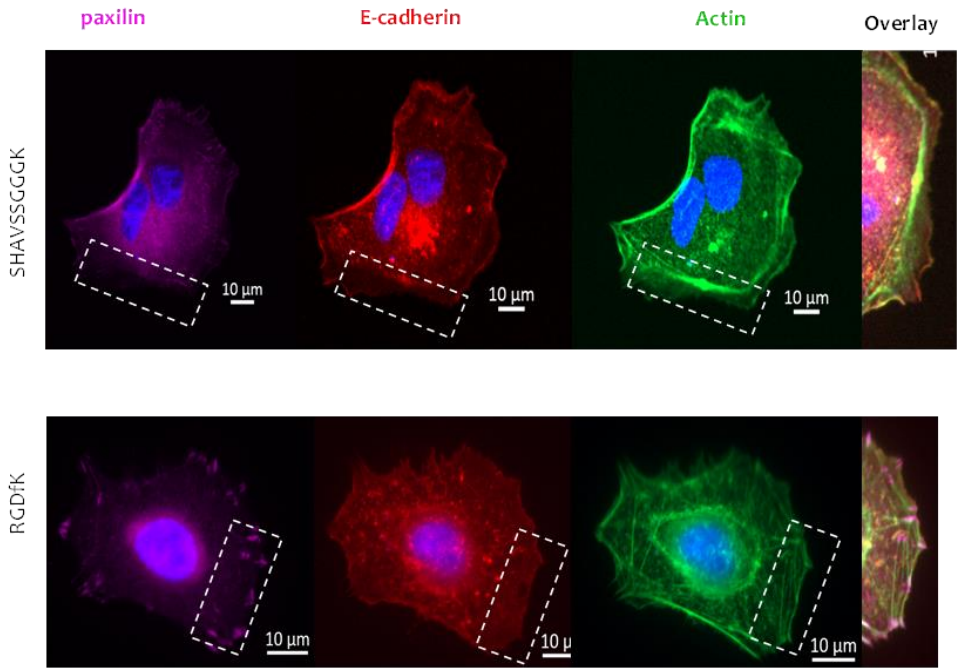

Fig. 4.12 *Immunofluorescence images of single MCDK cell on hydrogels functionalized with (A) HAV10 and (B) cyclo(RGDfK) peptides for 24 h, F-actin (Green), E-cadherin (Red), Paxillin (Magenta)and nuclei (Blue). Data are presented as mean ± standard deviation.*

The interaction between E-cadherin expressing cells and E-cadherin mimicking homophilic substrate was characterized by two striking features: (1) the formation of lamellipodium protrusions; and (2) actin filament the reorganization in cadherin adhesions. For cadherin adhesions, E-cadherin molecules that initially recognize the functionalized E-cadherin

substrates at the edge of lamellipodium, form sites of nascent contacts. This requires a tight co-ordination with actin cytoskeleton. It is interesting to observe that the cadherin mimetic peptides form matrix adhesions similar to the matrix adhesions formed by cyclo(RGDfK) mediated integrin interactions. The role of signaling proteins involved in the recruitment of adhesion proteins is not studied in this thesis.

4.3 Conclusion

Different E-cadherin peptidomimetic sequences were screened to find the best candidate to fabricate a p(AAm) based hydrogel system to mimic E-cadherin – E-cadherin interaction. Length and concentration of the peptides are two key important factors affecting the binding. Also, the rigidity of the substrates affected the cell attachment. A peptide from the groove region, containing the conserved HAV sequence flanked by Ser amino acids with a linker residue (HAV10) showed better cell attachment and spreading closer to Ecad-Fc protein than the short HAV6 peptide. Nevertheless, peptides from the bulge region ADT10 and SWEL also supported cell attachment but also showed paxillin staining in focal adhesion like structures. Since these peptides are less studied and the specificity of these peptides has not been studied in detail, we further proceeded with HAV10 peptides for the detailed analysis of the binding between peptide and protein from the living cell. A new coupling strategy with a Fc-binding peptide was developed to couple E-cadherin protein on p(AAm) hydrogels. p(AAm) hydrogels functionalized with E-cadherin mimetic peptides were investigated in detail to understand the effect of E-cadherin mimetic peptide mediated homophilic interaction in cell adhesion and membrane dynamics. MDCK cells specifically interacted with E-cadherin mimetic peptides and adhered to E-cadherin mimetic cell-like surfaces. Cadherin specific adhesion shows specific rearrangement of the actin cytoskeleton and lamellipodia protrusions, which are essential to promote cell-cell attachment and spreading. These results show that the E-cadherin mimetic peptide, HAV10 functionalized hydrogels interacts with E-cadherin protein from cell membrane, and impacts on cell morphology, membrane dynamics and actin organization.

4.4 Experimental section

4.4.1 Functionalization of p(AAm) hydrogel

The 100 kPa p(AAm-MS) or p(AAm-AA) hydrogels were prepared and functionalized by following the protocol described in section 3.2.4. The functionalized hydrogels were

transferred to a 24 well cell culture plate and sterilized with 70% ethanol for 5 min. Then the samples were washed with PBS (pH 7.4) (3 x) and incubated with cells under laminar flow.

4.4.2 Adhesion of MDCK cells

MDCK cells stably expressing E-cadherin-DsRed (received from Dr. Johan de Rooij and Dr. Martijn Gloerich, Center of Molecular Medicine, UMC Utrecht) was cultured in DMEM medium (Gibco) containing 10% fetal bovine serum (Invitrogen) and 1% penicillin-streptomycin (Invitrogen) at 37 °C and 5% CO2. 5 × 104 MDCK cells were seeded in each well having sterilized hydrogel samples and incubated at 37 °C and 5% CO2. The cell culture was incubated for 24 h. The cells were fixed with 4% PFA solution for 10 minutes. All the experiments were performed as triplets. Bright field images have been taken with the Zeiss axio observer epi-fluorescence microscope.

4.4.3 Adhesion of fibroblast L929 cells

Fibroblast L929 cell line was cultured in RPMI medium (Gibco) containing with 10% fetal bovine serum (Invitrogen) and 1% penicillin-streptomycin (Invitrogen) at 37 °C and 5% CO2. 5 × 104 L929 cells were seeded in each well having sterilized hydrogel samples and incubated at 37 °C and 5% CO2. The cell culture was incubated for 24 h. The cells were fixed with 4% PFA solution for 10 minutes. All the experiments were performed as triplets. Bright field images have been taken with Zeiss axio observer epi-fluorescence microscope.

4.4.4 Adhesion of fibroblast MEFs cells

Fibroblast MEFs cell line was cultured in DMEM medium (Gibco) containing with 10% fetal bovine serum (Invitrogen) and 1% penicillin-streptomycin (Invitrogen) at 37 °C and 5% CO2. 5 × 104 MEFs cells were seeded in each well having sterilized hydrogel samples and incubated at 37 °C and 5% CO2. The cell culture was incubated for 24 h. The cells were fixed with 4% PFA solution for 10 minutes. All the experiments were performed as triplets. Bright field images have been taken with Zeiss axio observer epi-fluorescence microscope.

4.4.5 Immunostaining

Cells were fixed in 4% PFA solution for 10 minutes and then three times washed with cold PBS pH 7.4. Fixed samples were treated with 0.1% (v/v) Triton-X in PBS for 10 min at room temperature for permeabilization and washed with PBS (3 x). The samples were incubated with 1% BSA in PBS at room temperature for 30 min to block non-specific binding of antibody. Then

the samples were incubated with respective primary antibodies of desired concentration in PBS containing 1% BSA for 1 h at room temperature followed by washing with PBS (3 x). Subsequently incubated with their respective secondary antibodies of desired concentration in PBS containing 1% BSA for 1 h at room temperature and washed with PBS (3 x). Finally, the samples were mounted on microscopy cover slips using mounting medium containing DAPI (Dinova) to stain nucleus by following standard protocols.

Primary antibody (anti-mouse paxillin) was used in 1:100 concentration. Secondary antibodies Alexa α mouse 647 (1:1000) and Alexa fluor 488 phalloidin (1:80) were used in the respective concentrations.

4.4.6 Analysis and quantification

Imaging was performed using Zeiss axio observer epi-fluorescence microscope. All the image analysis was done using ImageJ and graphs were plotted using Microsoft spread sheet for three independent experiments. Adhesion of cells were quantified by calculating the number of cells on the surfaces. Protrusion length: On each substrate, five areas from at least four separate colonies were analyzed, resulting in a quantification of 100 protrusions per substrate.

4.5 Supporting figures

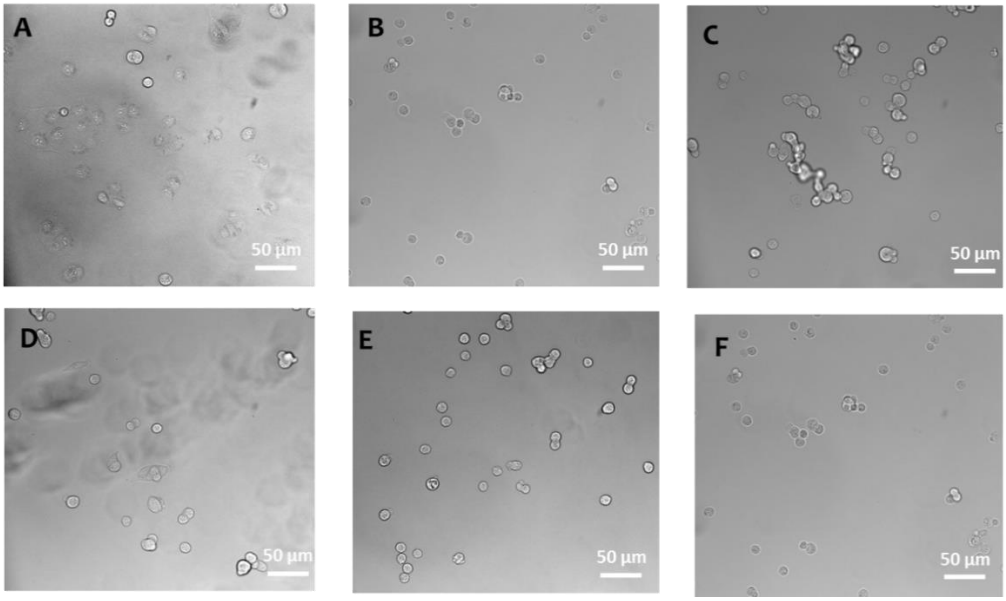

Fig. 4.13 *Brightfield images of MDCK cells cultured on NEXTERION® slides functionalized with (A) 0,01 mg/mL RGDfC, (B) 1% BSA, (C) 1 mg/mL HAV6, (D) 0.1 mg/mL HAV6, (E) 0.01 mg/mL, and (F) 0.001 mg/mL HAV6 for 24 h.*

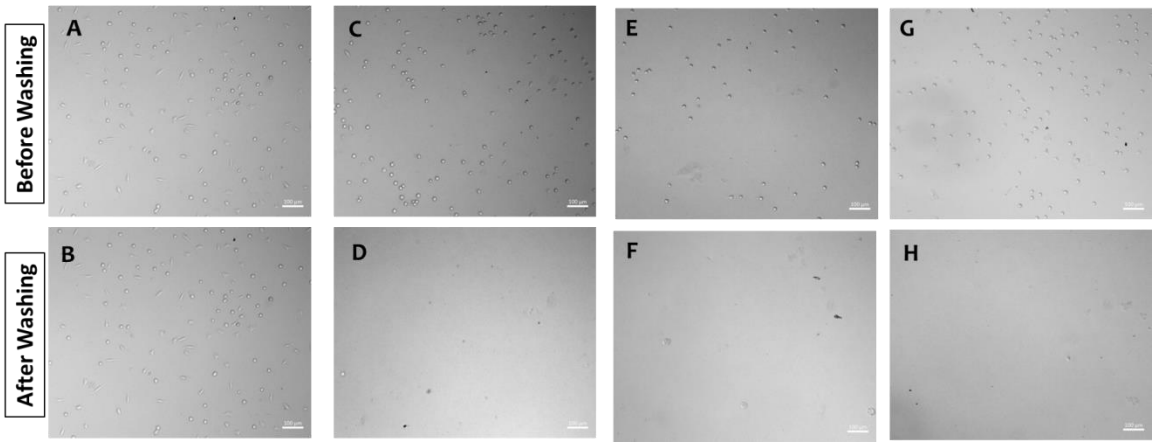

Fig. 4.14 *Bright field images of L929 cells cultured 100 kPa p(AAm) hydrogels functionalized with (A&B) cyclo(RGDfK), (C&D) ScrbHAV10, (E&F) HAV10, and (G&H) E-cadherin for 24 h.*

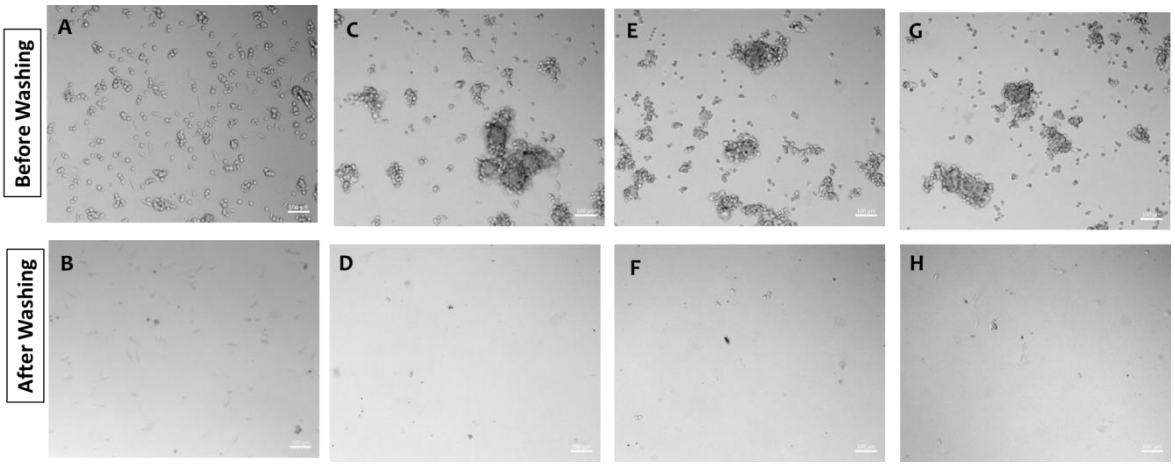

Fig. 4.15 *Bright field images of MEFs cells cultured on 100kPa p(AAm) hydrogels functionalized with (A&B) cyclo(RGDfK), (C&D) ScrbHAV10, (E&F) HAV10, and (G&H)E-cadherin for 24 h.*

Chapter 5

Photoactivatable N-cadherin peptide can regulate the behavior of C2C12 myoblasts on polarized biointerfaces

In this chapter, a micropatterned hydrogel with a basolateral distribution of matrix and cell adhesion ligands was used to test the myogenic differentiation of C2C12 cells as function of the presentation of N-cadherin peptidomimetic. 2.5D poly(Acrylamide) hydrogels were immobilized with ECM mimetic cyclo(RGDfK) peptide and N-cadherin mimetic HAVDIGGGC, AGVGDHIGC, and H[Ru(bpy)2(PPh3)]AVDIGGGC peptides on the basal and lateral directions respectively. Photoactivatable N-cadherin mimetic peptide, H[Ru(bpy)2(PPh3)]AVDIGGGC allowed the study of myogenesis as function of N-cadherin binding with temporal control.

5.1 Introduction

N-cadherin mediated cell-cell interactions are essential for morphogenetic processes, transduction of long-range growth and differentiation signals[159], and also plays key role in differentiation of various cell types, like muscle cells[102], chondrocytes[160], osteoclasts[161],and neural cells[162]. In skeletal myogenesis, cell- matrix and cell-cell adhesion are involved[163,164]. The developing skeletal muscle expresses N-, M-, R-, and 11-cadherins[165]. Antibodies that disrupt N-cadherin activity prevent the development of myotubes and inhibit myosin accumulation[165]. Also, the expression of N-cadherin stimulates expression of MyoD and sacromyosin in baby hamster kidney cells[166]. N-cadherin coated beads have induced myogenesis in cultured myoblast, indicating the relevance of the formation of N-cadherin adhesive complexes in myogenesis[159]. A recent study showed that hyaluronic acid (HA) co-modified with N-cadherin mimetic peptides and ECM mimetic peptides enhanced MSC chondrogenesis and osteogenesis[57,62,167]. Altogether these results suggest and to some extend demonstrate that hydrogel platforms incorporating N-cadherin protein, or its peptidomimetics, can enhance myogenesis.

The myoblast cell line C2C12 can be used to study myogenesis. These cells proliferate in vitro and, once confluence is reached and cell-cell contacts can be established, they upregulate N-cadherin expression and undergo differentiation[168]. This is accompanied by clear morphological changes, i.e., elongation and formation of post-mitotic mononucleated myocytes, which finally fuse into multinucleated myotubes and differentiate into muscle fibers. Therefore, this system seems suitable to test the activity of the photoactivatable N-cadherin peptide described in Chapter 2.

Previous experiments in the group performed by Dr. Aleeza Farrukh had demonstrated that the 2.5D model hydrogels described in section 3.2.7 are appropriate platform to study N-cadherin mediated myogenesis. C2C12 cells seeded on these hydrogels modified with ECM cyclo(RGDfK) and N-cadherin ligands at the bottom and walls of the micropatterned channels respectively, underwent myogenesis. In this chapter, a non-invasive N-cadherin peptidomimetic containing a photoremovable protecting group was used to regulate N-cadherin mediated myogenic differentiation in vitro on 2.5D hydrogels. The application of a light at particular wavelength can remove the protecting group and the activity of N-cadherin mimetic peptide can be restored in a controlled manner.

5.2 Results and Discussion

5.2.1 Behavior of C2C12 myoblasts on 2D hydrogels modified with N-cadherin peptidomimetic (HAVDIGGGC)

The behavior of C2C12 fibroblasts on p(AAm-AA-MS) hydrogels modified with N-cadherin peptidomimetic HAVDIGGGC (HAV) and/or with cyclo(RGDfC) matrix ligand was studied. The scrambled peptide AGVGDHIGC (AGV)was used as a negative control. Hydrogels were modified with individual peptides or with peptide mixtures as described in Chapter 2. The peptide incubation concentrations had been optimized in previous studies in the group and were 0.1 mg/mL for cyclo(RGDfK) (RGD) and 0.05 mg/mL for the N-cadherin peptides. Lower concentrations of cyclo(RGDfK) peptide did not support cell adhesion to the bottom of the channels and lower concentrations of HAVDIGGC were not sufficient to trigger cell responses. Higher concentration of cyclo(RGDfK) peptide lead monolayer formation in the channels and myogenic differentiation was observed. A higher concentration of N-cadherin peptide did not lead to differences in the cell behavior (unpublished work). Hydrogels with Young's modulus

of 10 kPa were selected for the studies. This rigidity is close to that of muscle tissue and is expected to support myogenic differentiation[139,140].

The behavior of C2c12 cells was first tested on 2D p(AAm-AA-MS) hydrogels. C2C12 cells were seeded on the hydrogels and imaged after 24hrs. C2C12 cells spread and proliferated on cyclo[RGDfK] modified hydrogels (**Fig. 5.1A**). In contrast, C2C12 cells were loosely attached to the N-cadherin peptide and to the scrambled control, they showed a rounded morphology and no significant spreading. Staining of the cells with N-cadherin, CD2 antibody (green) revealed accumulation of N-cadherin on the basal side of C2C12 cells seeded on HAV modified hydrogels (**Fig. 5.1A**), indicating interaction of N-cadherin at the cell membrane of the C2C12 with the peptide. In contrast, C2C12 seeded on hydrogels modified with the scrambled N-cadherin peptidomimetic or with the RGD peptide showed even distribution of N cadherin over the whole cell (**Fig. 5.1A**). C2C12 myoblasts seeded on bifunctional hydrogels modified with a mixture of RGD and HAVDIGGGC ligands attached to the substrate and showed spread morphologies, as seen on hydrogels modified with RGD only. However, whereas C2C12 cells on RGD proliferated during 4 days, reached confluency and established cell-cell contacts, cells on mixtures of RGD with N-cadherin peptides failed to proliferate and establish cell-cell interactions at day 4 (**Fig. 5.1A**). In summary, the presentation of N-cadherin mimetic ligand, alone or together with RGD on a 2D hydrogel surface, did not facilitate the attachment and inhibit cell-cell contact.

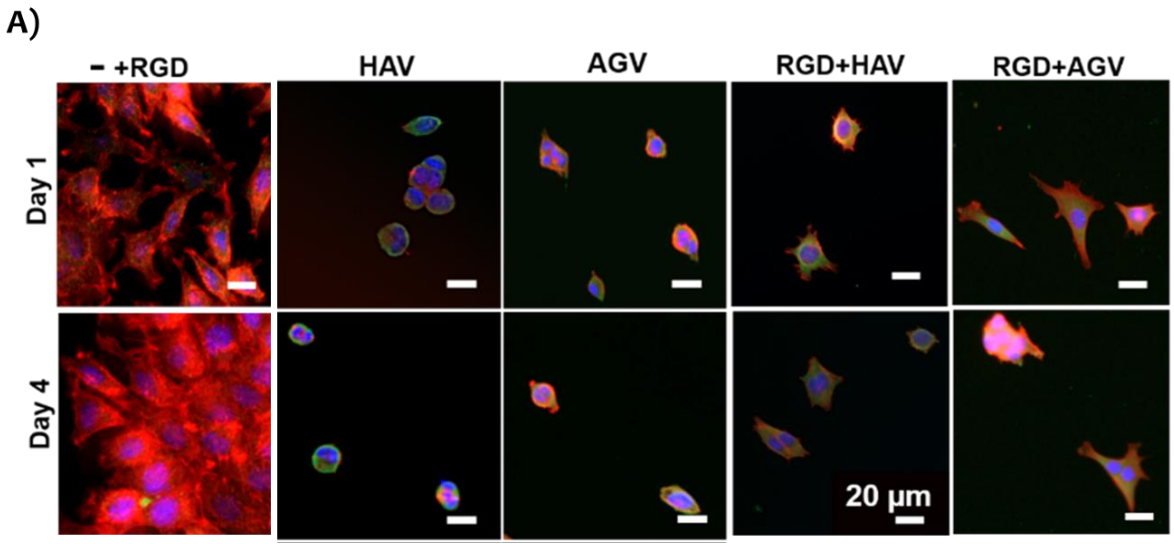

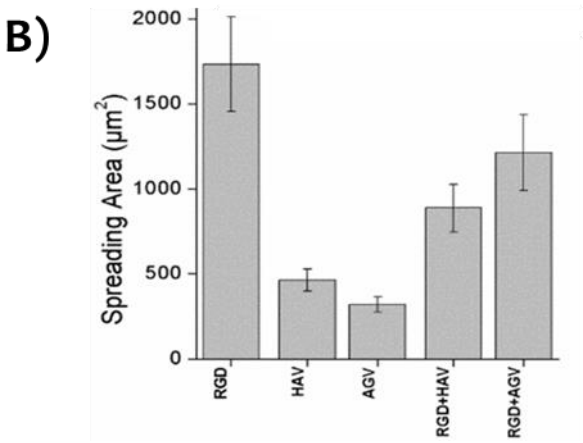

Fig. 5.1 *(A) Immunofluorescence images of C2C12 myoblast on 2D P(AAm-AA-MS) hydrogels modified with RGD, HAV, AGV or their mixtures after 1 and 4 days of culture. Actin (red), N-cadherin (green) and nucleus(blue). (B) Quantification of cell spreading area on the different hydrogels(n=90-420cells/sample).*

5.2.2 Myogenic differentiation of C2C12 myoblast cells on 2.5D hydrogels

Experiments in this section were done in collaboration with Dr. Aleeza Farrukh. C2C12 myoblast cells were cultured on 2.5D hydrogel models consisting of micropatterned channels in the hydrogel, which were functionalized at the bottom with cyclo[RGDfK] peptide and at the walls with the N-cadherin peptide HAVDIGGGC, with the scrambled peptide AGVGDHIGC or with the N-cadherin fragment CD2, immobilized by direct coupling via Cys. Channels were 5 μm wide, 6 μm height and separated by 50 μm thick walls. The elongated geometry is expected to favor the natural morphology of C2C12 cells during differentiation. The spatial differentiation between matrix (bottom) and cell-cell (walls) adhesive ligands in the channels mimics the natural arrangement of cell-cell and cell-matrix interfaces of the cells in natural tissue.

C2C12 myoblasts entered the 5 μm wide channels modified with RGD at the bottom and spread on day 1. When the walls of the channels were functionalized with N-cadherin mimetic peptide, C2C12 adopted an elongated morphology and contacted the walls of the channels. This morphology was also visible in channels modified with CD2, indicating that cells sense the N-cadherin functionalization by establishing contact with the functionalized interface. Elongated morphologies were also observed in C2C12 seeded in channels with the scrambled peptide, suggesting that this peptide still retains some affinity for the N-cadherin receptor. However, nucleus and actin staining revealed differences between cells on channels with HAV or CD2 vs. AGV functionalization (**Fig. 5.2A**). Cells in CD2/RGD and HAV/RGD channels showed

actin stress fibers aligned along the channel, whereas no aligned actin fibers were observed on AGV/ RGD and -/RGD channels. Elongated cell and nuclear shapes are characteristic of muscle cells, and this morphology was only observed when C2C12 were exposed to the 2.5D polarized microenvironments with HAV or CD2 cell-cell ligands on the walls.

Besides morphological differences in the polarized environments, proliferation and differentiation levels were also tested. Proliferation rate at day 1 was independent of the presence of N-cadherin ligands on the channel wall (**Fig. 5.2A**). In contrast, a higher expression of sarcomeric myosin (MF-20 staining) was observed in cells within CD2/RGD and HAV/RGD channels vs. -/RGD and AGV/RGD ones, already at day 1. These differences become more pronounced at longer culture time. At day 4, C2C12 on CD2/RGD and HAV/RGD channels showed high proliferation levels and high sarcomeric myosin expression values. Fusion of myogenic cells into polynucleated myocytes were also observed (**Fig. 5.2A**). Proliferation levels and sarcomeric myosin expression on -/RGD and AGV/RGD channels were significantly lower, and no fused cells were observed. Enhanced myogenesis on substrate morphologies supporting cellular alignment had been demonstrated in previous reports[169–171]. The data here show that the combination of alignment and spatially resolved presentation of matrix and cell-cell adhesive cues significantly accelerates myogenic proliferation and differentiation of C2C12 myoblasts.

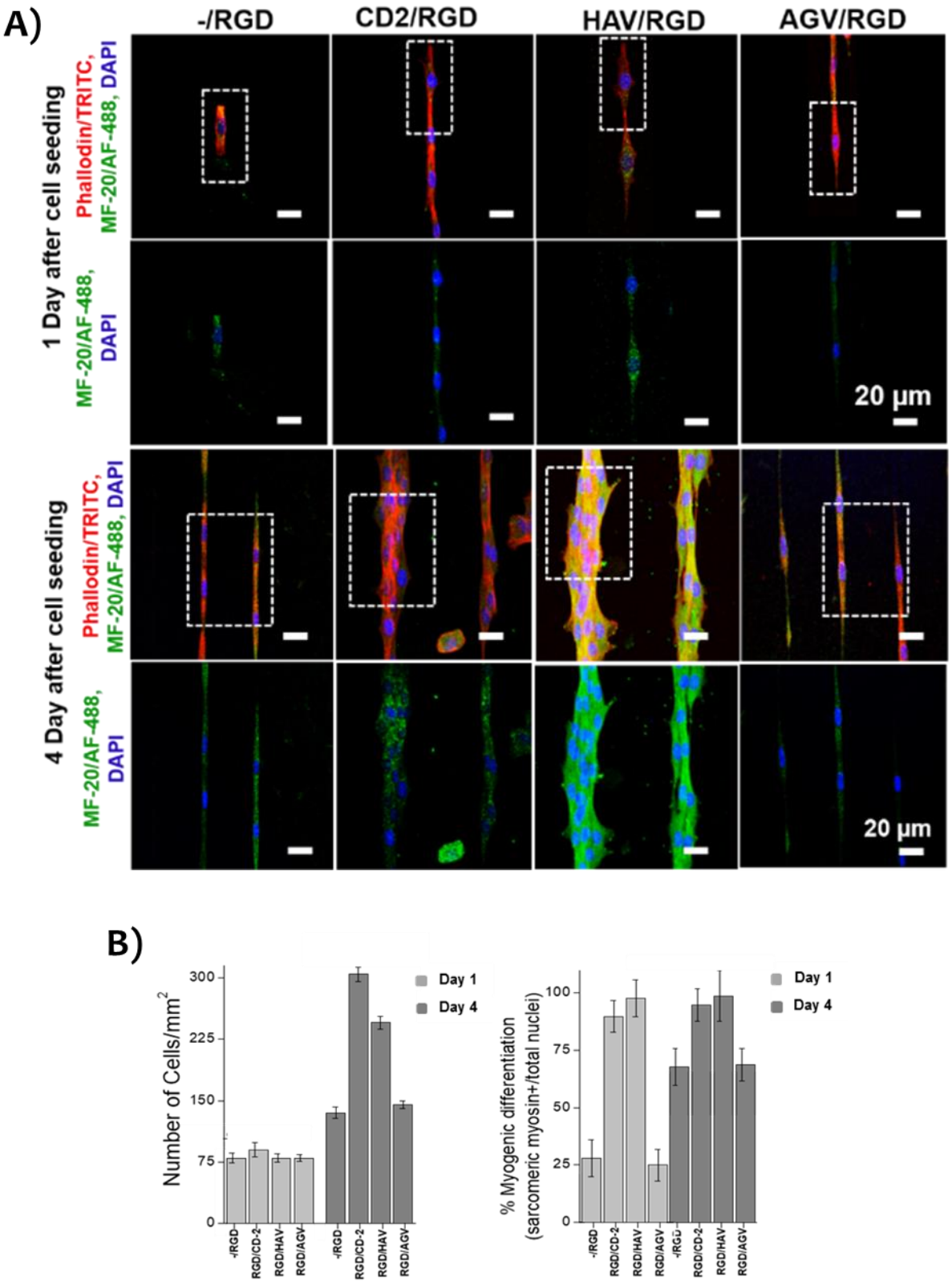

Fig. 5.2. *Myogenic differentiation of C2C12 myoblast in 2.5D polarized microenvironments.* ***(A)*** *Immunofluorescence images of cells after 24h and 4 days culture seeded on bifunctional channels modified with RGD at the base and CD2, HAV or AGV on the walls. Actin (red), sarcomeric myosin*

(green), and nuclei (Blue). ***(B)*** *Quantification of cell density i.e. number of cells, and myogenic positive cells on different substrates.*

5.2.3 Regulation of myogenic differentiation of C2C12 myoblasts with light using the photoactivatable N-cadherin peptidomimetic

Photoactivatable N-cadherin peptidomimetic, H[Ru(bpy)2(PPh3)]AVDIGGGC mentioned in section 2.2.4 was studied to verify the inhibitory action of the photo protected peptide and activation of peptide using light. The experiments described in section 5.2.2 were repeated on gels functionalized at the walls with the N-cadherin peptide, H[Ru(bpy)2(PPh3)]AVDIGGGC. The ability of photoactivatable N-cadherin peptide H[Ru(bpy)2(PPh3)]AVDIGGGC peptide to phototrig<ger N-cadherin dependent myogenic differentiation of C2C12 was tested by performing the experiments on irradiated *vs.* non irradiated hydrogels. (Irradiation conditions: 10 min at 423 nm, 0.34 $mWcm^{-2}$). This exposure dose had been proven sufficient to photocleavage the $[Ru(bpy)_2(PPh_3)]^{2+}$complex (**section 3.2.6**).

Cells cultured on 5µm wide channels functionalized at the walls with H[Ru(bpy)2(PPh3)]AVDIGGGC and at the bottom with RGD entered into channels, spread and proliferated (Fig 5.3(a)). The morphology of cells was similar to the morphology in the channels that were only functionalized with RGD at the bottom (Figure 5.2). No significant elongation of the cells was observed. In contrast, C2C12 cells on pre-irradiated H[Ru(bpy)2(PPh3)]AVDIGGGC channels showed an elongated morphology, similar to the observations in channels with HAVDIGGGC or CD2 modified walls. This result indicates a successful activation of the N-cadherin peptide in the hydrogel. This was confirmed by quantifying the expression levels of myogenic differentiation marker. Low expression values were obtained when the channel walls were either not modified or modified with the H[Ru(bpy)2(PPh3)]AVDIGGGC peptide (no irradiation). The myogenic differentiation marker was upregulated on the channels modified with H[Ru(bpy)2(PPh3)]AVDIGGGC and exposed to light, up to similar levels to the channels modified with HAVDIGGGC (**Fig. 5.3B**).

Proliferation levels were not affected by the functionalization of the channel wall at day 1, as observed in previous experiments (**Fig. 5.2**). However, proliferation ratio after 4 days

culture between non irradiated and preirradiated substrates with H[Ru(bpy)2(PPh3)]AVDIGGGC modification did show significant differences. Low proliferation levels were observed in channels with walls modified with H[Ru(bpy)2(PPh3)]AVDIGGGC, with similar values to channels with no wall modification. In contrast, preirradiated channels showed much higher proliferation ratios, similar to the values observed on the positive control (HAVDI/RGD channel). MF-20 expression levels were also significantly higher in cells cultured on pre-irradiated substrates compared to those with the protected peptide. Formation of multinucleated myocytes was also observed upon light activation of the wall functionality. These results confirm the lack of bioactivity of the H[Ru(bpy)2(PPh3)]AVDIGGGC peptide, and the possibility to restore it upon irradiation. Moreover, the observed results also indicate that the Ru complex in H[Ru(bpy)2(PPh3)]AVDIGGGC remains stable under cell culture condition, at least for 4 days.

In order to exclude that the light exposure step was responsible for the observed changes, substrates functionalized with cyclo(RGDfK) at the bottom were irradiated at the same conditions, and proliferation and differentiation of C2C12 cells was quantified. Fig.5.4 shows the results. Cells on these microchannels showed a very similar behavior to cells on non-irradiated microchannels (**Fig. 5.3**). Number of cells attached on hydrogels functionalized with H[Ru(bpy)2(PPh3)]AVDIGGGC peptide was same as non-functionalized substrates. Whereas the preirradiated substrates had regained its bioactivity and shown to have number of cells attached close to HAVDIGGGC peptide functionalized substrates. Moreover, the preirradiated substrates promoted myogenic differentiation of C2C12 cells after 4days of cell culture, as observed on HAVDIGGGC (**Fig. 5.2**). These results confirm that the photolysis reaction on N-cadherin mimetic peptide immobilized on p(AAm-MS) hydrogel was successful and the bioactivity of peptide could be restored after light exposure.

In summary, the attachment of [Ru(bpy)2(PPh3)] complex to the His residue of the N-cadherin peptidomimetic HAVDIGGGC inhibits the N-cadherin specific responses of cells to the presence of this peptide in a biointerface. This inhibitory effect can be maintained in cell culture at least for 4 days. Light exposure is able to restore functionality at similar cell response levels to the original peptide.

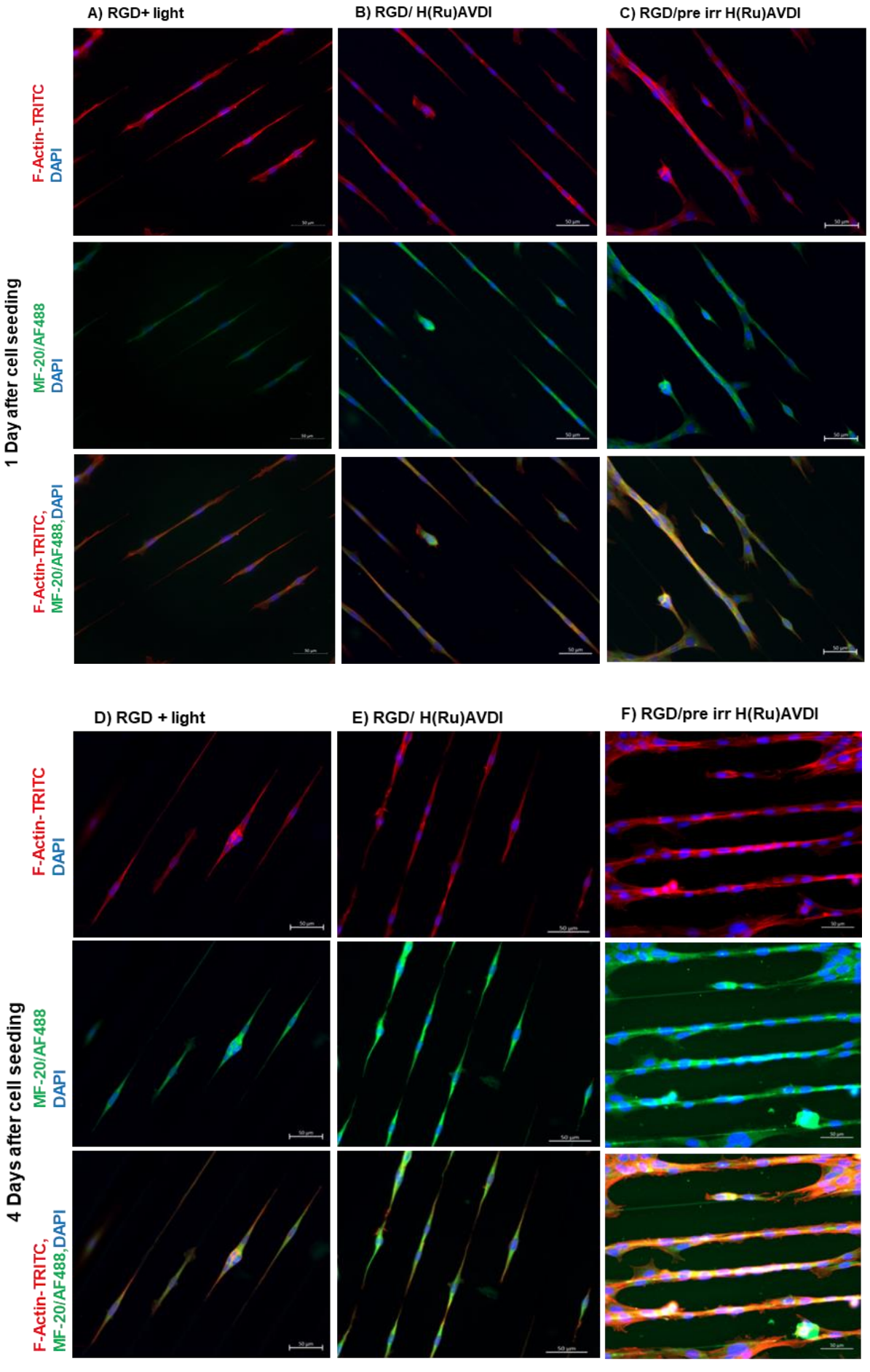
A) RGD+ light
B) RGD/ H(Ru)AVDI
C) RGD/pre irr H(Ru)AVDI
1 Day after cell seeding
F-Actin-TRITC
DAPI
MF-20/AF488
DAPI
F-Actin-TRITC,
MF-20/AF488,DAPI
D) RGD + light
E) RGD/ H(Ru)AVDI
F) RGD/pre irr H(Ru)AVDI
4 Days after cell seeding
F-Actin-TRITC
DAPI
MF-20/AF488
DAPI
F-Actin-TRITC,
MF-20/AF488,DAPI

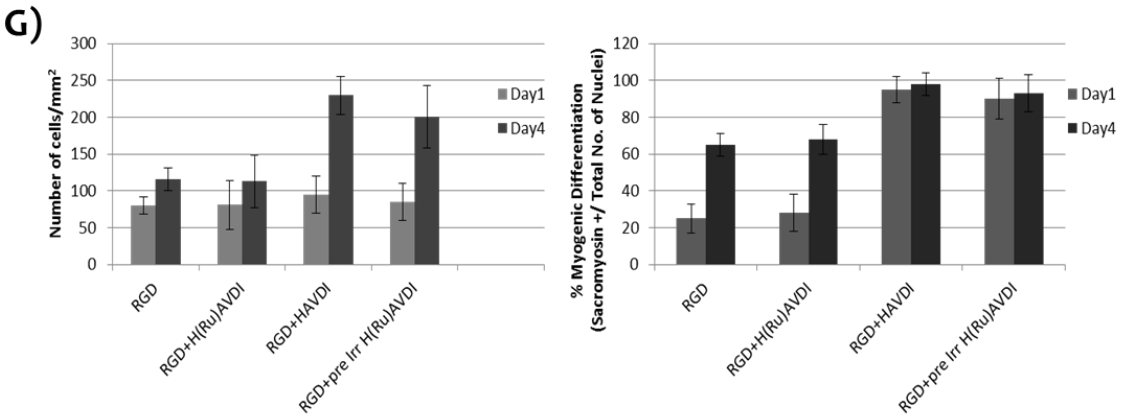

Fig. 5.3 *Myogenic differentiation of C2C12 myoblast in 2.5D polarized microenvironments: (A-F) Immunofluorescence images of cells after 24h and 4 days culture on bifunctional channels modified with RGD at the base and with H[Ru(bpy)2(PPh3)]AVDIGGGC at the walls. Samples that were not irradiated and samples that were irradiated are shown. As control, experiments performed on preirradiated hydrogels with RGD modification at the bottom and no modification at the walls are also shown. Actin (red), sarcomeric myosin (green) and nucleus (blue). (G) Quantification of cell density and ratio of myogenic positive cells on different hydrogels (n=200-600 cell/sample).*

5.3 Conclusion

In this chapter the possibility to photoregulate myogenic differentiation on hydrogels presenting a H[Ru(bpy)2(PPh3)]AVDIGGGC biointerface was studied. A bifunctional hydrogel with micropatterned channels modified with N-cadherin cell-cell adhesive ligand at the walls and with an RGD matrix adhesive ligand at the bottom were shown to promote myogenic differentiation of C2C12 cells in 4 days. This polarized exposure of cell-matrix and cell-cell ligands allowed to study the effect the establishment of N-cadherin mediated cell-cell contacts on the myogenic differentiation of C2C12 cells, and to test its regulation with light. The light-triggered interaction of the hydrogel-bound photoactivatable H[Ru(bpy)2(PPh3)]AVDIGGGC peptide with N-cadherins at the cell membrane was confirmed. The spatial differentiation of cell-cell and cell-matrix adhesive ligands in the 2.5D gels was important for the interaction between cadherin peptide on the gel and N-cadherin protein at the membrane. This study shows that N-cadherin mediated cellular process can be regulated with light by using photoactivatable H[Ru(bpy)2(PPh3)]AVDIGGGC.

5.4 Materials and methods

5.4.1 Preparation and functionalization of p(AAm-AA) and p(AAm-AA-MS) hydrogels

The hydrogels were prepared by following the protocol described in chapter 3.

5.4.2 Preparation and functionalization bilayer p(AAm-AA-MS) hydrogels

The hydrogels were prepared by following the protocol described in chapter 3.

5.4.3 Cell culture

C2C12 mouse myoblast cell line (ATCC, CRL-1772) were grown at 37° C and 5% CO2 in DMEM-HG medium (CLS cell lines service Germany, 820300a) contain 20% fetal bovine serum (Invitrogen) and 1% penicillin-streptavidin (Invitrogen). Hydrogel samples were sterilized by placing in 30% ethanol for 10 minutes in a laminar flow, followed by washing twice with sterile PBS. Cells were seeded on the sterilized peptide functionalized hydrogel films placed in 24-well plates. 500 µL of medium was used per well and culture was kept between 24h -14 days. 260 cell/mm2 were used for 1-2 days of culture, and 200 cell/mm2 for 4 days culture of culture to avoid over confluency of cells. Medium was changed after every 48h during myogenic differentiation studies.

5.4.4 Staining Protocol

Cells were fixed with 4% PFA solution after 1-4 days of culture, permeabilized with 0.1% Triton for 5 minutes and incubated with primary antibodies for sarcomeric myosin MF-20 (1:500, antibodies online, ABIN457406) or with N-Cadherin (1:100, antibodies online, ABIN969038) prepared in 1% BSA for 2h at r.t. Samples were washed three times with PBS and incubated for 2h at r.t with secondary antibodies solution prepared in water. Anti-mouse AF-488 (1:500) was used for MF-20 or N-cadherin, actin fibers and nuclei were stained with TRITC-phalloidin (1:200) and DAPI (1:500) respectively. Samples were mounted using mounting medium (Dinova) following standard protocols. Imaging was performed using Zeiss axio observer epi-fluorescence microscope or Zeiss-LSM 880 with Airyscan.

5.4.5 Statistical Analysis

All experiments were performed as three independent experiments and data are expressed in ± SD. Cell number, spreading area, sarcomeric positive cells were counted from fluorescence images taken after fixation and staining. The area of cells and nucleus were

measured using Zen blue software. The numbers of sarcomeric positive cells were counted manually.

Chapter 6

Summary

In this PhD thesis, photoactivatable E and N-cadherin peptidomimetics have been developed by attaching a bisbipyridyl ruthenium (II) complex as protecting group to a His residue of the peptidomimetic sequence. The photo protecting group temporarily inhibits the cadherin mediated bioactivity, which can be regained by exposure at visible wavelengths. Hydrogel surfaces modified with these peptides were used to culture cells and reconstitute a biomimetic cell-cell interface. E-cadherin peptide functionalized hydrogels allowed interaction with the E-cadherin protein on cell membrane of epithelial cells, resulting in cell adhesion and spreading on the hydrogels. On micropatterned hydrogels with spatially polarized presentation of cadherin and matrix mimetic peptides, N-cadherin dependent myogenic differentiation was regulated by light.

The major conclusions of this work are as follows:

1) The study of cell-cell adhesive interactions at molecular scale at the natural cell-cell interface is complicated, and the use of simplified synthetic interfaces with cadherin peptidomimetics can experimentally simplify such studies.
2) The control of cell-cell interaction spatiotemporally and noninvasively is challenging. The developed cadherin mimetic HAVDIGGGC(N-cadherin) and SHAVSSC (E-cadherin) peptides modified with photolabile [Ru(bpy)2(PPh3)] group at His residue provide a useful approach to control cadherin mediated cell-cell interaction on biomaterials with light.
3) Past fundamental studies on E-cadherin mediated cell-cell interactions were mainly focused on E-cadherin proteins. This thesis demonstrates that the E-cadherin mimetic peptide SHAVSSGGGC immobilized on polyacrylamide hydrogels activates E-cadherin mediated cellular response on epithelial cells in a similar way to surface immobilized E-cadherin fragments. Selective interaction with E-cadherin and E-cadherin mediated cellular response was also observed on hydrogels modified with ADTPPVGGGC and SWEL peptides.

4) Functionalized micropatterned hydrogels with matrix and cadherin adhesive peptides in a polarized manner, as observed in specific natural cellular niches, can support

differentiation processes on artificial substrates which are dependent on cell-cell contacts.

5) Photoactivatable N-cadherin peptide H[Ru(bpy)2(PPh3)]AVDIGGGC allows control of N-cadherin regulated myogenesis with temporal resolution. This system and peptides can be further explored to understand the cadherin regulated biological process.

List of scientific contributions

Articles

1. A. Farrukh, **D. Joseph**, R. V. Nair, A. del Campo, A Biomaterials Platform to Decouple Cell-Matrix and Cell-Cell Interactions and Mechanics (In preparation).

Poster Presentations

1. A. Farrukh, **D. Joseph**, R. V. Nair, A. del Campo, A Biomaterials Platform to Decouple Cell-Matrix and Cell-Cell Forces; FEBS Workshop – Biological Surfaces and Interfaces: Interface Dynamics. 02 – 07 July **2017**, Hotel Eden Roc, Sant Feliu de Guixols, Catalonia, Spain
2. A. Farrukh, **D. Joseph**, R. V. Nair, A. del Campo, A Biomaterials Platform to Decouple Cell-Matrix and Cell-Cell Forces; Cell Physics Conference, 11-13 October **2017**, Saarland University, Saarbrücken
3. **D. Joseph**, A. Farrukh, R. V. Nair, A. del Campo, Synthetic Bio-interfaces that can talk to Cells; N^2 Science Communication Conference, 06-08 November **2017**, Museum für Naturkunde, Berlin
4. A. Farrukh, **D. Joseph**, R. V. Nair, A. del Campo, A Biomaterials Platform to Decouple Cell-Matrix and Cell-Cell Forces; Bio inspired and Biomimetic Hydrogels, A Theodore von Kármán Discussion Conference Materials for Life, 15 – 18 April **2018**, Kardinal-Schulte-HausBergisch-Gladbach, Germany

Workshops

1. Basic cell culture course, Promo cell academy, Heidelberg, January **2018**

Participation in lectures

1. Modern Laser Microscopy in cell biology; University of Saarland, Summer **2016** Department of Biophotonics and laser Technology; Lecturer: Prof. Dr. Hanil. Karsten König, Dr. Uchugonova
2. Carbohydrate chemistry; University of Saarland and HIPS, Summer **2017**; Lecturer: Dr. Alexander Titz

3. Electrochemistry; University of Saarland and KIST; winter **2017-2018**, Lecturer: Dr. Ruiyong Chen
4. Biopolymers course; University of Saarland and INM, Summer **2018**, Lecturer: Prof. Aranzazu del campo

Teaching assistantships for masters courses

1. Biopolymers practicum, Summer **2017**; Preparation of pAAM hydrogels and functionalization with peptides.

2. Biopolymers practicum, Summer **2018**; Preparation of pAAM hydrogels and functionalization with peptides.

Curriculum Vitae

Desna Joseph

Personal Details

Date of Birth	17th June 1992
Place of Birth	Kerala, India

Professional Experience

10.2019 – present	ABX Advanced biochemical compounds, Radeberg, Germany **Research Scientist, Peptide Chemistry, Department of Medicinal Chemistry**
02.2016 – 07.2019	INM-Leibniz Institute for New Materials Saarbrücken, Germany **Doctorate studies, Dynamic Biomaterials**
07.2015 – 12.2015	IISER-Indian Institute of Science Education and Research, Bhopal, India **Research Assistant, Organic Chemistry**
05.2014 – 04.2015	IISER-Indian Institute of Science Education and Research, Bhopal, India **MS thesis, Organic Chemistry**
05.2013 – 07.2013	IIST-Indian Institute of Space Science and Technology, Trivandrum, India, **Summer Internship, Organic Chemistry**
05.2012 – 07.2012	IIT-Indian Institute of Technology Madras, Chennai, India **Summer Internship, Organometallic Chemistry**

Education

02.2016 – Present	**PhD in Chemistry** INM-Leibniz Institute for New Materials, University of Saarland, Germany **Tentative title of the thesis**: Light responsive cell-cell like biointerface using cadherin peptidomimetics **Supervisor:** Prof. Dr. A. del Campo
07.2010 – 05.2015	**BS-MS (Dual Degree) in Chemistry** IISER-Indian Institute of Science Education and Research Bhopal, India **Master thesis:** Synthesis of atropisomeric pyrroles via (4+1) pyrrolannulations of Ru(II) enalcarbenoids with 2,6-disubstituted anilines **Supervisor:** Dr. Sreenivas Katukojvala

References

(1) Cooper, G. M. *The Cell: A Molecular Approach. 2nd Edition*; **2000**. https://doi.org/10.1016/B978-0-12-387738-3.00003-2.

(2) McMillen, P.; Holley, S. A. Integration of Cell-Cell and Cell-ECM Adhesion in Vertebrate Morphogenesis. *Current Opinion in Cell Biology*. **2015**. https://doi.org/10.1016/j.ceb.2015.07.002.

(3) Yan, Z.; Qin, H.; Ren, J.; Qu, X. Photocontrolled Multidirectional Differentiation of Mesenchymal Stem Cells on an Upconversion Substrate. *Angew. Chem. - Int. Ed.* **2018**. https://doi.org/10.1002/anie.201803939.

(4) Bartelt, S. M.; Chervyachkova, E.; Ricken, J.; Wegner, S. V. Mimicking Adhesion in Minimal Synthetic Cells. *Adv. Biosyst.* **2019**, *1800333*, 1800333. https://doi.org/10.1002/adbi.201800333.

(5) Rekka, N. C. I.; Sathiyawathie, R. S.; Abilasha, R. Cell Adhesion Molecules. *Drug Invent. Today* **2019**.

(6) Garcia-Gonzalez, E.; Swerlick, R. A.; Lawley, T. J. Cell Adhesion Molecules. *Am. J. Dermatopathol.* **1990**, *12* (2), 188–192. https://doi.org/10.1097/00000372-199004000-00011.

(7) Lodish, H.; Berk, A.; Zipursky, S. Cell Biology. 4th Edition. In *Section 22.1 Cell-Cell Adhesion and Communication*; **2000.**

(8) Rosso, F.; Giordano, A.; Barbarisi, M.; Barbarisi, A. From Cell-ECM Interactions to Tissue Engineering. *Journal of Cellular Physiology*. **2004**. https://doi.org/10.1002/jcp.10471.

(9) Takada, Y.; Ye, X.; Simon, S. The Integrins. *Genome Biol.* **2007**, *8* (5), 215. https://doi.org/10.1186/gb-2007-8-5-215.

(10) Campbell, I. D.; Humphries, M. J. Integrin Structure, Activation, and Interactions. *Cold Spring Harb. Perspect. Biol.* **2011**. https://doi.org/10.1101/cshperspect.a004994.

(11) Goldfinger, L. E. Integrin Signaling. In *Encyclopedia of Biological Chemistry: Second Edition*; **2013**. https://doi.org/10.1016/B978-0-12-378630-2.00447-3.

(12) Aplin, A. E.; Howe, A.; Alahari, S. K.; Juliano, R. L. Signal Transduction and Signal Modulation by Cell Adhesion Receptors: The Role of Integrins, Cadherins, Immunoglobulin-Cell Adhesion Molecules, and Selectins. *Pharmacol. Rev.* **1998**.

(13) Geiger, B.; Yamada, K. M. Molecular Architecture and Function of Matrix Adhesions. *Cold Spring Harb. Perspect. Biol.* **2011**. https://doi.org/10.1101/cshperspect.a005033.

(14) Hartsock, A.; Nelson, W. J. Adherens and Tight Junctions: Structure, Function and Connections to the Actin Cytoskeleton. *Biochim. Biophys. Acta BBA - Biomembr.* **2008**, *1778* (3), 660–669. https://doi.org/10.1016/j.bbamem.2007.07.012.

(15) Knudsen, K. A.; Soler, A. P. Cadherin-Mediated Cell-Cell Interactions. In *Developmental Biology Protocols*; Humana Press: New Jersey, **2000**; Vol. 137, pp 409–440. https://doi.org/10.1385/1-59259-066-7:409.

(16) Ranscht, B. Cadherins and Catenins: Interactions and Functions in Embryonic Development. *Curr. Opin. Cell Biol.* **1994**. https://doi.org/10.1016/0955-0674(94)90102-3.

(17) Takeichi, M. The Cadherins: Cell-Cell Adhesion Molecules Controlling Animal Morphogenesis. *Dev. Camb. Engl.* **1988**.

(18) Tsukita, S.; Tsukita, S.; Nagafuchi, A.; Yonemura, S. Molecular Linkage between Cadherins and Actin Filaments in Cell-Cell Adherens Junctions. *Curr. Opin. Cell Biol.* **1992**. https://doi.org/10.1016/0955-0674(92)90108-O.

(19) Benjamin, J. M.; Kwiatkowski, A. V.; Yang, C.; Korobova, F.; Pokutta, S.; Svitkina, T.; Weis, W. I.; Nelson, W. J. AE-Catenin Regulates Actin Dynamics Independently of Cadherin-Mediated Cell–Cell Adhesion. *J. Cell Biol.* **2010**, *189* (2), 339–352. https://doi.org/10.1083/jcb.200910041.

(20) Van Roy, F.; Berx, G. The Cell-Cell Adhesion Molecule E-Cadherin. *Cell. Mol. Life Sci.* **2008**, *65* (23), 3756–3788. https://doi.org/10.1007/s00018-008-8281-1.
(21) Akaike, T. The Curses and the Blesses of E-Cadherin. *Hum. Genet. Embryol.* **2014**, *04* (01). https://doi.org/10.4172/2161-0436.1000118.
(22) Paridah, M. t; Moradbak, A.; Mohamed, A. Z.; Owolabi, F. abdulwahab taiwo; Asniza, M.; Abdul Khalid, S. H. P. We Are IntechOpen , the World ' s Leading Publisher of Open Access Books Built by Scientists , for Scientists TOP 1 %. *Intech* **2016**, *i* (tourism), 13. http://dx.doi.org/10.5772/57353.
(23) AWATA, R.; SAWAI, H.; IMAI, K.; TERADA, K.; SENOO, H.; SUGIYAMA, T. Morphological Comparison and Functional Reconstitution of Rat Hepatic Parenchymal Cells on Various Matrices. *J. Gastroenterol. Hepatol.* **1998**. https://doi.org/10.1111/jgh.1998.13.s1.55.
(24) Atwood, C. S.; Meethal, S. V. *Pluripotent Stem Cell Biology - Advances in Mechanisms, Methods and Models*; **2014**. https://doi.org/10.5772/57025.
(25) Carrasco, S.; Meyer, T. N E W S A N D V I E W S Cracking CRAC. *Nat. CELL Biol.* **2010**.
(26) Larue, L.; Antos, C.; Butz, S.; Huber, O.; Delmas, V.; Dominis, M.; Kemler, R. A Role for Cadherins in Tissue Formation. *Dev. Camb. Engl.* **1996**.
(27) Charest, J. L.; Jennings, J. M.; King, W. P.; Kowalczyk, A. P.; García, A. J. Cadherin-Mediated Cell-Cell Contact Regulates Keratinocyte Differentiation. *J. Invest. Dermatol.* **2009**. https://doi.org/10.1038/jid.2008.265.
(28) Young, P.; Boussadia, O.; Halfter, H.; Grose, R.; Berger, P.; Leone, D. P.; Robenek, H.; Charnay, P.; Kemler, R.; Suter, U. E-Cadherin Controls Adherens Junctions in the Epidermis and the Renewal of Hair Follicles. *EMBO J.* **2003**. https://doi.org/10.1093/emboj/cdg560.
(29) Thiery, J. P.; Acloque, H.; Huang, R. Y. J.; Nieto, M. A. Epithelial-Mesenchymal Transitions in Development and Disease. *Cell* **2009**, *139* (5), 871–890. https://doi.org/10.1016/j.cell.2009.11.007.
(30) Stemmler, M. P. Cadherins in Development and Cancer. *Molecular BioSystems*. **2008**, pp 835–850. https://doi.org/10.1039/b719215k.
(31) Hatta, K.; Takeichi, M. Expression of N-Cadherin Adhesion Molecules Associated with Early Morphogenetic Events in Chick Development. *Nature* **1986**. https://doi.org/10.1038/320447a0.
(32) Xu, L.; Overbeek, P. A.; Reneker, L. W. Systematic Analysis of E-, N- and P-Cadherin Expression in Mouse Eye Development. *Exp. Eye Res.* **2002**. https://doi.org/10.1006/exer.2002.1175.
(33) Linask, K. K. N-Cadherin Localization in Early Heart Development and Polar Expression of Na+, K+-ATPase, and Integrin during Pericardial Coelom Formation and Epithelialization of the Differentiating Myocardium. *Dev. Biol.* **1992**. https://doi.org/10.1016/0012-1606(92)90228-9.
(34) Hatta, K.; Takagi, S.; Fujisawa, H.; Takeichi, M. Spatial and Temporal Expression Pattern of N-Cadherin Cell Adhesion Molecules Correlated with Morphogenetic Processes of Chicken Embryos. *Dev. Biol.* **1987**. https://doi.org/10.1016/0012-1606(87)90119-9.
(35) George-Weinstein, M.; Gerhart, J.; Blitz, J.; Simak, E.; Knudsen, K. A. N-Cadherin Promotes the Commitment and Differentiation of Skeletal Muscle Precursor Cells. *Dev. Biol.* **1997**. https://doi.org/10.1006/dbio.1997.8542.
(36) Liu, Z.-P.; Wang, Z.; Yanagisawa, H.; Olson, E. N. Phenotypic Modulation of Smooth Muscle Cells through Interaction of Foxo4 and Myocardin Nisms That Link These Signaling Pathways to the Program for SMC Gene Expression. *Dev. Cell* **2005**. https://doi.org/10.1016/j.devcel.2005.05.017.
(37) Nag, K.; Adnan, N.; Kutsuzawa, K.; Akaike, T. Cadherin-Fc Chimeric Protein-Based Biomaterials: Advancing Stem Cell Technology and Regenerative Medicine Towards Application. *Pluripotent Stem Cell Biol. - Adv. Mech. Methods Models* **2014**. https://doi.org/10.5772/58287.

(38) Shapiro, L.; Fannon, A. M.; Kwong, P. D.; Thompson, A.; Lehmann, M. S.; Gerhard, G.; Als-Nielsen, J.; Als-Nielsen, J.; Colman, D. R.; Hendrickson, W. A. Structural Basis of Cell-Cell Adhesion by Cadherins. *Nature* **1995**. https://doi.org/10.1038/374327a0.

(39) Hatta, K.; Nose, A.; Nagafuchi, A.; Takeichi, M. Cloning and Expression of CDNA Encoding a Neural Calcium-Dependent Cell Adhesion Molecule: Its Identity in the Cadherin Gene Family. *J. Cell Biol.* **1988**. https://doi.org/10.1083/jcb.106.3.873.

(40) Harrison, O. J.; Jin, X.; Hong, S.; Bahna, F.; Ahlsen, G.; Brasch, J.; Wu, Y.; Vendome, J.; Felsovalyi, K.; Hampton, C. M.; Troyanovsky, R. B.; Ben-Shaul, A.; Frank, J.; Troyanovsky, S. M.; Shapiro, L.; Honig, B. The Extracellular Architecture of Adherens Junctions Revealed by Crystal Structures of Type i Cadherins. *Structure* **2011**. https://doi.org/10.1016/j.str.2010.11.016.

(41) Brasch, J.; Harrison, O. J.; Honig, B.; Shapiro, L. Thinking Outside the Cell: How Cadherins Drive Adhesion. *Trends in Cell Biology*. **2012**. https://doi.org/10.1016/j.tcb.2012.03.004.

(42) Blaschuk, O. W.; Sullivan, R.; David, S.; Pouliot, Y. Identification of a Cadherin Cell Adhesion Recognition Sequence. *Dev. Biol.* **1990**, *139* (1), 227–229. https://doi.org/10.1016/0012-1606(90)90290-Y.

(43) Williams, E.; Williams, G.; Gour, B. J.; Blaschuk, O. W.; Doherty, P. A Novel Family of Cyclic Peptide Antagonists Suggests That N-Cadherin Specificity Is Determined by Amino Acids That Flank the HAV Motif. *J. Biol. Chem.* **2000**, *275* (6), 4007–4012. https://doi.org/10.1074/jbc.275.6.4007.

(44) Blaschuk, O. W. N-Cadherin Antagonists as Oncology Therapeutics. *Philosophical Transactions of the Royal Society B: Biological Sciences*. Royal Society of London January 5, **2015**. https://doi.org/10.1098/rstb.2014.0039.

(45) Biswas, K. H.; Hartman, K. L.; Zaidel-Bar, R.; Groves, J. T. Sustained α-Catenin Activation at E-Cadherin Junctions in the Absence of Mechanical Force. *Biophys. J.* **2016**, *111* (5), 1044–1052. https://doi.org/10.1016/j.bpj.2016.06.027.

(46) Biswas, K. H.; Hartman, K. L.; Yu, C.; Harrison, O. J.; Song, H.; Smith, A. W.; Huang, W. Y. C.; Lin, W.-C.; Guo, Z.; Padmanabhan, A.; Troyanovsky, S. M.; Dustin, M. L.; Shapiro, L.; Honig, B.; Zaidel-Bar, R.; Groves, J. T. E-Cadherin Junction Formation Involves an Active Kinetic Nucleation Process. *Proc. Natl. Acad. Sci.* **2015**, *112* (35), 10932–10937. https://doi.org/10.1073/pnas.1513775112.

(47) Andreasson-Ochsner, M.; Romano, G.; Håkanson, M.; Smith, M. L.; Leckband, D. E.; Textor, M.; Reimhult, E. Single Cell 3-D Platform to Study Ligand Mobility in Cell-Cell Contact. *Lab. Chip* **2011**, *11* (17), 2876–2883. https://doi.org/10.1039/c1lc20067d.

(48) Adams, C. L.; Chen, Y.-T.; Smith, S. J.; James Nelson, W. Mechanisms of Epithelial Cell–Cell Adhesion and Cell Compaction Revealed by High-Resolution Tracking of E-Cadherin– Green Fluorescent Protein. *J. Cell Biol.* **1998**, *142* (4), 1105–1119. https://doi.org/10.1083/jcb.142.4.1105.

(49) Evans, S. F.; Docheva, D.; Bernecker, A.; Colnot, C.; Richter, R. P.; Knothe Tate, M. L. Solid-Supported Lipid Bilayers to Drive Stem Cell Fate and Tissue Architecture Using Periosteum Derived Progenitor Cells. *Biomaterials* **2013**, *34* (8), 1878–1887. https://doi.org/10.1016/j.biomaterials.2012.09.024.

(50) Zobel, K.; Choi, S. E.; Minakova, R.; Gocyla, M.; Offenhäusser, A. N-Cadherin Modified Lipid Bilayers Promote Neural Network Formation and Circuitry. *Soft Matter* **2017**, *13* (44), 8096–8107. https://doi.org/10.1039/c7sm01214d.

(51) Li, J.; Di Russo, J.; Hua, X.; Chu, Z.; Spatz, J. P.; Wei, Q. Surface Immobilized E-Cadherin Mimetic Peptide Regulates the Adhesion and Clustering of Epithelial Cells. *Adv. Healthc. Mater.* **2019**, *8* (8), 1801384. https://doi.org/10.1002/adhm.201801384.

(52) Zhang, Y.; Mao, H.; Qian, M.; Hu, F.; Cao, L.; Xu, K.; Shuai, Q.; Gao, C.; Lang, R.; Akaike, T.; Yang, J. Surface Modification with E-Cadherin Fusion Protein for Mesenchymal Stem Cell Culture. *J. Mater. Chem. B* **2016,** *4*, 4267-4277. https://doi.org/10.1039/c6tb00765a.

(53) Gavard, J.; Lambert, M.; Grosheva, I.; Marthiens, V.; Irinopoulou, T.; Riou, J.-F.; Bershadsky, A.; Mège, R.-M. Lamellipodium Extension and Cadherin Adhesion: Two Cell Responses to Cadherin Activation Relying on Distinct Signalling Pathways. *J. Cell Sci.* **2004**, *117* (2), 257. https://doi.org/10.1242/jcs.00857.

(54) Fichtner, D.; Lorenz, B.; Engin, S.; Deichmann, C.; Oelkers, M.; Janshoff, A.; Menke, A.; Wedlich, D.; Franz, C. M. Covalent and Density-Controlled Surface Immobilization of E-Cadherin for Adhesion Force Spectroscopy. *PLoS ONE* **2014,** *9* (3), e93123. https://doi.org/10.1371/journal.pone.0093123.

(55) Kristensen, S. H.; Pedersen, G. A.; Nejsum, L. N.; Sutherland, D. S. Nanoscale E-Cadherin Ligand Patterns Show Threshold Size for Cellular Adhesion and Adherence Junction Formation. *Nano Lett.* **2012**, *12* (4), 2129–2133. https://doi.org/10.1021/nl300514v.

(56) Lin, E.; Sikand, A.; Wickware, J.; Hao, Y.; Derda, R. Peptide Microarray Patterning for Controlling and Monitoring Cell Growth. *Acta Biomater.* **2016**, *34*, 53–59. https://doi.org/10.1016/j.actbio.2016.01.028.

(57) Cosgrove, B. D.; Mui, K. L.; Driscoll, T. P.; Caliari, S. R.; Mehta, K. D.; Assoian, R. K.; Burdick, J. A.; Mauck, R. L. N-Cadherin Adhesive Interactions Modulate Matrix Mechanosensing and Fate Commitment of Mesenchymal Stem Cells. *Nat. Mater.* **2016**, *15* (12), 1297–1306. https://doi.org/10.1038/nmat4725.

(58) Collins, C.; Denisin, A. K.; Pruitt, B. L.; Nelson, W. J. Changes in E-Cadherin Rigidity Sensing Regulate Cell Adhesion. *Proc. Natl. Acad. Sci.* **2017**, *114* (29), E5835–E5844. https://doi.org/10.1073/pnas.1618676114.

(59) Caliari, S. R.; Burdick, J. A. A Practical Guide to Hydrogels for Cell Culture. *Nat. Methods* **2016**, *13* (5), 405–414. https://doi.org/10.1038/nmeth.3839.

(60) Ladoux, B.; Anon, E.; Lambert, M.; Rabodzey, A.; Hersen, P.; Buguin, A.; Silberzan, P.; Mège, R. M. Strength Dependence of Cadherin-Mediated Adhesions. *Biophys. J.* **2010**, *98* (4), 534–542. https://doi.org/10.1016/j.bpj.2009.10.044.

(61) Bian, L.; Guvendiren, M.; Mauck, R. L.; Burdick, J. A. Hydrogels That Mimic Developmentally Relevant Matrix and N-Cadherin Interactions Enhance MSC Chondrogenesis. *Proc. Natl. Acad. Sci.* **2013**, *110* (25), 10117–10122. https://doi.org/10.1073/pnas.1214100110.

(62) Zhu, M.; Lin, S.; Sun, Y.; Feng, Q.; Li, G.; Bian, L. Hydrogels Functionalized with N-Cadherin Mimetic Peptide Enhance Osteogenesis of HMSCs by Emulating the Osteogenic Niche. *Biomaterials* **2016**, *77*, 44–52. https://doi.org/10.1016/j.biomaterials.2015.10.072.

(63) Moreno-Bueno, G.; Peinado, H.; Molina, P.; Olmeda, D.; Cubillo, E.; Santos, V.; Palacios, J.; Portillo, F.; Cano, A. The Morphological and Molecular Features of the Epithelial-to-Mesenchymal Transition. *Nat. Protoc.* **2009**, *4* (11), 1591–1613. https://doi.org/10.1038/nprot.2009.152.

(64) Yüz, S. G.; Rasoulinejad, S.; Mueller, M.; Wegner, A. E.; Wegner, S. V. Blue Light Switchable Cell-Cell Interactions Provide Reversible and Spatiotemporal Control Towards Bottom-Up Tissue Engineering. *Adv. Biosyst.* **2019**, *1800310*, 1800310. https://doi.org/10.1002/adbi.201800310.

(65) STEINBERG, M. S. Reconstruction of Tissues by Dissociated Cells. Some Morphogenetic Tissue Movements and the Sorting out of Embryonic Cells May Have a Common Explanation. *Science* **1963,** *141* (3579), 401-408. https://doi.org/10.1126/science.141.3579.401.

(66) Duguay, D.; Foty, R. A.; Steinberg, M. S. Cadherin-Mediated Cell Adhesion and Tissue Segregation: Qualitative and Quantitative Determinants. *Dev. Biol.* **2003**, *253* (2), 309-323. https://doi.org/10.1016/S0012-1606(02)00016-7.

(67) Shao, Q.; Xing, B. Photoactive Molecules for Applications in Molecular Imaging and Cell Biology. *Chemical Society Reviews*. **2010,** *39*, 2835-2846. https://doi.org/10.1039/b915574k.

(68) Petersen, S.; Alonso, J. M.; Specht, A.; Duodu, P.; Goeldner, M.; Del Campo, A. Phototriggering of Cell Adhesion by Caged Cyclic RGD Peptides. *Angew. Chem. - Int. Ed.* **2008**, *47* (17), 3192–3195. https://doi.org/10.1002/anie.200704857.

(69) Wirkner, M.; Weis, S.; San Miguel, V.; Álvarez, M.; Gropeanu, R. A.; Salierno, M.; Sartoris, A.; Unger, R. E.; Kirkpatrick, C. J.; del Campo, A. Photoactivatable Caged Cyclic RGD Peptide for Triggering Integrin Binding and Cell Adhesion to Surfaces. *ChemBioChem* **2011**, *12* (17), 2623–2629. https://doi.org/10.1002/cbic.201100437.

(70) Salierno, M. J.; García, A. J.; Del Campo, A. Photo-Activatable Surfaces for Cell Migration Assays. *Adv. Funct. Mater.* **2013**, *23* (48), 5974–5980. https://doi.org/10.1002/adfm.201300902.

(71) Farrukh, A. B. for L.-G. A.; Paez, J. I.; Campo, A. 4D Biomaterials for Light-Guided Angiogenesis. **2018**, *1807734*, 1–11. https://doi.org/10.1002/adfm.201807734.

(72) Ohmuro-Matsuyama, Y.; Tatsu, Y. Photocontrolled Cell Adhesion on a Surface Functionalized with a Caged Arginine-Glycine-Aspartate Peptide. *Angew. Chem. - Int. Ed.* **2008**, *47* (39), 7527–7529. https://doi.org/10.1002/anie.200802731.

(73) Farrukh, A.; Fan, W.; Zhao, S.; Salierno, M.; Paez, J. I.; del Campo, A. Photoactivatable Adhesive Ligands for Light-Guided Neuronal Growth. *ChemBioChem* **2018**, *19* (12), 1271–1279. https://doi.org/10.1002/cbic.201800118.

(74) Farrukh, A.; Zhao, S.; Paez, J. I.; Kavyanifar, A.; Salierno, M.; Cavalie, A. In Situ, Light-Guided Axon Growth on Biomaterials via Photoactivatable Laminin Peptidomimetic IK(HANBP)VAV. **2018**, 2–10. https://doi.org/10.1021/acsami.8b15517.

(75) Vagner, J.; Qu, H.; Hruby, V. J. Peptidomimetics, a Synthetic Tool of Drug Discovery. *Curr. Opin. Chem. Biol.* **2008**, *12* (3), 292–296. https://doi.org/10.1016/j.cbpa.2008.03.009.

(76) Klán, P.; Šolomek, T.; Bochet, C. G.; Blanc, A.; Givens, R.; Rubina, M.; Popik, V.; Kostikov, A.; Wirz, J. Photoremovable Protecting Groups in Chemistry and Biology: Reaction Mechanisms and Efficacy. *Chem. Rev.* **2013**, *113* (1), 119–191. https://doi.org/10.1021/cr300177k.

(77) Lizama, C. O.; Zovein, A. C. Polarizing Pathways: Balancing Endothelial Polarity, Permeability, and Lumen Formation. *Exp. Cell Res.* **2013**, *319* (9), 1247–1254. https://doi.org/10.1016/j.yexcr.2013.03.028.

(78) Worzfeld, T.; Schwaninger, M. Apicobasal Polarity of Brain Endothelial Cells. *J. Cereb. Blood Flow Metab.* **2016**, *36* (2), 340–362. https://doi.org/10.1177/0271678X15608644.

(79) Gillard, G.; Nicolle, O.; Brugière, T.; Prigent, S.; Pinot, M.; Michaux, G. Force Transmission between Three Tissues Controls Bipolar Planar Polarity Establishment and Morphogenesis. *Curr. Biol. - CB* **2019**, *29* (8), 1360-1368.e4. https://doi.org/10.1016/j.cub.2019.02.059.

(80) Borghi, N.; Lowndes, M.; Maruthamuthu, V.; Gardel, M. L.; Nelson, W. J. Regulation of Cell Motile Behavior by Crosstalk between Cadherin- and Integrin-Mediated Adhesions. *Proc. Natl. Acad. Sci.* **2010**, *107* (30), 13324–13329. https://doi.org/10.1073/pnas.1002662107.

(81) Lowndes, M.; Rakshit, S.; Shafraz, O.; Borghi, N.; Harmon, R. M.; Green, K. J.; Sivasankar, S.; Nelson, W. J. Different Roles of Cadherins in the Assembly and Structural Integrity of the Desmosome Complex. *J. Cell Sci.* **2014**, *127* (10), 2339. https://doi.org/10.1242/jcs.146316.

(82) Sim, J. Y.; Moeller, J.; Hart, K. C.; Ramallo, D.; Vogel, V.; Dunn, A. R.; Nelson, W. J.; Pruitt, B. L. Spatial Distribution of Cell–Cell and Cell–ECM Adhesions Regulates Force Balance While Main-taining E-Cadherin Molecular Tension in Cell Pairs. *Mol. Biol. Cell* **2015**, *26* (13), 2456–2465. https://doi.org/10.1091/mbc.E14-12-1618.

(83) Li, Q.; Zhang, Y.; Pluchon, P.; Robens, J.; Herr, K.; Mercade, M.; Thiery, J.-P.; Yu, H.; Viasnoff, V. Extracellular Matrix Scaffolding Guides Lumen Elongation by Inducing Anisotropic Intercellular Mechanical Tension. *Nat. Cell Biol.* **2016**, *18* (3), 311–318. https://doi.org/10.1038/ncb3310.

(84) Cohen, D. J.; Gloerich, M.; Nelson, W. J. Epithelial Self-Healing Is Recapitulated by a 3D Biomimetic E-Cadherin Junction. *Proc. Natl. Acad. Sci. U. S. A.* **2016,** *113*(51):14698-14703. https://doi.org/10.1073/pnas.1612208113.

(85) Hart, K. C.; Tan, J.; Siemers, K. A.; Sim, J. Y.; Pruitt, B. L.; Nelson, W. J.; Gloerich, M. E-Cadherin and LGN Align Epithelial Cell Divisions with Tissue Tension Independently of Cell Shape. *Proc. Natl. Acad. Sci.* **2017**, *114* (29), E5845–E5853. https://doi.org/10.1073/pnas.1701703114.

(86) Tsai, J.; Kam, L. Rigidity-Dependent Cross Talk between Integrin and Cadherin Signaling. *Biophys. J.* **2009,** *96* (6), L39-L41. https://doi.org/10.1016/j.bpj.2009.01.005.
(87) Gloerich, M.; Bianchini, J. M.; Siemers, K. A.; Cohen, D. J.; Nelson, W. J. Cell Division Orientation Is Coupled to Cell-Cell Adhesion by the E-Cadherin/LGN Complex. *Nat. Commun.* **2017**, *8*, 1–11. https://doi.org/10.1038/ncomms13996.
(88) Noë, V.; Willems, J.; Vandekerckhove, J.; Roy, F. Van; Bruyneel, E.; Mareel, M. Inhibition of Adhesion and Induction of Epithelial Cell Invasion by HAV-Containing E-Cadherin-Specific Peptides. *J. Cell Sci.* **1999**, *112*, 127–135.
(89) Lutz, K. L.; Siahaan, T. J. E-Cadherin Peptide Sequence Recognition by Anti-E-Cadherin Antibody. *Biochem. Biophys. Res. Commun.* **1995,** *211* (1),21-27. https://doi.org/10.1006/bbrc.1995.1772.
(90) Makagiansar, I. T.; Avery, M.; Hu, Y.; Audus, K. L.; Siahaan, T. J. Improving the Selectivity of HAV-Peptides in Modulating E-Cadherin-E-Cadherin Interactions in the Intercellular Junction of MDCK Cell Monolayers. *Pharm. Res.* **2001**, *18* (4), 446–453. https://doi.org/10.1023/A:1011094025008.
(91) Sinaga, E.; Jois, S. D. S.; Avery, M.; Makagiansar, I. T.; Tambunan, U. S. F.; Audus, K. L.; Siahaan, T. J. Increasing Paracellular Porosity by E-Cadherin Peptides: Discovery of Bulge and Groove Regions in the EC1-Domain of E-Cadherin. *Pharm. Res.* **2002**, *19* (8), 1170–1179. https://doi.org/10.1023/A:1019850226631.
(92) Kiptoo, P.; Sinaga, E.; Calcagno, A. M.; Zhao, H.; Kobayashi, N.; Tambunan, U. S. F.; Siahaan, T. J. Enhancement of Drug Absorption through the Blood-Brain Barrier and Inhibition of Intercellular Tight Junction Resealing by E-Cadherin Peptides. *Mol. Pharm.* **2011**, *8* (1), 239–249. https://doi.org/10.1021/mp100293m.
(93) On, N. H.; Kiptoo, P.; Siahaan, T. J.; Miller, D. W. Modulation of Blood-Brain Barrier Permeability in Mice Using Synthetic E-Cadherin Peptide. *Mol. Pharm.* **2014**, *11* (3), 974–981. https://doi.org/10.1021/mp400624v.
(94) Laksitorini, M. D.; Kiptoo, P. K.; On, N. H.; Thliveris, J. A.; Miller, D. W.; Siahaan, T. J. Modulation of Intercellular Junctions by Cyclic-ADT Peptides as a Method to Reversibly Increase Blood-Brain Barrier Permeability. *J. Pharm. Sci.* **2015**, *104* (3), 1065–1075. https://doi.org/10.1002/jps.24309.
(95) Alaofi, A.; On, N.; Kiptoo, P.; Williams, T. D.; Miller, D. W.; Siahaan, T. J. Comparison of Linear and Cyclic His-Ala-Val Peptides in Modulating the Blood-Brain Barrier Permeability: Impact on Delivery of Molecules to the Brain. *J. Pharm. Sci.* **2016**, *105* (2), 797–807. https://doi.org/10.1016/S0022-3549(15)00188-4.
(96) Kiptoo, P.; Sinaga, E.; Calcagno, A. M.; Zhao, H.; Kobayashi, N.; Tambunan, U. S. F.; Siahaan, T. J. Enhancement of Drug Absorption through the Blood-Brain Barrier and Inhibition of Intercellular Tight Junction Resealing by E-Cadherin Peptides. *Mol. Pharm.* **2011**, *8* (1), 239–249. https://doi.org/10.1021/mp100293m.
(97) Segal, J. M.; Ward, C. M. Novel Peptides for Deciphering Structural and Signalling Functions of E-Cadherin in Mouse Embryonic Stem Cells. *Sci. Rep.* **2017**, *7* (December 2016), 1–12. https://doi.org/10.1038/srep41827.
(98) Devemy, E.; Blaschuk, O. W. Identification of a Novel Dual E- and N-Cadherin Antagonist. *Peptides* **2009**, *30* (8), 1539–1547. https://doi.org/10.1016/j.peptides.2009.05.010.
(99) Pertz, O. A New Crystal Structure, Ca2+ Dependence and Mutational Analysis Reveal Molecular Details of E-Cadherin Homoassociation. *EMBO J.* **1999,** *18* (7), 1738-47. https://doi.org/10.1093/emboj/18.7.1738.
(100) Blaschuk, O. W. Discovery and Development of N-Cadherin Antagonists. *Cell and Tissue Research*. May **2012**, pp 309–313. https://doi.org/10.1007/s00441-011-1320-5.
(101) Doherty, P.; Rowett, L. H.; Moore, S. E.; Mann, D. A.; Walsh, F. S. Neurite Outgrowth in Response to Transfected N-CAM and N-Cadherin Reveals Fundamental Differences in Neuronal Responsiveness to CAMs. *Neuron* **1991,** *6* (2), 247-258. https://doi.org/10.1016/0896-6273(91)90360-C.

(102) Mege, R. M.; Goudou, D.; Diaz, C.; Nicolet, M.; Garcia, L.; Geraud, G.; Rieger, F. N-Cadherin and N-CAM in Myoblast Fusion - Compared Localisation and Effect of Blockade by Peptides and Antibodies. *J Cell Sci* **1992,** *103*, 897-906.
(103) Wilby, M. J.; Muir, E. M.; Fok-Seang, J.; Gour, B. J.; Blaschuk, O. W.; Fawcett, J. W. N-Cadherin Inhibits Schwann Cell Migration on Astrocytes. *Mol. Cell. Neurosci.* **1999,** *14* (1), 66-84. https://doi.org/10.1006/mcne.1999.0766.
(104) Williams, G.; Williams, E. J.; Doherty, P. Dimeric Versions of Two Short N-Cadherin Binding Motifs (HAVDI and INPISG) Function as N-Cadherin Agonists. *J. Biol. Chem.* **2002,** *277* (6), 4361-7. https://doi.org/10.1074/jbc.M109185200.
(105) Blaschuk, O. W.; Devemy, E. Cadherins as Novel Targets for Anti-Cancer Therapy. *European Journal of Pharmacology*. **2009**, *625* (1-3),195-8. https://doi.org/10.1016/j.ejphar.2009.05.033.
(106) Thota, S.; Vallala, S.; Yerra, R.; Rodrigues, D. A.; Raghavendra, N. M.; Barreiro, E. J. Synthesis, Characterization, DNA Binding, DNA Cleavage, Protein Binding and Cytotoxic Activities of Ru(II) Complexes. *Int. J. Biol. Macromol.* **2016,** *82*, 663-670. https://doi.org/10.1016/j.ijbiomac.2015.09.045.
(107) Li, A.; Turro, C.; Kodanko, J. J. Ru(II) Polypyridyl Complexes as Photocages for Bioactive Compounds Containing Nitriles and Aromatic Heterocycles. *Chem. Commun.* **2018**, *54* (11), 1280–1290. https://doi.org/10.1039/c7cc09000e.
(108) Donato, L.; Mourot, A.; Davenport, C. M.; Herbivo, C.; Warther, D.; Léonard, J.; Bolze, F.; Nicoud, J. F.; Kramer, R. H.; Goeldner, M.; Specht, A. Water-Soluble, Donor-Acceptor Biphenyl Derivatives in the 2-(o-Nitrophenyl)Propyl Series: Highly Efficient Two-Photon Uncaging of the Neurotransmitter γ-Aminobutyric Acid at Λ=800 Nm. *Angew. Chem. - Int. Ed.* **2012**, *51* (8), 1840–1843. https://doi.org/10.1002/anie.201106559.
(109) Zayat, L.; Noval, M. G.; Campi, J.; Calero, C. I.; Calvo, D. J.; Etchenique, R. A New Inorganic Photolabile Protecting Group for Highly Efficient Visible Light GABA Uncaging. *ChemBioChem* **2007**, *8* (17), 2035–2038. https://doi.org/10.1002/cbic.200700354.
(110) *Luminescent and Photoactive Transition Metal Complexes as Biomolecular Probes and Cellular Reagents*; **2015**; Vol. 165. https://doi.org/10.1007/978-3-662-46718-3.
(111) Mari, C.; Pierroz, V.; Ferrari, S.; Gasser, G. Combination of Ru(II) Complexes and Light: New Frontiers in Cancer Therapy. *Chem. Sci.* **2015**, *6* (5), 2660–2686. https://doi.org/10.1039/c4sc03759f.
(112) Sgambellone, M. A.; David, A.; Garner, R. N.; Dunbar, K. R.; Turro, C. Cellular Toxicity Induced by the Photorelease of a Caged Bioactive Molecule: Design of a Potential Dual-Action Ru(II) Complex. *J. Am. Chem. Soc.* **2013**, *135* (30), 11274–11282. https://doi.org/10.1021/ja4045604.
(113) Mosquera, J.; Sánchez, M. I.; Mascareñas, J. L.; Eugenio Vázquez, M. Synthetic Peptides Caged on Histidine Residues with a Bisbipyridyl Ruthenium(Ii) Complex That Can Be Photolyzed by Visible Light. *Chem. Commun.* **2015**, *51* (25), 5501–5504. https://doi.org/10.1039/c4cc08049a.
(114) Zayat, L.; Filevich, O.; Baraldo, L. M.; Etchenique, R. Ruthenium Polypyridyl Phototriggers : From Beginnings to Perspectives Subject Areas : Author for Correspondence : *Phil Trans R Soc A* **2013**, *371*.
(115) Durham, B.; Caspar, J. V.; Nagle, J. K.; Meyer, T. J. Photochemistry of Ru(Bpy) 32+. *J. Am. Chem. Soc.* **1982**, *104* (18), 4803–4810. https://doi.org/10.1021/ja00382a012.
(116) Zayat, L.; Salierno, M.; Etchenique, R. Ruthenium(II) Bipyridyl Complexes as Photolabile Caging Groups for Amines. *Inorg. Chem.* **2006**, *45* (4), 1728–1731. https://doi.org/10.1021/ic0512983.
(117) Pinnick, D. V.; Durham, B. Photosubstitution Reactions of Ru(Bpy)2XYn+ Complexes. *Inorg. Chem.* **1984**, *23* (10), 1440–1445. https://doi.org/10.1021/ic00178a028.

(118) Zhu, M.; Lin, S.; Sun, Y.; Feng, Q.; Li, G.; Bian, L. Hydrogels Functionalized with N-Cadherin Mimetic Peptide Enhance Osteogenesis of HMSCs by Emulating the Osteogenic Niche. *Biomaterials* **2016**, *77* (January), 44–52. https://doi.org/10.1016/j.biomaterials.2015.10.072.
(119) San Miguel, V.; Álvarez, M.; Filevich, O.; Etchenique, R.; Del Campo, A. Multiphoton Reactive Surfaces Using Ruthenium(II) Photocleavable Cages. *Langmuir* **2012**, *28* (2), 1217–1221. https://doi.org/10.1021/la2033687.
(120) Nesrinne, S.; Djamel, A. Synthesis, Characterization and Rheological Behavior of PH Sensitive Poly(Acrylamide-Co-Acrylic Acid) Hydrogels. *Arab. J. Chem.* **2017**, *10* (4), 539–547. https://doi.org/10.1016/j.arabjc.2013.11.027.
(121) EL-Sharif, H. F.; Stevenson, D.; Warriner, K.; Reddy, S. M. CHAPTER 3:Hydrogel-Based Molecularly Imprinted Polymers for Biological Detection. In *Advanced Synthetic Materials in Detection Science*; **2014**; pp 75–115. https://doi.org/10.1039/9781849737074-00075.
(122) Denisin, A. K.; Pruitt, B. L. Tuning the Range of Polyacrylamide Gel Stiffness for Mechanobiology Applications. *ACS Applied Materials and Interfaces*. **2016**, *8* (34), 21893-21902. https://doi.org/10.1021/acsami.5b09344.
(123) Fischer, R. S.; Myers, K. A.; Gardel, M. L.; Waterman, C. M. Stiffness-Controlled Three-Dimensional Extracellular Matrices for High-Resolution Imaging of Cell Behavior. *Nat. Protoc.* **2012,** 7, 2056-2066. https://doi.org/10.1038/nprot.2012.127.
(124) Farrukh, A.; Paez, J. I.; Salierno, M.; del Campo, A. Bioconjugating Thiols to Poly(Acrylamide) Gels for Cell Culture Using Methylsulfonyl Co-Monomers. *Angew. Chem. Int. Ed.* **2016**, *55* (6), 2092–2096. https://doi.org/10.1002/anie.201509986.
(125) Wen, J. H.; Vincent, L. G.; Fuhrmann, A.; Choi, Y. S.; Hribar, K. C.; Taylor-Weiner, H.; Chen, S.; Engler, A. J. Interplay of Matrix Stiffness and Protein Tethering in Stem Cell Differentiation. *Nat. Mater.* **2014,** *13*, 979-987. https://doi.org/10.1038/nmat4051.
(126) Hermanson, G. T. *Bioconjugate Techniques: Third Edition*; **2013**. https://doi.org/10.1016/C2009-0-64240-9.
(127) Pande, C. S.; Sharma, A. Functionalization of Crosslinked Polyacrylamide through γ-Radiation-Induced Grafting of 4-Vinylpyridine. *J. Appl. Polym. Sci.* **2002**, 84, 2613-2620. https://doi.org/10.1002/app.10413.
(128) Grevesse, T.; Versaevel, M.; Circelli, G.; Desprez, S.; Gabriele, S. A Simple Route to Functionalize Polyacrylamide Hydrogels for the Independent Tuning of Mechanotransduction Cues. *Lab. Chip* **2013,** 13, 777-780. https://doi.org/10.1039/c2lc41168g.
(129) Farrukh, A.; Paez, J. I.; Salierno, M.; Fan, W.; Berninger, B. Bifunctional Poly (Acrylamide) Hydrogels through Orthogonal Coupling Chemistries. *Biomacromolecules* **2017**, 18, 3, 906–913. https://doi.org/10.1021/acs.biomac.6b01784.
(130) Farrukh, Aleeza: Photo-triggerable laminin mimetic peptides for directional neural regeneration https://publications.ub.uni-mainz.de/theses/frontdoor.php?source_opus=100001678&la=en (accessed 2020 -05 -24).
(131) Paez, J. I.; Farrukh, A.; Ustahüseyin, O.; del Campo, A. Biofunctionalization of Poly(Acrylamide) Gels. In *Biomaterials for Tissue Engineering*; Chawla, K., Ed.; Methods in Molecular Biology; Springer New York: New York, NY, **2018**; Vol. 1758, pp 101–114. https://doi.org/10.1007/978-1-4939-7741-3_8.
(132) Thiele, J.; Ma, Y.; Bruekers, S. M. C.; Ma, S.; Huck, W. T. S. 25th Anniversary Article: Designer Hydrogels for Cell Cultures: A Materials Selection Guide. *Adv. Mater.* **2014**, *26* (1), 125–148. https://doi.org/10.1002/adma.201302958.
(133) Ahearne, M.; Yang, Y.; El Haj, A. J.; Then, K. Y.; Liu, K. K. Characterizing the Viscoelastic Properties of Thin Hydrogel-Based Constructs for Tissue Engineering Applications. *J. R. Soc. Interface* **2005**, *2* (5), 455–463. https://doi.org/10.1098/rsif.2005.0065.
(134) Anseth, K. S.; Bowman, C. N.; Brannon-Peppas, L. Mechanical Properties of Hydrogels and Their Experimental Determination. *Biomaterials* **1996**, *17* (17), 1647–1657. https://doi.org/10.1016/0142-9612(96)87644-7.

(135) Martins, A. de O.; Canalli, V. M.; Azevedo, C. M. N.; Pires, M. Degradation of Pararosaniline (C.I. Basic Red 9 Monohydrochloride) Dye by Ozonation and Sonolysis. *Dyes Pigments* **2006**. https://doi.org/10.1016/j.dyepig.2005.02.002.
(136) Kister, A. E.; Roytberg, M. A.; Chothia, C.; Vasiliev, J. M.; Gelfand, I. M. The Sequence Determinants of Cadherin Molecules. *Protein Sci. Publ. Protein Soc.* **2001**, *10* (9), 1801–1810.
(137) Reid, R. A.; Hempertly, J. Human N-Cadherin: Nucleotide and Deduced Amino Acid Sequence. *Nucleic Acids Res.* **1990**, *18* (19), 5896–5896. https://doi.org/10.1093/nar/18.19.5896.
(138) Choe, W.; Durgannavar, T. A.; Chung, S. J. Fc-Binding Ligands of Immunoglobulin G: An Overview of High Affinity Proteins and Peptides. *Materials* **2016**, *9* (12). https://doi.org/10.3390/ma9120994.
(139) Zouani, O. F.; Kalisky, J.; Ibarboure, E.; Durrieu, M.-C. Effect of BMP-2 from Matrices of Different Stiffnesses for the Modulation of Stem Cell Fate. *Biomaterials* **2013**, *34* (9), 2157–2166. https://doi.org/10.1016/j.biomaterials.2012.12.007.
(140) Engler, A. J.; Sen, S.; Sweeney, H. L.; Discher, D. E. Matrix Elasticity Directs Stem Cell Lineage Specification. *Cell* **2006**, *126* (4), 677–689. https://doi.org/10.1016/j.cell.2006.06.044.
(141) Moshayedi, P.; Costa, L. da F.; Christ, A.; Lacour, S. P.; Fawcett, J.; Guck, J.; Franze, K. Mechanosensitivity of Astrocytes on Optimized Polyacrylamide Gels Analyzed by Quantitative Morphometry. *J. Phys. Condens. Matter* **2010**, *22* (19), 194114. https://doi.org/10.1088/0953-8984/22/19/194114.
(142) Greiner, C.; del Campo, A.; Arzt, E. Adhesion of Bioinspired Micropatterned Surfaces: Effects of Pillar Radius, Aspect Ratio, and Preload. *Langmuir* **2007**, *23* (7), 3495–3502. https://doi.org/10.1021/la0633987.
(143) Campo, A. del; Greiner, C. SU-8: A Photoresist for High-Aspect-Ratio and 3D Submicron Lithography. *J. Micromechanics Microengineering* **2007**, *17* (6), R81–R95. https://doi.org/10.1088/0960-1317/17/6/R01.
(144) Xia, Y.; Whitesides, G. M. Soft Lithography. *Angew. Chem. Int. Ed.* **1998**, *37* (5), 550–575. https://doi.org/10.1002/(SICI)1521-3773(19980316)37:5<550::AID-ANIE550>3.0.CO;2-G.
(145) Xue, L.; Iturri, J.; Kappl, M.; Butt, H.-J.; del Campo, A. Bioinspired Orientation-Dependent Friction. *Langmuir* **2014**, *30* (37), 11175–11182. https://doi.org/10.1021/la502695d.
(146) Humphrey, J. D.; Dufresne, E. R.; Schwartz, M. A. Mechanotransduction and Extracellular Matrix Homeostasis. *Nature Reviews Molecular Cell Biology*. **2014,** 15, 802–812. https://doi.org/10.1038/nrm3896.
(147) Yamada, S.; Pokutta, S.; Drees, F.; Weis, W. I.; Nelson, W. J. Deconstructing the Cadherin-Catenin-Actin Complex. *Cell* **2005,** *123* (5), 889-901. https://doi.org/10.1016/j.cell.2005.09.020.
(148) Buckley, C. D.; Tan, J.; Anderson, K. L.; Hanein, D.; Volkmann, N.; Weis, W. I.; Nelson, W. J.; Dunn, A. R. The Minimal Cadherin-Catenin Complex Binds to Actin Filaments under Force. *Science* **2014***, 346* (6209), 1254211. https://doi.org/10.1126/science.1254211.
(149) Collins, C.; Denisin, A. K.; Pruitt, B. L.; Nelson, W. J. Changes in E-Cadherin Rigidity Sensing Regulate Cell Adhesion. *Proc. Natl. Acad. Sci.* **2017**, *114* (29), E5835–E5844. https://doi.org/10.1073/pnas.1618676114.
(150) Yamada, S.; Nelson, W. J. Localized Zones of Rho and Rac Activities Drive Initiation and Expansion of Epithelial Cell-Cell Adhesion. *J. Cell Biol.* **2007,** *178* (3), 517-527. https://doi.org/10.1083/jcb.200701058.
(151) Borghi, N.; Sorokina, M.; Shcherbakova, O. G.; Weis, W. I.; Pruitt, B. L.; Nelson, W. J.; Dunn, A. R. E-Cadherin Is under Constitutive Actomyosin-Generated Tension That Is Increased at Cell-Cell Contacts upon Externally Applied Stretch. *Proc. Natl. Acad. Sci. U. S. A.* **2012**, *109* (31), 12568-12573. https://doi.org/10.1073/pnas.1204390109.
(152) Weber, G. F.; Bjerke, M. A.; DeSimone, D. W. A Mechanoresponsive Cadherin-Keratin Complex Directs Polarized Protrusive Behavior and Collective Cell Migration. *Dev. Cell* **2012,** *22* (1), 104-115. https://doi.org/10.1016/j.devcel.2011.10.013.

(153) Le Duc, Q.; Shi, Q.; Blonk, I.; Sonnenberg, A.; Wang, N.; Leckband, D.; De Rooij, J. Vinculin Potentiates E-Cadherin Mechanosensing and Is Recruited to Actin-Anchored Sites within Adherens Junctions in a Myosin II-Dependent Manner. *J. Cell Biol.* **2010**, *189* (7), 1107–1115. https://doi.org/10.1083/jcb.201001149.

(154) Barry, A. K.; Wang, N.; Leckband, D. E. Local VE-Cadherin Mechanotransduction Triggers Long-Ranged Remodeling of Endothelial Monolayers. *J. Cell Sci.* **2015,** *128* (7), 1341-51. https://doi.org/10.1242/jcs.159954.

(155) Yeung, T.; Georges, P. C.; Flanagan, L. A.; Marg, B.; Ortiz, M.; Funaki, M.; Zahir, N.; Ming, W.; Weaver, V.; Janmey, P. A. Effects of Substrate Stiffness on Cell Morphology, Cytoskeletal Structure, and Adhesion. *Cell Motil. Cytoskeleton* **2005,** *60* (1), 24-34. https://doi.org/10.1002/cm.20041.

(156) Engler, A.; Bacakova, L.; Newman, C.; Hategan, A.; Griffin, M.; Discher, D. Substrate Compliance versus Ligand Density in Cell on Gel Responses. *Biophys. J.* **2004,** *86* (1),617-628. https://doi.org/10.1016/S0006-3495(04)74140-5.

(157) Suraneni, P.; Rubinstein, B.; Unruh, J. R.; Durnin, M.; Hanein, D.; Li, R. The Arp2/3 Complex Is Required for Lamellipodia Extension and Directional Fibroblast Cell Migration. *J. Cell Biol.* **2012,** *197* (2), 239-251. https://doi.org/10.1083/jcb.201112113.

(158) Beckham, Y.; Vasquez, R. J.; Stricker, J.; Sayegh, K.; Campillo, C.; Gardel, M. L. Arp2/3 Inhibition Induces Amoeboid-like Protrusions in MCF10A Epithelial Cells by Reduced Cytoskeletal-Membrane Coupling and Focal Adhesion Assembly. *PLoS ONE* **2014**, *9* (6), e100943. https://doi.org/10.1371/journal.pone.0100943.

(159) Goichberg, P.; Geiger, B. Direct Involvement of N-Cadherin-Mediated Signaling in Muscle Differentiation. *Mol. Biol. Cell* **1998,** *9* (11), 3119-3131. https://doi.org/10.1091/mbc.9.11.3119.

(160) Oberlender, S. A.; Tuan, R. S. Expression and Functional Involvement of N-Cadherin in Embryonic Limb Chondrogenesis. *Development* **1994,** *120* (1), 177-87.

(161) Mbalaviele, G.; Chen, H.; Boyce, B. F.; Mundy, G. R.; Yoneda, T. The Role of Cadherin in the Generation of Multinucleated Osteoclasts from Mononuclear Precursors in Murine Marrow. *J. Clin. Invest.* **1995,** *95* (6), 2757-65. https://doi.org/10.1172/JCI117979.

(162) Doherty, P.; Walsh, F. S. Signal Transduction Events Underlying Neurite Outgrowth Stimulated by Cell Adhesion Molecules. *Curr. Opin. Neurobiol.* **1994,** *4* (1), 49-55. https://doi.org/10.1016/0959-4388(94)90031-0.

(163) Buckingham, M. Skeletal Muscle Formation in Vertebrates. *Current Opinion in Genetics and Development*. **2001**. https://doi.org/10.1016/S0959-437X(00)00215-X.

(164) Charrasse, S.; Meriane, M.; Comunale, F.; Blangy, A.; Gauthier-Rouvière, C. N-Cadherin-Dependent Cell-Cell Contact Regulates Rho GTPases and β-Catenin Localization in Mouse C2C12 Myoblasts. *J. Cell Biol.* **2002**, *158* (5), 953–965. https://doi.org/10.1083/jcb.200202034.

(165) Knudsen, K. A.; Myers, L.; McElwee, S. A. A Role for the Ca2+-Dependent Adhesion Molecule, N-Cadherin, in Myoblast Interaction during Myogenesis. *Exp. Cell Res.* **1990**, *188* (2), 175–184. https://doi.org/10.1016/0014-4827(90)90157-6.

(166) Redfield, A.; Nieman, M. T.; Knudsen, K. A. Cadherins Promote Skeletal Muscle Differentiation in Three-Dimensional Cultures. *J. Cell Biol.* **1997,** *138* (6), 1323-1331. https://doi.org/10.1083/jcb.138.6.1323.

(167) Bian, L.; Guvendiren, M.; Mauck, R. L.; Burdick, J. A. Hydrogels That Mimic Developmentally Relevant Matrix and N-Cadherin Interactions Enhance MSC Chondrogenesis. *Proc. Natl. Acad. Sci.* **2013**, *110* (25), 10117–10122. https://doi.org/10.1073/pnas.1214100110.

(168) Tanaka, K.; Sato, K.; Yoshida, T.; Fukuda, T.; Hanamura, K.; Kojima, N.; Shirao, T.; Yanagawa, T.; Watanabe, H. Evidence for Cell Density Affecting C2C12 Myogenesis: Possible Regulation of Myogenesis by Cell–Cell Communication. *Muscle Nerve* **2011**, *44* (6), 968–977. https://doi.org/10.1002/mus.22224.

(169) Bajaj, P.; Reddy, B.; Millet, L.; Wei, C.; Zorlutuna, P.; Bao, G.; Bashir, R. Patterning the Differentiation of C2C12 Skeletal Myoblasts. *Integr. Biol.* **2011**, *3* (9), 897–909. https://doi.org/10.1039/c1ib00058f.

(170) Kilian, K. A.; Bugarija, B.; Lahn, B. T.; Mrksich, M. Geometric Cues for Directing the Differentiation of Mesenchymal Stem Cells. *Proc. Natl. Acad. Sci.* **2010**, *107* (11), 4872–4877. https://doi.org/10.1073/pnas.0903269107.

(171) Griffin, M. A.; Engler, A. J.; Barber, T. A.; Healy, K. E.; Sweeney, H. L.; Discher, D. E. Patterning, Prestress, and Peeling Dynamics of Myocytes. *Biophys. J.* **2004**, *86* (2), 1209–1222. https://doi.org/10.1016/S0006-3495(04)74195-8.